UNIVERSITY OF CALIFORNIA

Santa Barbara

Controlling Polymer Conformation and Hydration with Monomer Sequence

A dissertation submitted in partial satisfaction of the

requirements for the degree Doctor of Philosophy

in Chemical Engineering

by

Audra Jean DeStefano

Committee in charge:

Professor Rachel Segalman, Co-chair

Professor Songi Han, Co-chair

Professor M. Scott Shell

Professor Angela Pitenis

September 2023

The dissertation of Audra Jean DeStefano is approved.

_____

Angela Pitenis

_____

M. Scott Shell

_____

Songi Han, Committee Co-chair

_____

Rachel Segalman, Committee Co-chair

September 2023

Controlling Polymer Conformation and Hydration with Monomer Sequence

Audra Jean DeStefano

Acknowledgements

First, I am grateful to my family for their continual support. I am so lucky to have parents that gave me the freedom, resources, and encouragement to explore ideas (and the mountains) from a young age. Thank you for encouraging me be my own person, even when that path takes me far away from home. My sisters continually help me recenter myself, my grandmothers inspired and encouraged me to pursue a scientific career, and my partner, Drew, brightens all of my days. Infinite thanks to all of you.

My graduate mentors, Prof. Rachel Segalman and Prof. Songi Han, have been essential to my growth as a researcher and as a human. Thank you both for giving me this opportunity, for providing the patience and resources necessary for me to learn and combine entirely new skillsets, and for helping me become a more confident and capable person. I have learned tremendously from your examples.

Prof. Scott Shell and Prof. Angela Pitenis have been exemplary committee members. I collaborated closely with Scott throughout my PhD and he contributed immensely to the technical depth of my projects. Angela brings a fresh perspective and thoughtful questions each time that we meet. I leave every discussion with Angela feeling more motivated than when I came, in large part because she helps me see new ways in which my work can be applicable. Thank you both for sharing your time and expertise with me.

I also want to thank my collaborators. Sally Jiao and Prof. Scott Shell have been close computational collaborators throughout my time at UCSB. Both are incredibly generous with their time and their insightful feedback has been instrumental, even on projects in which we haven't collaborated directly. Discussions with and simulations by My Nguyen and Prof. Glenn Fredrickson have greatly enhanced the depth of my work. Benjamin Predetti spent

many patient hours teaching me anionic synthesis and making PEO polymers for me, while Prof. Nate Lynd has been a great resource on all things block copolymer synthesis. Further collaborations with Dr. Ethan Crumlin, Prof. Lynn Walker, Prof. Abigail Knight, Prof. Julia Ortony, Prof. Ansgar Seimer, Prof. Ralf Langen, and their groups have been both informative and enjoyable.

I am grateful to have been surrounded by smart, helpful, and fun people in the Han and Segalman groups. Working with good people from diverse backgrounds has enriched my experience and broadened my world. Several people deserve special thanks. In particular, Mikayla Barry taught me how to do the polypeptoid synthesis that is central to this thesis and Segolene Antoine introduced me to anionic polymerization. Timothy Keller and Thomas Casey helped me get started with electron paramagnetic resonance techniques and Thomas Webber and Karen Tsay have answered many questions (and fixed many instrumentation problems) in subsequent years. Shawn Mengel's attention to detail and perfect polypeptoids have made our work together fun and successful. Thank you all for your help and encouragement.

The work described in this thesis was made possible by the efforts of UCSB user facility staff. Rachel Behrens, Morgan Bates, Shamon Walker, Jaya Nolt, Jerry Hu, and Jen Smith went above and beyond to provide reliable instrumentation and technical support. I am so thankful to have had access to well-maintained instruments and rapid response help anytime something looked awry.

I am also appreciative of Katie Li-Oakey who advised me at the University of Wyoming and provided my first research experience. Her example as a woman with a career enabled by an advanced engineering degree drastically lowered the barrier to envisioning a similar life

for myself. I still benefit from lessons I learned by working with Katie, especially in learning how to write. Thank you for helping me see my potential and pointing me toward UCSB.

Finally, Santa Barbara has brought too many wonderful friends into my life to list. I feel incredibly lucky to have kind people to climb, bike, surf, backpack, hike, ski, rollerblade, dance, make art, sing songs, play games, eat food, and talk late into the night with. You have made me happy to be here and sad to leave.

Curriculum Vitae

Audra Jean DeStefano

EDUCATION

Sep 2018 – Sep 2023	Ph.D. in Chemical Engineering (expected), University of California, Santa Barbara Co-advisors: Professor Rachel A. Segalman and Professor Songi Han
Jun 2016 – May 2018	M.S. in Chemical Engineering, University of Wyoming Advisor: Professor Dongmei Li-Oakey
Aug 2012 – May 2016	B.S. in Chemical Engineering, University of Wyoming Advisor: Professor Dongmei Li

PUBLICATIONS

11. A. DeStefano*, S. Mengel*, M. Bates, S. Jiao, M. S. Shell, S. Han, R. Segalman. *Control Over Conformational Landscapes of Short Polypeptoids by Monomer Sequence*, *submitted*. (*equal contribution)
10. E. Day, K. Cunha, J. Zhao, A. DeStefano, J. Dodds, M. Yu, S. Han, E. Baker, J.-E. Shea, R. Berlow, A. Knight, *Insights into Conformational Ensembles of Compositionally Identical Disordered Peptidomimetics, submitted.*
9. S. Oh, P. Nguyen, T. Tran, A. DeStefano, K. Tagami, D. Yuan, A. Nikolaev, M. Condarcure, S. Han, J. Read de Alaniz, M. Chabinyc, *Interfacial Doping of Semiconducting Polymers with Phenothiazine-based Polymer Ionic Liquids, submitted.*
8. A. DeStefano, M. Nguyen, G. Fredrickson, S. Han, R. Segalman. *Design of Soft Material Surfaces with Rationally Tuned Water Diffusivity*, ACS Central Science, 2023, 9 (5), 1019-1024.
7. S. Jiao, D. Rivera Mirabel, A. DeStefano, R. Segalman, S. Han, M. S. Shell. *Sequence Modulates Hydration Water Structure and Dynamics*, Biomacromolecules, 2022, 23 (4), 1745-1756.
6. M. Barry, P. Aydogan Gokturk, A. DeStefano, A. Leonardi, C. Ober, E. Crumlin, R. Segalman. *Effects of Amphiphilic Polypeptoid Side Chains on Polymer Surface Chemistry and Hydrophilicity.* ACS Applied Materials and Interfaces, 2022, 14 (5), 7340-7349.
5. A. DeStefano, R. Segalman, S. Han. *Where Biology and Traditional Polymer Meet: The Potential of Associating Sequence-Defined Polymers for Materials Science.* Journal of the American Chemical Society Au, 2021, 1 (10), 1556-1571.
4. S. Jiao, A. DeStefano, J. Monroe, M. Barry, N. Sherck, T. Casey, R. Segalman, S. Han, M. S. Shell. *Quantifying Polypeptoid Conformational Landscapes Through Integrated Experiment and Simulation.* Macromolecules, 2021, 54, 5011-5021.

3. N. Sherck, T. Webber, D. Robinson Brown, T. Keller, M. Barry, A. DeStefano, S. Jiao, R. Segalman, G. Fredrickson, M. S. Shell, S. Han. *End-to-end Distance Probability Distributions of Dilute Poly(ethylene oxide) in Aqueous Solution.* Journal of the American Chemical Society, 2020, 142, 19631-19641.
2. J. Monroe, M. Barry, A. DeStefano, P. Gokturk, S. Jiao, D. Robinson-Brown, T. Webber, E. Crumlin, S. Han, M. S. Shell. *Water Structures and Properties at Hydrophilic and Hydrophobic Surfaces.* Annual Review of Chemical and Biomolecular Engineering, 2020, 11, 523-57.
1. A. DeStefano, J. Yin, T. Kraus, B. Parkinson, and D. Li. *Elucidation of Titanium Dioxide Nucleation and Growth on Polydopamine Modified Nanoporous Polyvinylidene Fluoride Substrate via Low-Temperature Atomic Layer Deposition.* ACS Omega, 2018, 3, 10493-10502.

Abstract

Controlling Polymer Conformation and Hydration with Monomer Sequence

by

Audra Jean DeStefano

While most synthetic polymers are best described by their statistical nature, many biological polymers derive their highly tailored functions from precisely defined monomeric sequences. Sequence-controlled polymers, such as polypeptoids, present a unique tool for controlling material properties by harnessing both the robustness of synthetic polymers and the ability to tailor the inter- and intra-molecular interactions so crucial to many biological materials. Significant progress has been made towards predicting how protein folding is controlled by monomer sequence and interactions with water, but a thorough understanding of how to use polymer sequence to similarly control chain conformation and resulting functionality in synthetic polymer assemblies is lacking. Similarly, advances in understanding the effect of polymer surface chemistry and topology on hydration water dynamics and resulting polymer-solute interactions lags behind analogous protein hydration studies. Together, the ability to control polymer structure and hydration water behavior via sequence-control offers an avenue to pursue polymeric materials with protein-like functionality. This work focuses on how polypeptoid sequence can be utilized to control polymer conformation and nearby water behavior. First, monomer sequence effects on polymer conformation are probed, primarily making use double electron-electron resonance (DEER) spectroscopy. Second, the sequence specificity of polypeptoids enables observation of multiple hydration environments within

multi-chain assemblies via Overhauser dynamic nuclear polarization (ODNP) spectroscopy. Finally, these differences in water behavior are utilized to tune catalytic activity within micelles, much like proteins.

TABLE OF CONTENTS

LIST OF FIGURES

LIST OF TABLES

Chapter 1 - Introduction

1.1 Abstract

Polymers with precisely defined monomeric sequences present an exquisite tool for controlling material properties by harnessing both the robustness of synthetic polymers and the ability to tailor the inter- and intra-molecular interactions so crucial to many biological materials. While polymer scientists traditionally synthesized and studied the physics of long molecules best described by their statistical nature, many biological polymers derive their highly tailored functions from precisely controlled sequences. Significant progress has been made towards understanding, but a thorough understanding of how to use polymer sequence to similarly control interactions and chain conformation, and through them spatial patterning and resulting functionality, in synthetic polymer assemblies is needed. Similarly, advances in understanding the effect of polymer surface chemistry and topology on hydration water dynamics and resulting polymer-solute interactions lag behind protein hydration studies. Together, the ability to control polymer assembly and hydration water behavior via sequence-control could offer an avenue to pursue polymeric materials with protein-like functionality.

This chapter was reproduced in part with permission from:

1. DeStefano, A. J.; Segalman, R. A.; Davidson, E. C. Where Biology and Traditional Polymers Meet: The Potential of Associating Sequence-Defined Polymers for Materials Science *JACS Au*, 2021, 1 (10), 1556-1571. DOI: 10.1021/jacsau.1c00297. Copyright 2021 American Chemical Society.
2. Jiao, S.; DeStefano, A.; Monroe, J.; Barry, M.; Sherck, N.; Casey, T.; Segalman, R. A.; Han, S.; Shell, M. S. Quantifying Conformational Landscapes through Integrated Experiment and Simulation *Macromolecules*, 2021, 54 (11), 5011-5021. DOI: 10.1021/acs.macromol.1c00550. Copyright 2021 American Chemical Society.

1.2 Introduction

The development of synthetic sequence-defined polymers represents the achievement of a longstanding 'grand challenge' in polymer science.[1] The inspiration for pursuing sequence control as a means of attaining unique material properties largely is derived from nature. Many biological systems precisely control the arrangement of monomers within polymer chains into specific orders, or sequences, to achieve diverse functions such as information storage,[2] signaling and circuitry,[3] templating of biomineralization,[4] and hierarchical assembly[5] that facilitates binding, transport, and material properties. Synthetic techniques capable of directly producing polypeptides,[6] RNA, and DNA have been developed,[7] but lack the chemical diversity and stability of synthetic polymers. At the other end of the spectrum, traditional synthetic polymers feature distributions of molecular weight and, where multiple monomers are included, the monomers are arranged into statistical or blocky regions that vary from chain to chain. Sequence-defined polymers bridge both classes of polymers by precisely ordering diverse chemical functionalities with non-natural backbones and side chains (**Figure 1.1**). These diverse chemistries have spanned from biomimetic polypeptoids for protein-mimetic

folding and function in solution[8, 9] to sequences with the goal of achieving synthetic materials capable of information storage.[10, 11] Control over precise monomer sequence confers significant tools to tune monomer-monomer associations over multiple length scales, while also allowing the integration of elements of chemical functionality.

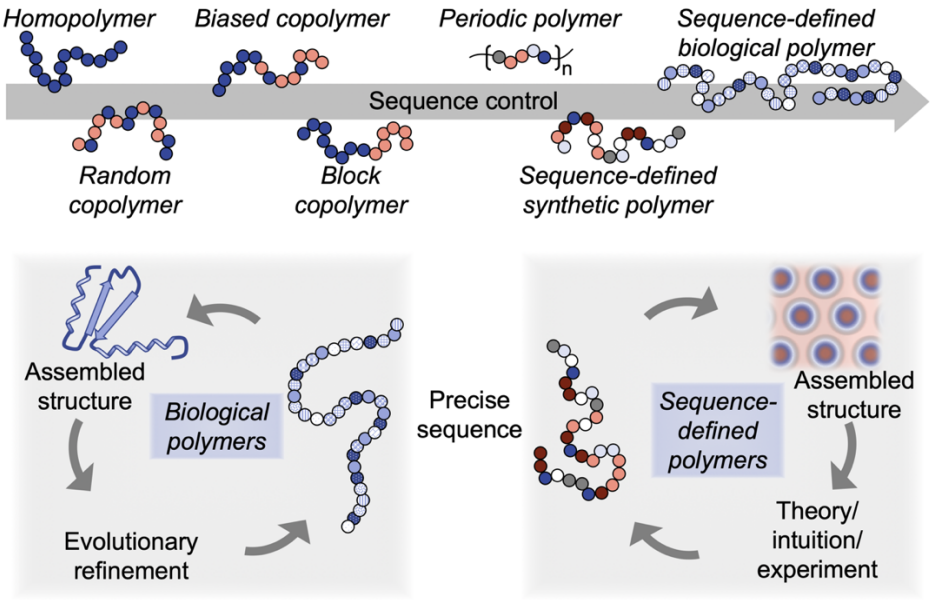

Figure 1.1. Sequence-defined polymers bridge biological and traditional synthetic polymers.

Biological materials, such as proteins, and traditional synthetic polymers make up two well established classes of polymers. While traditional synthetic polymers feature broad molecular weight distributions with statistically controlled sequences, many biological polymers are characterized by precise monomer sequences. Synthetic sequence-defined polymers contain perfectly controlled monomer sequences, where the difference from chain-to-chain is comparable to that of protein or small molecule purity but are capable of incorporating a broader range of functionalities. Depicted cycles represent that while many sequence-defined biological polymers evolve over many generations (in nature or in laboratories) to access precise architectures capable of achieving specific functions, sequences guiding synthetic polymer assembly and function are engineered through intuition, experiment, and, ultimately, theory.

The fields of polymer physics, foldamers, and protein engineering have largely advanced independently; sequence-defined polymers bridge these fields. Unique material architectures and properties can be accessed by encoding intra- and inter-molecular interactions in polymer sequence. Significant progress has been made towards predicting how protein folding is controlled by monomer sequence and interactions with water, but a thorough understanding of how to use polymer sequence to similarly control chain conformation and resulting functionality in synthetic polymer assemblies is lacking. Similarly, advances in understanding the effect of polymer surface chemistry and topology on hydration water dynamics and resulting polymer-solute interactions lags behind analogous protein hydration studies. Together, the ability to control polymer structure and hydration water behavior via sequence-control offers an avenue to pursue polymeric materials with protein-like functionality. This thesis advances our fundamental understanding of how sequence impacts polymer chain formation and guides hydration water diffusivity and, consequently, interactions with nearby solutes. Further development of such fundamental knowledge will transform the use of synthetic polymers in a myriad of applications, such as membrane science, antifouling coatings, and catalysis.

1.3 Defining and quantifying perfection

In studies of associating polymer chains, it is important to consider the properties of not just an individual chain, but of collections of chains; indeed, this has formed the basis of many traditional studies in polymer science. While assembly of a single chain in solution concerns only the interactions of that chain with its solvent and itself, in bulk and concentrated polymer systems, interactions of many polymer chains with each other must be considered. Traditional synthetic polymer samples contain many chains, with properties including molecular weight,

amount and distribution of each monomer, and spatial conformation varying from chain to chain. These differences in overall composition and/or sequence influence associating and bulk material properties[12] and, therefore, are crucial to contextualizing material systems containing sequence-defined polymers.

Informative quantification of forms of variation and dispersity in a sample requires polymer scientists to move beyond standard measurements of dispersity (**Figure 1.2a**). The classic measure of variation between polymer chains in a sample is the molecular weight distribution via the ratio of the number average (M_n) and weight average (M_w) molecular weights, defining a dispersity index, Đ. This value gives only general information about the shape of the distribution (in other words, a bimodal vs. a broad single modal distribution could in principle have identical Đ, but very different impacts on assembly and other properties[12-14]). As samples with more complexity are synthesized – for example, random copolymers and block copolymers – materials begin to also be characterized by an average volume fraction and composition profile defined by the monomers available and biasing of the polymerization statistics.[15] Underneath this is the realization that individual chains are composed of a distribution of these available monomers. For example, for a given volume fraction f_A of monomer in a sample, individual chains will vary regarding their individual volume fraction of A; f_A simply represents a population average.[16] This form of dispersity is referred to as compositional dispersity. Likewise, the sequence of monomers along a polymer chain can vary. Even in a population of chains where the monomers are randomly distributed from end-to-end, individual chains will deviate to greater or lesser extents from even spacing (indeed, a single chain cannot be evenly distributed due to the discrete nature of monomers!)[16]. Separately examining the impacts of compositional and sequence dispersity on behavior and

assembly is nearly impossible in traditional polymer systems but may be achieved leveraging controlled combinations of sequence-defined polymers.

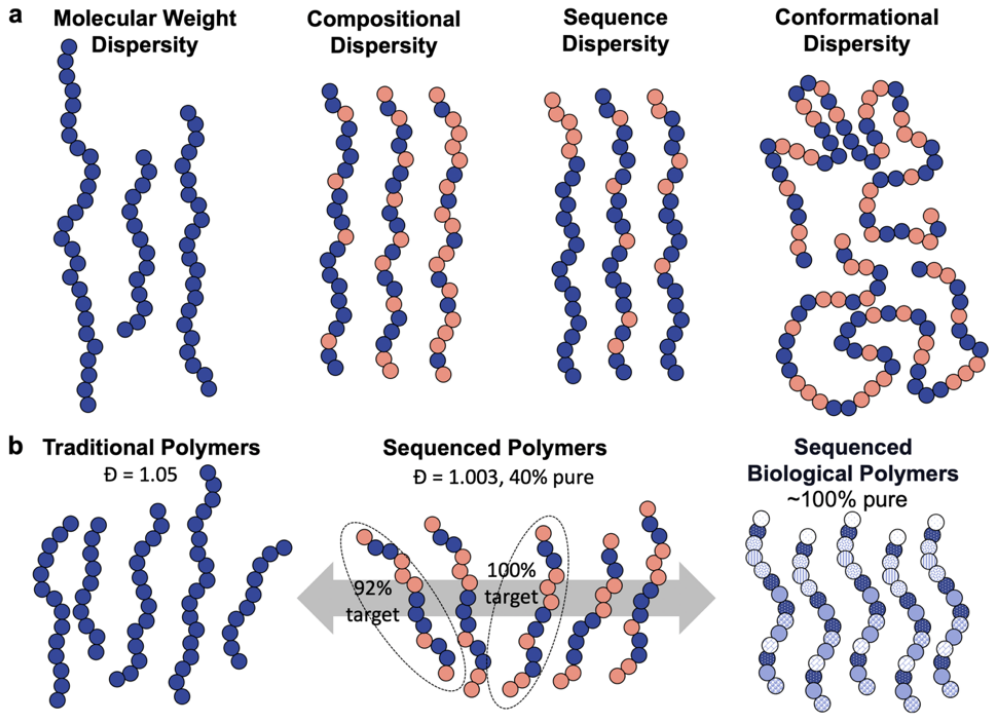

Figure 1.2. Describing precision in linear polymer chains.

a) Measures of dispersity often describe only the molecular weight distribution of a sample of polymer chains. In a population of chains with multiple monomers, the sample may be characterized by an overall fraction of monomer A and monomer B, but this composition may vary from chain to chain. Similarly, in a population of chains with an identical fraction of each monomer, the sequence of those monomers may not be constant. A population of chains with identical sequence will still adopt a range of chain conformations whether in solution or in the bulk. b) The presence of multiple forms of dispersity in sequence-defined polymers demands that we quantify dispersity in multiple ways and weigh the impact of dispersity on material performance. Sequenced polymers in which many chains have minor deviations (e.g. 1-2 deletions) still have Đ far closer to unity than is attainable for traditional polymers. In terms of a yield of perfect sequences, however, even one deletion renders that chain an impurity, leading to low yields of the target sequence.

While a population of 'perfect' sequence-defined polymers lack all of the aforementioned forms of dispersity (perfectly defined in molecular weight, composition, and sequence, similar to a protein or small molecule level of purity), the statistical nature of polymer chains will still cause significant variability in adopted chain shape. In traditional polymer systems, monomer identity controls the polymer persistence length and resulting radius of gyration (polymer size). In polymer systems that exhibit self-assembly in the bulk, changes in polymer chain conformation, particularly near interfaces, have significant impacts on self-assembly.[17, 18] For example, block copolymers exhibit significant changes in assembly in response to changes in local persistence length and nematic interactions.[19-21] Further, even elements such as side chain chirality can drive significant changes in polymer conformation, such as from a coil to a helical moiety.[22] The extreme of sequence-biased chain shape is found in polymer chains such as proteins assembled into well-defined conformations; the 'foldamer' community works to build synthetic mimics of these materials.[23] Even in well-defined protein structures, significant conformational fluctuations and flexibility persist (and are important for function) and much of the utility in leveraging sequence ultimately is derived from the ability to selectively bias local polymer chain conformation.[24, 25] Notably, changes in chain conformation are often intricately linked to materials with significant stimuli-response. For example, micelles can be engineered to transition from helix to coil chain conformations useful for drug release,[26, 27] poly(*N*-isopropylacrylamide) demonstrates temperature responsive chain collapse/expansion,[28] and liquid crystalline polymers demonstrate stimuli-responsive changes in chain anisotropy.[29] Highly controlled incorporation of stimuli-responsive elements in sequence-defined materials is expected to enable the localization and degree of stimuli-responsive changes in material response, with implications for broader

material properties. There are biological inspirations for this: protein domains that, depending on their local environment, sample different sets of conformational states (only some of which are 'active') are capable of serving as feedback control elements.[30, 31] As we develop sequence-defined polymers for targeted material properties, it will be critical to develop more precise descriptors for the relationship between sequence and accessible chain conformation.

Notably, while biological systems leverage sequence-defined materials to excellent effects, many critical biological materials are not fully defined by sequence, such as polysaccharides. For example, seaweeds are largely composed of alginates, polysaccharides of mannuronate (M) and guluronate (G) residues. These residues are organized into blocks which are themselves primarily M, primarily G, or an alternating sequence of the two.[32] The block composition varies between species and tissue of the young vs. old seaweed, with accompanying differences in mechanical properties – an example of nature controlling properties via principles quite familiar to synthetic polymer science. Even in proteins, a precise sequence does not fully articulate the 3D arrangement of monomers; many proteins are now well-understood to lack a precisely defined structure, or are composed of a mixture of well controlled and disordered regions.[24] This suggests that while defined monomer sequence is truly transformative and worth the additional challenge in synthesis and purification in some applications, other applications may be best served by imperfect sequence control.

1.4 Synthetic approaches for controlling polymer sequence

Early synthetic polymerization approaches proceeded via mechanisms that resulted in poorly controlled materials (homopolymers and random copolymers), but methods attaining increasing levels of control over polymer sequence and molecular weight have evolved

(biased copolymers,[33, 34] block copolymers[35]). Biased copolymers leverage differences in reaction kinetics or controlled monomer addition to influence the arrangement of monomers while block copolymers allow complete reaction of one monomer type before adding the next. Modern methods that enable true sequence control generally fall into one of two categories (**Figure 1.3**). The first consists of methods with precise control over sequence and composition, but without molecular weight control (periodic polymers). These methods are generally based on repeats of precise monomers enabled via step growth or ring opening polymerization of precise, oligomeric monomers, enabling scalable synthesis. The second includes iterative methods that lead to both precise sequence and molecular weight control. Generally, it is this latter that are referred to as 'sequence-defined'. Here, scalable synthesis remains generally out of reach.

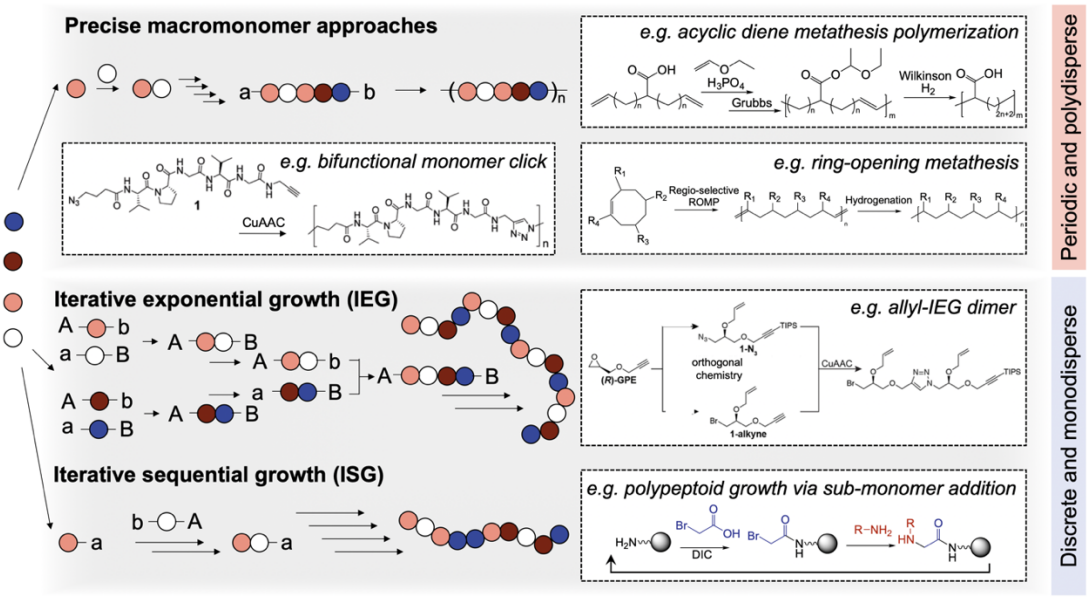

Figure 1.3. Synthetic methods for attaining sequence control.

Several polymerization methods produce sequence-controlled materials. Precise macromonomer approaches make use of sequence-specific macromonomers to make polymer with periodic sequences. Iterative exponential growth (IEG) and iterative sequential growth (ISG) approaches use sequential monomer additions to access complex sequences and control molecular weight.

Several industrially scalable routes for synthesizing polymers with periodic sequence control from precise macromonomers are illustrated in **Figure 1.3**. Acyclic diene metathesis polymerization (ADMET) relies on step growth polymerization of symmetric α,ω-diene monomers to regularly incorporate chemical functionalities along a polyethylene chain.[36-38] Both chain ends are identical, so ADMET forms precise sequences only when monomers are symmetrical. This means that non-symmetric monomers or polymers combining multiple monomers with different chemical functionality will not yield precise sequences. Other precise macromonomer addition methods address this limitation to some degree. Here, macromonomers containing a uniform sequence of chemical functionalities are polymerized

together, resulting in repeating blocks of a specific sequence. Polymerization schemes include click chemistry of bifunctional macromonomers[39] and regioselective ring opening metathesis (ROMP) of cyclic monomers.[40, 41] Of these methods, ROMP generally provides the best molecular weight control, but all three methods enable less molecular weight control and sequence complexity than iterative methods. Multicomponent reactions offer another route to sequence control and, when performed iteratively, can also achieve molecular weight control.[42, 43]

Methods for the synthesis of synthetic sequence-defined materials with uniform molecular weight generally rely on either iterative exponential (IEG) or iterative sequential (ISG) growth methods. Generally, both IEG and ISG achieve a single coupling at a time via some form of orthogonal chemistry. We note that for these methods, particularly in solution, coupling efficiency decreases with increasing polymer length. In the IEG approach, a sequence may be composed by first synthesizing the component dimers, from them the component tetramers, and so forth, until a final coupling forms the entire desired chain, as shown in **Figure 1.3**.[44, 45] Notably, stepwise product purification is required for these materials (**Figure 1.4a**). The doubling of molecular weight with each step enhances the efficiency and ease of separation, but even in-line purification via flow synthesis does not eliminate the requirement.[46] Further, IEG methods require orthogonal 'activation' chemistries on the end groups: that can be achieved either via high efficiency protection-deprotection chemistries[45] or, elegantly, via orthogonal light-based chemistries.[47] While IEG achieves some distinct advantages over ISG methods, both approaches remain limited to only certain polymer backbones, and are challenged by the efficiency of individual steps, limiting the overall molecular weight.

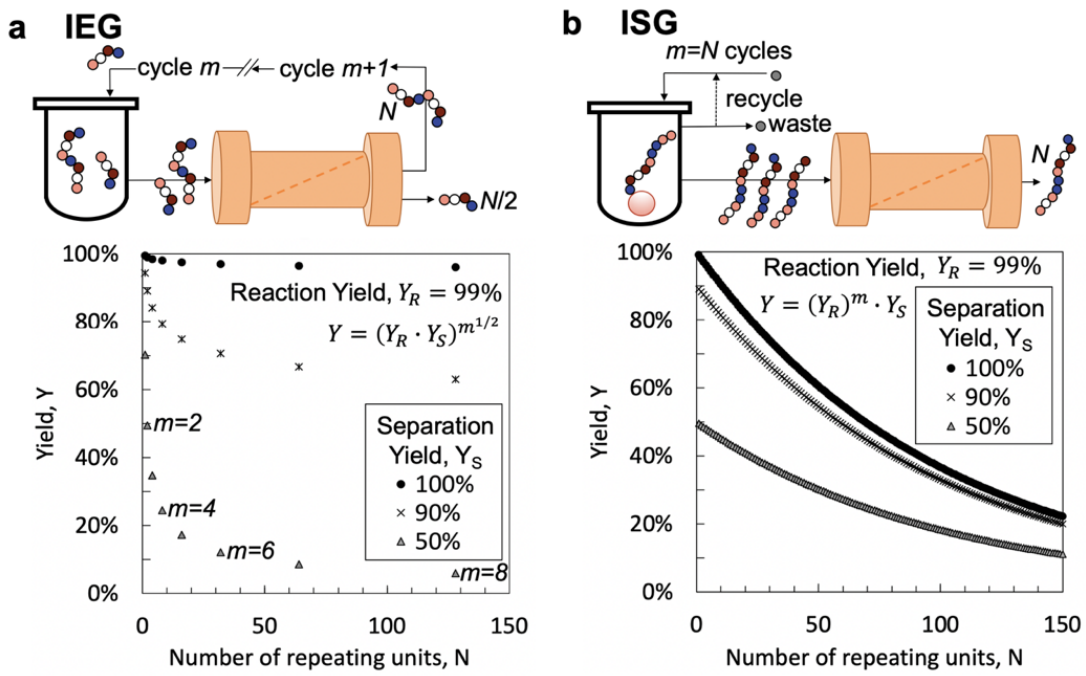

Figure 1.4. Synthesis and purification workflows for iterative growth methods.

a) IEG uses orthogonal deprotection chemistries to couple chains together, quickly leading to large molecular weight increases. Here, m reaction steps are needed to synthesize a polymer of length N, but molecular weight control depends on stepwise purification. Overall yields (Y) are plotted for several separation yields (Y_S) given a highly efficient individual reaction yield (Y_R) of 99%, demonstrating that highly efficient separations are necessary to attain reasonable yields. b) ISG methods, on the other hand, provide sequence control by adding each monomer individually. Reaction inefficiencies result in some chains missing at least one monomer. Subsequent purification generally involves isolating the target sequence via prep-HPLC. Overall yields are also plotted for ISG showing that very high reaction yields are necessary to attain even modest quantities of the target product.

In contrast to IEG, ISG adds a single monomer at a time. Many ISG methods are performed on solid-phase supports, allowing high reagent concentrations to push each individual step to high yield and enabling step-wise addition by retaining the growing polymer chain on the solid support while a solvent flush removes the excess reagent (**Figure 1.4b**).[48, 49] This strategy is best known for synthesis of biological and bio-inspired materials such as

polypeptides (via protecting groups) and polypeptoids (via a sub-monomer strategy), but is also applicable to other highly efficient chemistries, such as thiolactone-based approaches.[50] Drawbacks of solid-phase synthesis include that it requires large amounts of support beads relative to polymer grown and tremendous quantities of excess reagent and solvent. Further, materials synthesized via solid-phase ISG methods typically require further purification post-synthesis, with yields of the desired sequence scaling with molecular weight. If each synthetic step proceeds with 99% efficiency, a 10-mer will result in 90% of the desired product, while a 100-mer will result in only 37% of the desired product! This means that only reactions with extraordinarily high yields are useful in iterative growth strategies, thus limiting possible backbones. Rigorous chromatographic methods of purification consume additional solvent and restrict the attainable quantities of product. Solution-phase ISG methods suffer from similar drawbacks. While they do not consume the same degree of support beads and solvent during earlier synthetic steps, they often do so in return for a reduced yield and require similar purification during the final steps in order to achieve a near-perfect sequence-defined material for additional studies and application. Ultimately, the need for significant purification – even when using some of the most efficient known chemistries for couplings – remains a substantial hurdle in the scale-up of materials synthesized via either iterative method.

Of these sequence-defined materials, polypeptoids (**Figure 1.3**) are particularly useful for studying sequence effects due to their relative ease of synthesis, wide range of side chain functionality, lack of backbone hydrogen bonding, and ability to form secondary structures. Because of their advantages as model materials, polypeptoids are utilized extensively throughout this work.

1.5 Controlling spatial patterning

The explicit sequence of each polymer only tells part of the story in assembled polymer systems. A given monomer remains adjacent to the proceeding and subsequent monomer in its polymer chain; however, as that chain collapses into a single-chain polymer nanoparticle or is surrounded by other chains, the arrangement of monomers becomes much less obvious. Yes, directly adjacent monomers will always be nearest neighbors, but other nearest neighbors may reside in different segments of the polymer or different molecules entirely. Consequently, spatial patterning throughout assemblies is informed but not dictated by individual polymer sequence.

Proteins exemplify the impact of polymer sequence on spatial patterning and, thus, function. Polypeptide chains are composed of specific sequences of amino acids that use disulfide bonds and differences in hydrophobicity, hydrogen bonding, and electrostatic interactions to fold into unique structures (**Figure 1.5a**).[51] These structures vary widely with some being highly ordered and others intrinsically disordered, but all carry out critical biological functions. Protein functionality is largely enabled by areas of heterogeneity on the protein surface, both in chemistry and topology, that are an inherent result of the spatial arrangement of individual polypeptide repeating units.[52] For example, spatial variation on the protein Chemotaxis Y influences the behavior of water near its surface.[53] These variations in surface water behavior aid in site specific binding and are critical to its function. Furthermore, structural changes in response to external stimuli are also central to the function of many proteins, such as phototropin light switches in which the Jα-helix undocks and unfolds away from the protein.[54] Understanding the underlying protein sequence responsible for this behavior has enabled use of systematic mutations to enhance the range of photoswitching.[55,

[56] While, significant progress has been made towards understanding and even predicting protein folding,[55, 57-59] a thorough understanding of how to use polymer sequence to similarly control interactions and chain conformation, and through them spatial patterning and resulting functionality, in synthetic polymer assemblies is needed.

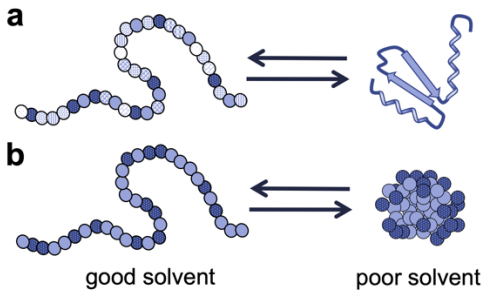

Figure 1.5. Assembled polymer morphology is directed by sequence.

a) A protein's folded structure is prescribed by its exact sequence of amino acids because these chemical moieties determine intramolecular interactions and interactions with the solvent. b) With as few as two chemical functionalities, protein-like synthetic polymer sequences mimic elements of protein folding in response to their solvent environment. Similar dramatic sequence-structure-function relationships observed in dilute systems provide inspiration for bulk materials.

Amphiphilic copolymers show great promise in mimicking protein folding, as discussed recently;[23] however, most studies of synthetic polymer collapse into single chain nanoparticles or globules have primarily focused on copolymers lacking the precise sequence control upon which proteins rely to achieve their structure. One class of sequence-defined polymers, polypeptoids, are particularly useful for studying sequence effects due to their ease of synthesis, wide range of side chain functionality, lack of backbone hydrogen bonding, and ability to form secondary structures. An example of sequence-controlled single chain collapse is the demonstration that polypeptoid sequences show sequence-dependent globule stability. Notably, these sequences have only two side chain functionalities, in contrast to the 20 amino

acids commonly found in proteins (**Figure 1.5b**).[9] Here, the placement of hydrophilic monomers in an otherwise hydrophobic chain controls the chain shape. In a good solvent, the chain extends, but in a poor solvent (water) the chain collapses with hydrophilic repeating units guiding which segments of the polymer chain are presented at the surface, thereby controlling surface patterning, globule density, and globule stability.

Multichain polypeptoid assemblies elegantly access other protein mimetic structures. A few examples include ribbons,[60] cyclic structures,[61, 62] helices,[63] multihelical bundles,[8] superhelices,[64] and nanosheets.[65] Of these, nanosheets are particularly interesting because they can be adapted to access a range of secondary structures,[66] such as loops,[67] and serve as scaffolds for further functionalization, as demonstrated with a biologically active streptavidin-binding peptide sequence.[68] Despite progress towards biomimicry, synthetic polymer folding fails to fully emulate the diversity and control over chain shape found in nature. However, given the extensive range of chemical diversity available to synthetic polymers, sequence-defined polymers have the potential to achieve functionalized architectures rivaling the complexity of proteins.

1.6 Characterizing polymer composition and conformation

Much of the practical challenge of characterization arises from the diversity of constituent chemistries. Tremendous progress has been made in the characterization of biological polymers, in large part due to the presence of limited backbones and monomers as well as central importance to medical fields. Approaches span from identifying DNA[69]/RNA[70] and protein sequences,[71] to quantifying supramolecular interactions within DNA using magnetic tweezers,[72] to characterizing structure via cryo-electron microscopy.[73] However, characterization in synthetic sequence-defined polymers has lagged. Much of the challenge

lies in the fact that synthetic sequence-defined materials have diverse chemical structures and assemble to form structures with less definition than the structures probed by cryo-EM. However, the field has seen progress. For example, the Kerr effect has been used to identify structures and their locations along polymer chains[74, 75] and 2D mass spectrometry techniques can consistently be leveraged to 'decode' or 'read' the sequences of non-natural polymers.[76-79] Despite this progress, significant process optimization per backbone and monomer chemistry is required, and computational methods must be used to identify ideal conditions and to interpret the data. Approaches to automate characterization processes for new chemistries will be essential for efficient implementation.

In addition to the chemical composition of synthetic sequence-defined polymers, chain conformation is also important to material function. Classical methods for characterizing chain shape, such as static light scattering (SLS),[80] small-angle X-ray scattering (SAXS),[81, 82] and small-angle neutron scattering (SANS),[82, 83] primarily probe average properties. For dilute polymers, properties accessible by scattering techniques include the globularity, shape, and radius of gyration (R_g). Small-angle scattering techniques, in particular, are advantageous in their ability to access time-resolved structures in near native conditions, but limited by low resolution (1-2 nm) and the need for additional parameters when using models to extract characteristics such as globule shape.[82] Other metrics of understanding chain conformation will provide additional awareness into how changes in sequence affect spatial arrangement.

Potential approaches for achieving detailed sequence-structure insights include borrowing methods from biophysics that allow probes to be installed in specific sites along a polymer chain that can then leverage, for example, nuclear magnetic resonance (NMR),[84, 85] fluorescence methods,[86] or electron paramagnetic resonance (EPR)[87, 88] to probe distributions

of distances in polymer chains. Of these methods, 2D NMR is unique in that it can determine the structure of small proteins without the use of labels, but extension to longer molecules is made challenging by loss of resolution and increasingly convoluted spectra. Here, automated peak assignment, perdeuteration, and selective labeling enable characterization of larger molecules.[85] Single molecule fluorescence resonance energy transfer (smFRET) and double electron-electron resonance (DEER), on the other hand, rely exclusively on interactions between label pairs to extract distances. The necessity of probes, however, may skew results in some instances and should be carefully considered. For example, smFRET and SAXS experiments routinely draw conflicting conclusions regarding protein response to chemical denaturation, indicating fluorophore interactions promote chain collapse.[89-91] In contrast, DEER utilizes smaller magnetic spin probes, requires fewer assumptions during data processing,[91, 92] and averages over more molecules, leading to more accurate distance distributions than smFRET. For all of these techniques, sequence-defined polymers offer a straightforward method to install probes anywhere in a sequence, opening doors to molecular-level information difficult to access through more traditional methods. Because of these advantages, DEER and other EPR-based methods are utilized extensively throughout this thesis.

1.7 EPR Methods for Characterizing Polymer Conformation

DEER is an electron paramagnetic resonance technique that provides unique access to conformational ensemble information by measuring the full distance distribution from a composite time domain signal that reports on distances between pairs of spin-labels.[88] It is especially advantageous for comparison with simulations because its probes are relatively small,[93] minimally perturb the conformational ensemble,[93] and can be directly simulated.[94]

DEER has traditionally been used to probe distances in structured biomacromolecules[88] or average distances in unstructured systems. In recent years, its ability to detail the full probability distribution over accessible distance ranges has garnered significant interest. The application of DEER to characterize disordered biological and synthetic polymeric systems through this distance distribution is emerging,[95-101] and methodological developments are continually improving the accurate resolution of the shape as well as the width of broad distributions.[102-106] Recent work on aqueous solutions of polyethylene oxide, a canonical disordered, synthetic polymer, demonstrates consistency between the broad distance distributions determined by DEER and simulation,[101] suggesting that DEER is well-positioned to characterize the conformational landscape of disordered macromolecules. Single-molecule Förster resonance energy transfer (FRET) also probes conformational distributions,[107] but DEER requires fewer assumptions[91, 92] and captures far more molecules, resulting in more accurate distance distributions. The accessible distance range for DEER is generally considered to be between 20 Å and 80 Å.[88, 108]

DEER spectroscopy probes conformational distributions, rather than just averaged quantities, because the time domain signal is a composite representing the product of individual dipole-dipole interactions of the molecular ensemble that can be decomposed into its constituents. **Figure 1.6a-c** provides an overview of the workflow by which DEER spectroscopy generates an end-to-end distance distribution. DEER involves the application of microwave pulses to doubly spin-labeled macromolecules in a static magnetic field according to the sequence illustrated in **Figure 1.6a**. The microwave pulses with the (probe) frequency ω_A excite a subset of electron spins (called "ω_A spins"), while the pulse with the (pump) frequency ω_B excites a separate subset (called "ω_B spins"). The ω_A sequence leads to a

refocused electron spin echo (ESE) at time $2(\tau_1 + \tau_2)$ with an amplitude that depends primarily on the bandwidths of the pulses and the relaxation times of the excited spins. With application of the pump pulse at ω_B that results in excitation of ω_B spins, any of the ω_A spins that are dipolar coupled to ω_B spins will experience changes in their local magnetic fields, communicated through their dipolar couplings. Because the relaxation mechanisms that govern the contributions of ω_A spins to the refocused ESE depend on the local magnetic fields at the ω_A spins, this will have the effect of attenuating the ESE relative to the ω_A sequence in the absence of the pump pulse at ω_B. As the ω_B pulse is moved in time between the second and third ω_A pulses, the ESE amplitude is modulated at the frequencies corresponding to the strengths of the dipolar couplings between ω_A and ω_B spins. In this way, a time domain signal is generated that consists of frequencies that can be related to dipole-dipole distances. In the time domain, the DEER signal consists of a form factor, $F(t)$, that contains the dipole-dipole interaction information of interest, and a background decay. The background decay is owed primarily to inter-molecular interactions and is removed using division of the overall signal by (typically) a stretched-exponential function.[103]

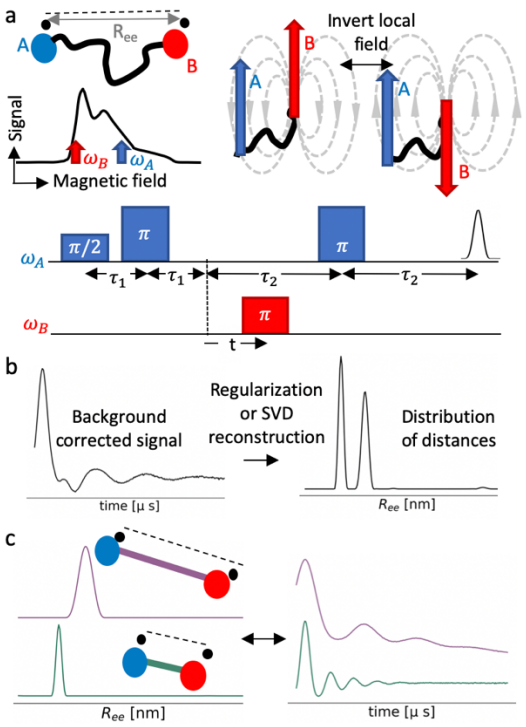

Figure 1.6. DEER enables resolution of distributions of distances.

(a) A pump pulse at frequency $\boldsymbol{\omega_B}$ *inverts the population of spins at that frequency (represented here by spin B), consequently inverting the local field of spin B on spins at the observer frequency,* $\boldsymbol{\omega_A}$*, (spin A, in this case). Interaction between the* $\boldsymbol{\omega_A}$ *and* $\boldsymbol{\omega_B}$ *spin populations changes the frequency of spin A, observed in the echo intensity measured at* $\boldsymbol{\omega_A}$ *as a function of the time corresponding to the pump pulse position. In the pulse schematic shown,* π *pulses fully invert spins while* $\pi/2$ *pulses tip the spins only 90°. The times between observer frequency pulses are denoted as* $\boldsymbol{\tau_1}$ *and* $\boldsymbol{\tau_2}$ *(b) Inversion of this time domain signal yields a distribution of distances in the form of a* $\boldsymbol{P(R_{ee})}$*. (c) The distance between the spin labels determines the frequency of the oscillations in the time domain data with shorter distances resulting in faster oscillations, so the observed time domain signal is a product of the frequencies corresponding to each distance in the ensemble.*

Most commonly, conversion of $F(t)$ to a distance distribution, $P(r)$, is achieved using Tikhonov regularization where the mathematical inversion of $F(t)$ occurs through a modified least-squares regression to find a solution for $P(r)$.[103] This method, however, can struggle to

find a unique solution, especially when $F(t)$ represents a broad and/or multi-modal $P(r)$. Method development for deriving reliable $P(r)$ from $F(t)$ is an active area of research, and several recent publications propose various solutions, e.g. neural network processing,[109] DeerLab,[103] and singular value decomposition.[105, 106] Of particular interest are the techniques using singular value decomposition (SVD) that have been developed by Srivastava and Freed (designated as SF-SVD). These methods involve factorization of the time domain signal into discrete distance regions, such that $P(r)$ is constructed from a linear combination of individual "singular valued" components.[105, 106] This approach has been shown to be robust for analyzing broad and multi-modal distributions.[110, 111] Each distance distribution is obtained by denoising the data using WavPDS,[112] then fitting the denoised data with the software SVDReconstruction.[105]

The lower limit of the DEER technique is approximately 20Å.[88, 108, 113] For this reason, DEER-derived distributions are presented with the region below 20Å in shaded. Supplementing DEER at shorter distances, is the analysis of Continuous Wave Electron Paramagnetic Resonance (cw-EPR, **Figure 1.7**) lineshapes where the dipolar interaction between two spin labels with distances between $8 - 25$ Å leads to broadening of the spectrum that can be related to the distances between them by spectral simulation. Unlike DEER, cw-EPR cannot fully resolve multi-featured distributions but is a complementary probe of the existence and approximate width and character of the distribution in the short-distance region.

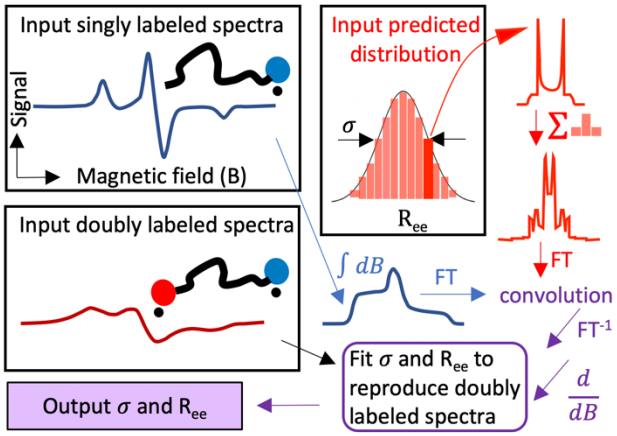

Figure 1.7. Cw-EPR probes distances less than 25Å.

Short distances inaccessible with DEER can be determined from dipolar broadening accessed with cw-EPR. Deconvolution analysis iteratively fits a Gaussian approximation of the distance distribution, $P(R_{ee})$, parameterized by average distance, $\langle R_{ee} \rangle$, and width, σ, to the EPR spectrum of a doubly labeled sample by convoluting the EPR spectrum of a singly labeled sample with the dipolar broadening from the distance distribution.

This technique extracts end-to-end distances from the effects of dipolar coupling between nearby unpaired electrons. When the extent of EPR line broadening by the dipole-dipole interactions exceeds the intrinsic cw-EPR linewidth of the spin label under the given experimental condition, its effect results in spectral broadening that can be related to dipolar distances through spectral simulation.[114] Line broadening is observed for doubly labeled polypeptoids where dipolar coupling originates from distances typically below 18-25 Å.[108, 115] Quantitative analyses leading to distance distributions are commonly performed using the ShortDistances spectral simulation software.[116, 117] As **Figure 1.7** illustrates, deconvolution analysis starts with generating Gaussian distance distributions parameterized by an average distance, $\langle R_{ee} \rangle$, and width, σ (full width at half maximum). The distributions are convoluted with EPR spectra of singly labeled samples (representing spectra unaffected by dipolar broadening) and compared to the experimental EPR spectra for doubly labeled samples. The

parameters, $\langle R_{ee} \rangle$ and σ, are iteratively varied until the parameters best reproduce the broadened EPR spectrum, and then are used to calculate the $P(R_{ee})$.

To demonstrate the ability of DEER and cw-EPR to capture polypeptoid conformations, we measured $P(R_{ee})$ for fully hydrophilic polypeptoids with increasing chain length. We synthesized the polypeptoid with alternating hydrophilic methoxyethyl and propanol groups, varying the number of hydrophilic monomers: $N = 9, 11, 15, 19$. We attached spin labels to both ends of all polypeptoids for DEER measurements and carried out 4-pulse DEER experiments and obtain the end-to-end distance distributions, $P(R_{ee})$, through SF-SVD. When compared to fully atomistic molecular dynamics simulations conducted by the Shell group at UCSB, both methods capture trends in conformation and demonstrate excluded-volume scaling.

Figure 1.8 shows the end-to-end distance distributions for lengths $N = 9, 11, 15, 19$. In the accessible region, simulations and DEER show excellent agreement, which offers strong cross-validation of both workflows. The locations of the peaks and the shapes of the long-distance tails of the distributions are especially well reproduced. Both methods consistently show not only the expected shift in the mean end-to-end distance, but also a broadening of the distribution with length, characteristic of disordered polymers.

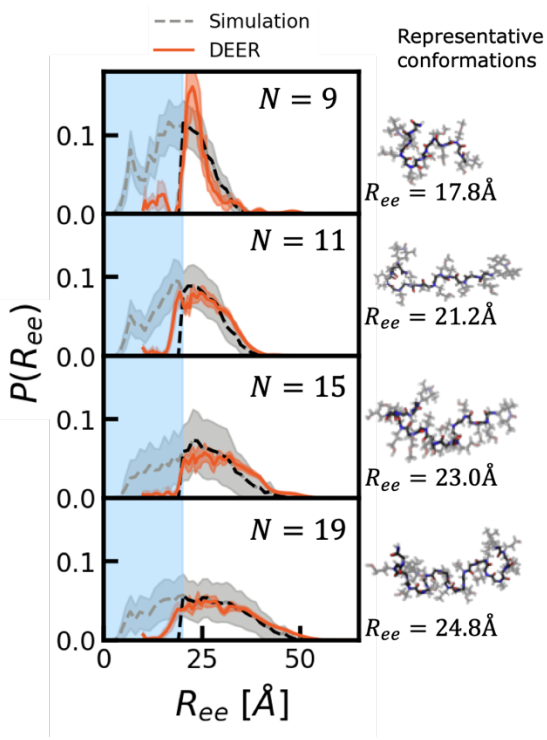

Figure 1.8. End-to-end distance distributions measured with DEER and computed from simulation are in excellent agreement.

The orange lines and shaded regions are the fitted DEER distributions and the grey lines are the simulated distributions (Shell group). All distributions are normalized such that the integral above 20Å *is 1. The light blue shaded box denotes the region below the accessible region for DEER. The snapshots to the right of the figures are representative conformations.*

We also validated cw-EPR as a probe the distance distributions whose end-to-end distance distribution largely lies below 20Å, and thus below the accessible region of DEER. **Figure 1.9** shows that the Gaussian approximation of the distance distribution of a 3-mer polypeptoid from the cw-EPR experiment agrees with the longer-distance peak in the simulated distribution. The simulated distribution also contains a shorter-distance peak at around 8Å that is also seen for longer polypeptoids, and here similarly indicates spin-label aggregation. While cw-EPR extends our insight into the experimental conformational distributions at distances

below the DEER-accessible regime, the narrow range of accessibility limits its utility in polymeric systems.

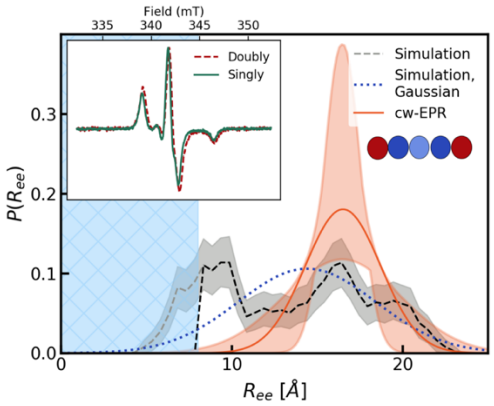

Figure 1.9. Continuous wave electron paramagnetic resonance allows access to the low-distance region and agrees with simulations.

For the $N = 3$ polypeptoid, the Gaussian approximation of the end-to-end distance distribution from cw-EPR (orange) agrees with the simulated distribution in the accessible region for cw-EPR (black dashed line gives the full distribution; the blue line is a Gaussian with the same mean and standard deviation as the simulated distribution in the cw-EPR accessible region). The shaded and hatched blue box denotes the region below the accessible region for cw-EPR. (Inset) The raw cw-EPR spectra for the doubly labeled 3mer (dashed red) and singly labeled 3mer (solid green) normalized by maximum peak height.

1.8 Mapping Hydration Water Diffusivity with ODNP

Overhauser dynamic nuclear polarization spectroscopy (ODNP) is unique among techniques for measuring water characteristics in that it can isolate water dynamics within about 1 nm of an experimental probe.[118, 119] The ability to control spin label position thus enables water property mapping throughout macromolecules and macromolecule assemblies. In particular, developments in the site directed spin labeling enables ODNP to characterize water diffusivity near specific regions of complex surfaces, such as proteins, under ambient conditions. Representative ODNP studies have, as a result, resolved spatial heterogeneities

in protein hydration, demonstrated that surface water behavior that impact protein and catalytic function, and mapped water dynamics throughout the cross-section of nanofibrils.[53, 120-124]

ODNP gains its site-sensitivity by combining EPR with NMR to measure water dynamics in the vicinity of precisely placed spin labels (**Figure 1.10**). Electrons spins have a vastly larger gyromagnetic ratio than ^{1}H nuclear spins. As a result, transfer of spin polarization from the electron spin of a spin label to surrounding water protons greatly enhances the NMR signal of water molecules in the vicinity of the spin label. Polarization transfer relies on close interaction between the electron and proton nuclear spin, so the relative speed of protons compared to the electron spin can be observed in the polarization transfer efficiency. Because polarization can only transfer within about 1 nm, observed signal amplifications isolate the water closest to the spin probe from bulk water.

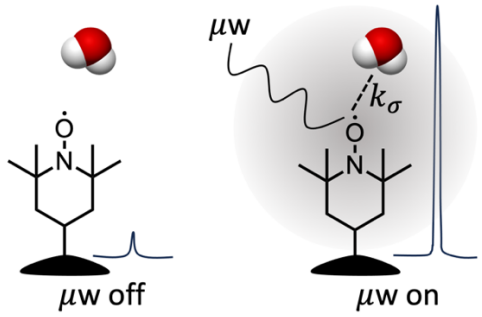

Figure 1.10. ODNP isolates water within 1 nm of a spin probe.

Microwave irradiation saturates the unpaired electron of the spin label. Polarization is then transferred to nearby waters, enhancing their NMR signal.

Practically, spin polarization is transferred by saturation of the EPR signal of the spin probe and the resulting NMR signal enhancement is tracked as a function of microwave power.[118, 119] NMR signal enhancements are used to determine the electron-nuclear spin cross-relaxation rate, k_σ. Translational motions of water in the 1-100 ps timescale impact

k_σ.[53] In order to access an overall local water diffusivity (D_{local}), proton spin-lattice relaxation times (T_1) for labeled and unlabeled samples ($T_{1,0,0}$) must be obtained by an inversion-recovery pulse sequence.[118] Then, D_{local} can be determined using previously established methods implemented through the Python-based software package called dnpLab.[118, 125] In brief, k_σ, is extracted from the NMR saturation and combined with $T_{1,0,0}$ to determine the self-relaxation rate (k_ρ). Dividing k_σ by the self-relaxation rate (k_ρ) yields the coupling factor (ξ). ξ is combined with the analytical form of the spectral density function using the force free hard sphere model to calculate the correlation time (τ_{corr}). Ultimately, D_{local} is calculated using Equation 1.1 where $\tau_{\text{corr,bulk}}$ is τ_{corr} for bulk water, $D_{\text{H}_2\text{O}}$ is the diffusivity of water, and D_{SL} is the diffusivity of the spin label.

$$D_{\text{local}} \equiv \frac{\tau_{\text{corr,bulk}}}{\tau_{\text{corr}}}(D_{\text{H}_2\text{O}} + D_{\text{SL}}) \qquad \text{(Equation. 1.1)}$$

1.9 Thesis Outline

This thesis provides a step towards protein-inspired functional soft materials. In particular, bio-inspired polypeptoids are used to control the sequence of monomers within each polymer chain, much like proteins. Sequence control enables incorporation of precisely placed functional groups with controlled polarity and charge that alter polymer structure and functionality (**Figure 1.11**). In addition, polypeptoids enable facile incorporation of nitroxide spin labels for EPR experiments. EPR techniques such as DEER and ODNP provide unique measures of polymer conformation and nearby water dynamics and are heavily utilized throughout this thesis.

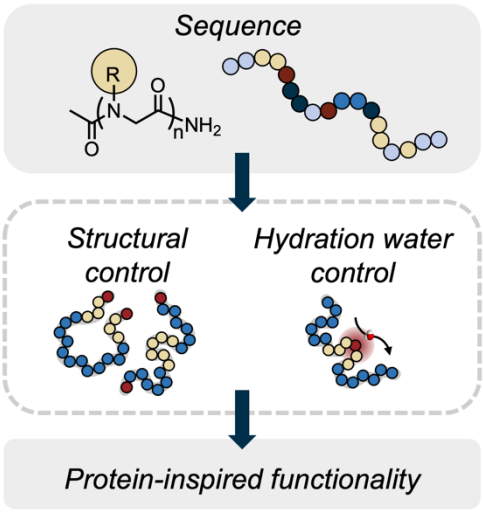

Figure 1.11. Dictating the sequence of monomers within a polymer chain controls polymer conformation and nearby water dynamics.

A fundamental understanding of how to guide polymer sequence effects could enable protein-like polymer-solute interactions in synthetic systems. Such control over polymer-solute interactions is of interest for catalysis, membrane science, and marine antifouling applications.

Chapter 2 demonstrates how polymer sequence can be used to tune polymer conformation in dilute solution. DEER spectroscopy is central to Chapter 2, but one limitation of this technique is that it is insensitive to distances below 2 nm. Chapter 3 pushes this lower limit with short polypeptoid chains to determine what information can be extracted when conformational landscapes largely extend below the lower cut-off of DEER.

While chemical patterning of polypeptoids influences their conformation and hydration in dilute solutions,[87, 126] more dramatic effects can often be achieved in assembled systems. Chapter 4 uses polymeric micelles to show that excluded volume tunes local water diffusivity in non-polar polymer assemblies. Chapter 5 builds on this work by drawing connections between local water diffusivity and protein-inspired organocatalysis in these assemblies.

Chapter 2 – Control Over Conformational Landscapes of Short Polypeptoids by Monomer Sequence Patterning

2.1 Abstract

The ability to program chain conformation and structure through control over the monomer sequence of synthetic polymers has broad implications for next-generation material design. While related problems of protein-folding and *de novo* design have generated accurate predictions of 3D folded chain structures, generalization to synthetic polymers remains intractable due to the requirement of large structural databases and the intrinsically disordered nature of polymeric building blocks. In this work, polypeptoids, a class of peptidomimetic synthetic polymers, are utilized to build a general workflow for the study of relationships between monomer sequence and dynamic 3D chain structure in solution. This work demonstrates how control over the monomer sequence can alter the conformational landscape

of synthetic polymers to deviate dramatically from classical chain statistics. Specifically, the distribution of end-to-end distances, as measured by double electron-electron resonance spectroscopy in dilute solvent, is systematically skewed towards shorter distances with an increasing number of hydrophobes and further refined by hydrophobe arrangement in amphiphilic polypeptoid chains.

All synthesis and much of the data analysis was performed by Shawn Mengel (Segalman group). Of key importance, he determined how to achieve nearly full spin labeling efficiency. Morgan Bates helped develop the polypeptoid purification strategy. Sally Jiao (Shell group) implemented the coarse-grained simulation model.

2.2 Introduction

Polymer properties relate to a hierarchy of chain structures that originates from the sequence of monomers and evolves due to combined effects of intramolecular forces and intermolecular interactions present in the given environment. The importance of sequence on chain conformation is best exemplified by biological macromolecules, such as proteins, where the precise arrangement of amino acids controls the formation of helical- and sheet-shaped segments, which guide the chain into a specific three-dimensional shape. The protein's folded shape then dictates its unique function. Replication of specificity in function through precise sequence control in synthetic polymer systems can similarly afford opportunities to design highly tunable materials for optoelectronic devices, catalysis, lithography, stimuli-responsive materials, and drug delivery.[127, 128] A large class of protein sequences give rise to partially or fully intrinsically disordered protein architectures that still exert important biological function, despite or because of this disorder, and whose ensemble conformational distribution is therefore critical to its property and function.

This grand challenge is closely related to the protein folding and *de novo* protein design problems, which rely heavily on AI-based algorithms for protein structure prediction. However, such methods lack fundamental insights into sequence/structure relationships and are ungeneralizable to synthetic backbone chemistries due to their reliance on statistical learning methods applied to large structural datasets of known protein structures in highly complex sequence space.[129-131] As a result, application of sequence control to synthetic polymers has been limited to block copolymers with relatively few blocks (typically ≤3) to restrict the design space to an experimentally manageable size, which has now been thoroughly explored. Increases in sequence complexity through post-functionalization of block copolymers with additional interaction types has demonstrated improved control over polymer structure and properties, motivating study of more precise sequence effects[132] and an expanded design space. Future advancements in synthetic polymer sequence design hence require new approaches to investigate this space and understand the interplay between chemical information and the resulting polymeric structure.[1, 133]

Polypeptoids bridge proteins and traditional synthetic polymers, providing an excellent platform for studying sequence-structure relationships. Solid-phase polypeptoid synthesis enables precise control over monomer sequence akin to polypeptides, while accessing a wider library of sidechain functionalities through the addition of primary amines rather than amino acids. *N*-substitution of the side chains simplifies intramolecular interactions by eliminating backbone chirality and hydrogen bonding.[48, 134] Previous studies leveraged these advantages to demonstrate sequence effects on solvent-induced single chain conformational changes and block copolymer self-assembly.[18, 135-139] It remains unclear, however, what design elements of the chain sequence stabilize polymer chain conformation. Inspired by the importance of

hydrophobic/hydrophilic patterning in determining protein structure,[140, 141] this study demonstrates relationships that describe how amphiphilic polymer sequences affects chain shape in dilute solution.

Intuitive rules of solvophobic/solvophilic interactions can inform limited design of sequence-defined polymers, but do not provide concrete sequence design principles. Further, even simple design motifs (e.g., binary) cannot be exhaustively searched through experiment, as their sequence possibilities grow exponentially with chain length. The lengths considered here exceed 69 trillion sequence possibilities. To navigate sequence space and resulting chain structures, low-cost computational models capable of high-throughput screening have become an important tool, particularly for protein-inspired macromolecular design.[133, 142] Validated atomistic simulations provide accurate and detailed conformational ensembles. However, their computational expense limits their utility in design workflows searching large sequence spaces, and they must be paired with coarser models or statistical learning methods. In particular, long conformational transition timescales prohibit the use of atomistic simulations for the 38-mer polypeptoids used in this study.[87] The sequences here are hence designed for compatibility with atomistic simulation methods and compared to a low-cost computational bead-spring model to validate the accuracy for future development of high-throughput sequence screening methods.

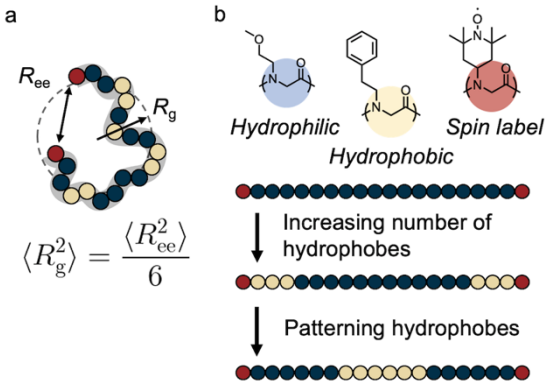

Figure 2.1. Amphiphilic patterns to control polypeptoid conformation.

(a) Flory theory connects the average end-to-end distance, $\langle R_{ee}^2 \rangle^{\frac{1}{2}}$, to the radius of gyration, $\langle R_g^2 \rangle^{\frac{1}{2}}$, but few methods exist for experimentally measuring $\langle R_{ee}^2 \rangle^{\frac{1}{2}}$. (b) Incorporation of nitroxide labels at both ends of each polypeptoid uniquely enables characterization of the distribution of R_{ee} from an ensemble of polypeptoids via double electron-electron resonance (DEER). Polypeptoids with varying hydrophobe content and arrangement along the polymer chain (patterning) modulate polymer conformation.

Achieving chain shape control requires both the ability to pattern intra- and inter-molecular interactions along the polymer backbone and a means for observing conformational changes. While folded proteins exhibit precise conformations with well-defined atomic locations and intrachain contacts, polymer chain conformations are disordered and transient. Ideal polymer chains are classically described by end-to-end distance, $\boldsymbol{R_{ee}}$, and radius of gyration, $\boldsymbol{R_g}$, vectors (**Figure 2.1a**), both of which exhibit Gaussian distributions.[143] These distributions can be extended to real polymer chains through use of renormalization group theory to account for excluded volume effects.[144] A combination of X-ray scattering and magnetic resonance techniques are widely used to characterize the structure of both folded and, more recently, intrinsically disordered proteins.[145, 146] In contrast, characterization of polymer chain conformations is typically limited to small angle neutron or X-ray scattering,

which yield an average radius of gyration, $\langle R_g^2 \rangle^{\frac{1}{2}}$. Few methods exist for experimentally determining $\langle R_{ee}^2 \rangle^{\frac{1}{2}}$.[87, 88, 101, 147, 148] Rather, the two are frequently linked by a proportionality constant predicted by Flory theory ($\langle R_g^2 \rangle = \frac{1}{6}\langle R_{ee}^2 \rangle$) with minor corrections for excluded volume effects.[144, 149-152] Introduction of protein-like sequence control will, by design, induce modest to complete deviation from Flory theory by programming chain shapes with narrower, non-Gaussian distributions of $\boldsymbol{R}_{ee}$ and $\boldsymbol{R}_g$. Theoretical predictions of such deviations already exist for block copolymers; however, validation of these theories is challenging by scattering alone and it remains unclear how to extrapolate to sequences of arbitrary complexity.[153-157]

Direct measurement of $\langle R_{ee}^2 \rangle^{\frac{1}{2}}$ is hence highly desirable to quantify sequence effects on polymer conformations. Critically, the average value $\langle R_{ee}^2 \rangle^{\frac{1}{2}}$ offers limited information. Instead, measurement of the entire end-to-end distance distribution, P(R_{ee}), is needed to obtain more detailed insight into the variation of conformations that reflect on the degree and nature of disorder. The P(R_{ee}) originating from the full conformational ensemble is uniquely accessible by double electron-electron resonance (DEER) spectroscopy, a pulsed electron paramagnetic resonance technique that can measure distances between 2-8 nm, depending on the experimental conditions. DEER is most widely used for studying structural biology of biomolecular complexes,[88] with comparatively few demonstrations in polymer physics.[101, 158] DEER measures a time domain decay of an ensemble of pairwise dipolar couplings between radical spin labels that is then transformed into an ensemble distribution of distances between the labels.[87, 88] In this case, these distances are the magnitude of the end-to-end vector, R_{ee}, without any angular information.

Here, control over the conformational ensembles of short, amphiphilic polypeptoids by precise monomer sequencing is demonstrated via DEER spectroscopy and coarse-grained molecular simulations. Sequence control and determination of the P(R_{ee}) uncovers how the number of hydrophobes and their arrangement affects the chains' conformational ensemble (**Figure 2.1b**). Nitroxide labels at both ends of all sequences enable detection of the intra-polymer distances between chain ends by DEER. Together, the synthetic, characterization, and simulation approaches described here provide foundations for a cohesive workflow capable of identifying polymer sequences with user-defined properties.

2.3 Experimental Methods

End-to-end distance distributions were measured for each polypeptoid sequence using DEER (**Figure 2.2**), as described previously.[87] Briefly, samples containing approximately 100 μM of polypeptoid were dissolved in 50/50 v/v D_2O/*d*-THF to ensure full solubility across a range of hydrophobic contents. Solutions were cryo-protected with 30% deuterated glycerol, by volume. Then, approximately 40 μL of solution was loaded into a 3 mm OD, 2 mm ID quartz tube. Samples were flash frozen in liquid nitrogen immediately prior to performing DEER. A Bruker/ColdEdge FlexLine Cryostat (Model ER 4118HV-CF100) maintained the sample temperature at 60 K. All DEER spectra were obtained using a Bruker QT-II resonator with a pulsed Q-band Bruker E580 Elexsys spectrometer with an Applied Systems Engineering, Model 177 Ka 300 W TWT amplifier. The following four pulse DEER sequence was applied to all samples: $\pi_{obs}/2$- τ_1-π_{obs}-(t-π_{pump})- (τ_2-t)-π_{obs}- τ_2-echo. Nutation experiments were used to determine optimal observer pulses (approximately 10 ns for 90 pulses and 20 ns for 180 pulses). The linear chirp π_{pump} frequency width was set at 80 MHz and its duration at 100 ns, while π_{obs} was 90 MHz above the center of the pump frequency range. τ_1 was set at

126 ns and τ_2 was set at 6 μs. All DEER experiments were signal averaged over at least 10 averages. Distance distributions were extracted from time-domain DEER signals using "model-free" Tikhonov regularization, as implemented by the LongDistances software.[159] Raw data, background-corrected data, and fits are plotted in the appendix.

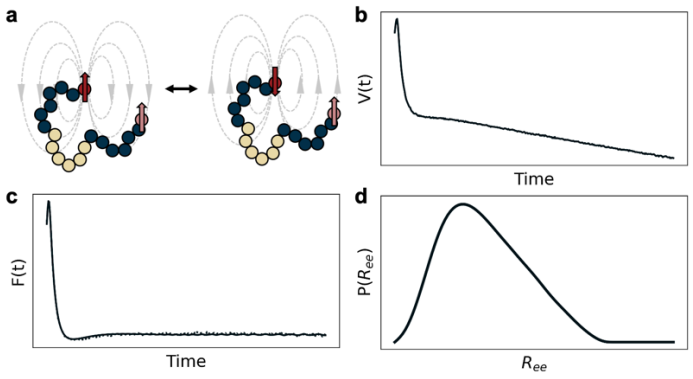

Figure 2.2. Measuring end-to-end distance distributions via DEER.

(a) A four-pulse sequence measures changes in the electron spin echo due to manipulation of the local microwave field between two spins on a macromolecule. (b) Raw DEER data (V(t)) contains the amplitude of the electron spin echo as a function of the pump pulse delay. (c) V(t) is background corrected to remove effects from intermolecular interaction and isolate intramolecular interactions. (d) Tikhonov regularization is typically used to extract a distribution of distances, in this case ($P(R_{ee})$), from the background corrected time-domain data (F(t)).

2.4 Results and Discussion

In this work, we present a combined computational and experimental platform for controlling polymer conformation via monomer sequence. Polypeptoids with precisely defined monomer sequences are synthesized with systematically changing hydrophobic compositions and patterning as a preliminary screening of the sequence design space. Experimental measurements of end-to-end distance distributions indicate the role of sequence parameters on chain conformations and offer new tools for quantifying chain shape. A

computationally inexpensive bead-spring model qualitatively reproduces the trends in the polymer R_{ee} obtained by DEER spectroscopy, suggesting the utility of coarse-grained molecular dynamics simulations in predicting material properties and motivating future development of high-throughput sequence screening algorithms.

This study considers conformations of polypeptoid sequences with increasing hydrophobicity and varying hydrophobe arrangement of two lengths (**Figure 2.3**). In particular, the effect of hydrophobic content is determined using sequences with increasing number of hydrophobic monomers at both ends ("0H" to "4H"). Because "3H" experimentally shows the maximum deviation from the fully hydrophilic sequence ("0H"), additional sequences of equivalent composition but varied placement of the hydrophobic monomers along the polymer backbone are considered to determine the extent to which sequence patterning can tune chain shape.

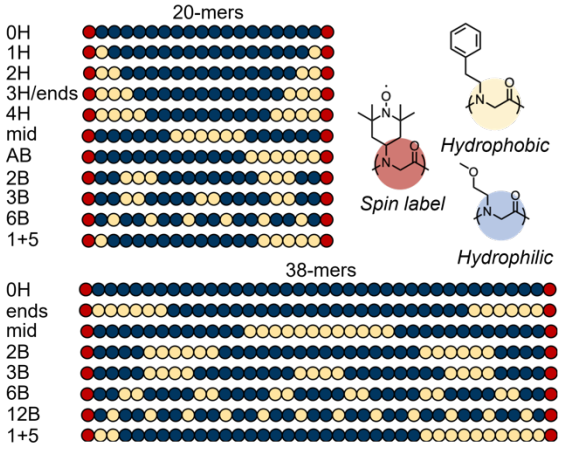

Figure 2.3. Complete list of polypeptoid sequences tested in this study.
Each sequence is comprised of precisely patterned hydrophilic (blue beads) and hydrophobic (yellow beads) monomers. TEMPO spin probes at the chain ends (red beads) enable measurement of $P(R_{ee})$ by DEER spectroscopy. These sequences probe the effects of increasing hydrophobic content and patterning.

The patterned set of sequences are designed using intuition from block copolymers and hydrophobic/hydrophilic patterning common to protein folding. Hydrophobic interactions between the aromatic side chains and the surrounding solvent are expected to drive the hydrophobes together to minimize solvent-hydrophobe contacts.[160] Sequences "ends," "AB," and "mid" therefore test the extremes of this effect. Sequences "2B" to "12B" vary the hydrophobic block size, which has previously been shown to control the density of hydrophobic/hydrophilic copolymer globules.[9, 161, 162]

While longer polypeptoids are expected to be more capable of achieving protein-like structural control, even state-of-the-art atomistic simulations possess chain length limitations of around 20 residues.[87] The development of coarse-grained methods capable of accurately simulating longer polymer sequences, therefore, will be necessary to reach the full potential of polypeptoids as biomimetic materials. Toward this goal, this work considers polypeptoids of two chain lengths, 20- and 38-mers. The longer 38-mers possess larger sequence effects and R_{ee} values centered in the 2–8 nm range, making them better suited for DEER spectroscopy. Although pushing the lower boundaries of the DEER technique, the 20-mers offer a bridge to connect experimental measurements with atomistic simulations for the future development of coarse-grained models. Together, these materials demonstrate that sequence can be used to tune chain shape and motivate the use of high throughput computational models to guide non-intuitive sequence discovery.

Distributions of R_{ee} ($P(R_{ee})$) obtained from DEER show that increasing the polypeptoid hydrophobicity at the chain ends drives them together, shifting the ensemble of chain conformations toward more compact structures (**Figure 2.4a**). This effect is most drastically seen in the root-mean-squared end-to-end distances of each sequence, with an increasing

number of hydrophobes resulting in shorter average R_{ee} values (**Figure 2.4b**). Despite equivalent contour lengths across all sequences, the more hydrophobic polypeptoids exhibit a clear trend toward more compact chain conformations, likely because increasing the hydrophobicity of the polymer changes the effective solvent quality experienced by the chains. As the chain becomes more hydrophobic, it is more poorly solvated, resulting in contraction of the chains toward the globule limit.

In addition to average chain composition, the arrangement of a fixed number of hydrophobes also influences the P(R_{ee}), as shown by the compositionally equivalent series of sequences (**Figure 2.5a**). Placing the hydrophobic residues at the center of the chain ("Mid" sequence, **Figure 2.5b**) extends the $\langle R_{ee}^2 \rangle^{\frac{1}{2}}$, while placement at the chain ends ("Ends") contracts $\langle R_{ee}^2 \rangle^{\frac{1}{2}}$ in comparison to the more evenly distributed "6B" sequence. This indicates that chain contraction due to solvent interaction is influenced by engineering of monomer sequence in the polypeptoids to achieve specific chain conformations, rather than averaged mixing effects. This result is consistent with previously observed sequence-dependent variations in polypeptoid hydration water diffusivity.[126] The $\langle R_{ee}^2 \rangle^{\frac{1}{2}}$ values of all the patterned sequences are smaller than that of the hydrophilic chain ("0H"), suggesting that some chain contraction still occurs, potentially due to global effects of decreased effective solvent quality with increasing peptoid hydrophobicity. However, placing the hydrophobic residues in the center or ends of the chain restricts globular collapse to those portions of the chain, while the rest fluctuates in a more extended state.

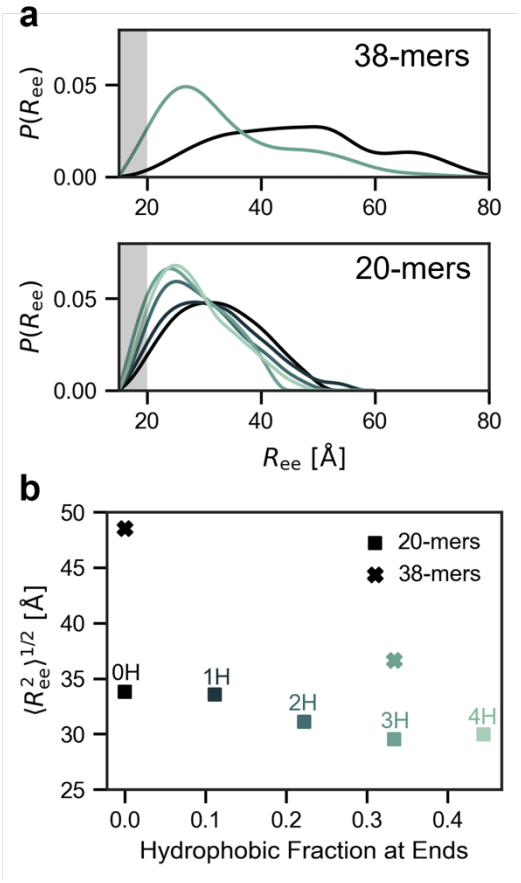

Figure 2.4. Increasing the number of hydrophobes on both ends leads to more compact conformations.

(a) P(R_{ee}) narrow and shift to shorter distances with increasing hydrophobicity for both 20-mer and 38-mer sequences. (b) The rotationally averaged end-to-end distance, $\langle R_{ee}^2 \rangle^{\frac{1}{2}}$, central to Flory theory reflects the trend of chain collapse with increased hydrophobic content.

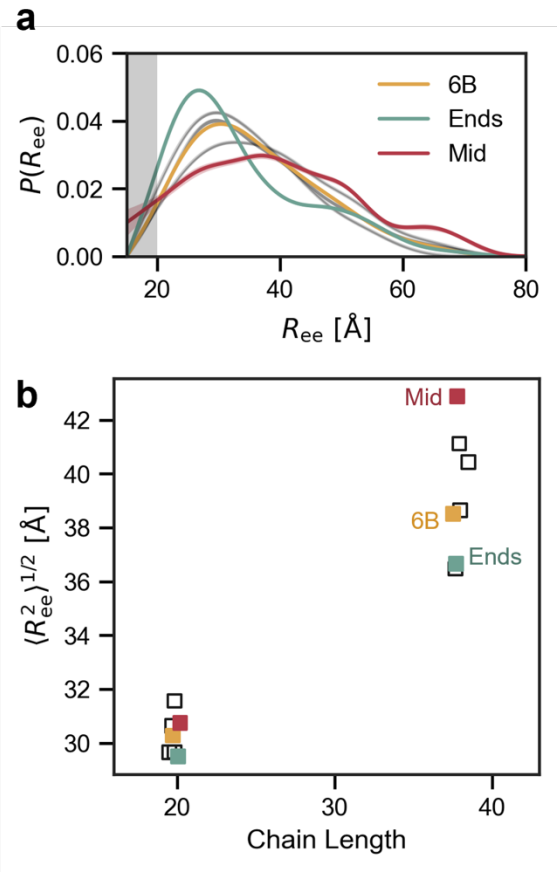

Figure 2.5. Patterning a set number of hydrophobes fine-tunes polymer conformation.

(a) The longest polymers considered in this study (38-mer) best exemplify sequence-dependent conformational changes. For ease of viewing, several sequences are highlighted. These sequences show that placing the hydrophobes on both ends ("Ends") leads to more compact conformations than more evenly distributed hydrophobes ("6B"). Placing all hydrophobes at the middle of the sequence ("Mid") leads to relatively extended conformations compared to the other patterns considered. (b) Trends in $\langle R_{ee}^2 \rangle^{\frac{1}{2}}$ *remain consistent for both chain lengths, suggesting that monomer sequence provides a handle to tune polymer conformation.*

Sequence-dependent variations in R_{ee} are generally consistent between the two chain lengths. In both lengths, the "mid" sequences possess greater $\langle R_{ee}^2 \rangle^{\frac{1}{2}}$ than the "ends" sequences, with the blocky "6B" in between. However, differences in P(R_{ee}) between the

sequences are more pronounced among the 38-mer polypeptoids compared to the 20-mers. This is likely due to the reduced conformational freedom of the shorter chains, which reduces the range of possible R_{ee} values, as well as limitations in the measurable length scale of the DEER technique. Based on the typical $\langle R_{ee}^2 \rangle^{\frac{1}{2}}$ values measured by DEER (approximately 3 nm), roughly 15% of the P(R_{ee}) distribution for the 20-mer sequences should lie outside of the range accessible to DEER, reducing the technique's ability to resolve differences in $\langle R_{ee}^2 \rangle^{\frac{1}{2}}$. Nonetheless, the general agreement of the shorter sequences with the 38-mers suggests that they can still provide basic information relating sequence to chain shape for future development of coarse-grained simulation models.

While atomistic simulations provide high resolution, they are prohibitively expensive for screening large design spaces for new, non-intuitive sequence designs. Bead-spring models by contrast are computationally inexpensive, even for long chains or multi-chain systems, but lack chemical information, making them difficult to relate to real materials. Coarse-grained models offer a compromise between cost and atomistic resolution, yet it is not currently understood what level of resolution is required to accurately model monomer sequence effects. To better understand this trade-off, a bead-spring model capturing the main interaction forces (hydrophobic attractions) is used to simulate the 20-mer and 38-mer sequences.

Simulations from the bead-spring model reflect trends in $\langle R_{ee}^2 \rangle^{\frac{1}{2}}$ due to changes in chain length, hydrophobic fraction, and sequence patterning effects. As seen in **Figure 2.6**, there exists a general positive correlation between the experimentally measured $\langle R_{ee}^2 \rangle^{\frac{1}{2}}$ and those calculated from the simulation. The 38-mers all possess larger average values than the 20-mers. The "0H" to "4H" series (represented as diamond symbols) and the 38-mer patterned

sequences (circle symbols) are also correlated. However, experiments show small differences in $\langle R_{ee}^2 \rangle^{\frac{1}{2}}$ among 20-mer patterned sequences that are not predicted by simulation. The 2 nm lower cut-off intrinsic to the DEER technique likely accounts for some of the deviation between the model and experiment for the shorter patterned polypeptoids, while extending sequences to 38 monomers largely overcomes this limitation. From the computational side, variations in chain stiffness not captured in the model may also contribute to differences in $\langle R_{ee}^2 \rangle^{\frac{1}{2}}$. While unable to resolve the most nuanced sequence effects, this simplistic model demonstrates a baseline of conformational resolution that predicts compositional and sequence effects well. We expect that incorporation of some atomistic detail through coarse-grained MD simulations will further improve predictions to enable nuanced, high throughput screening of vast sequence spaces.

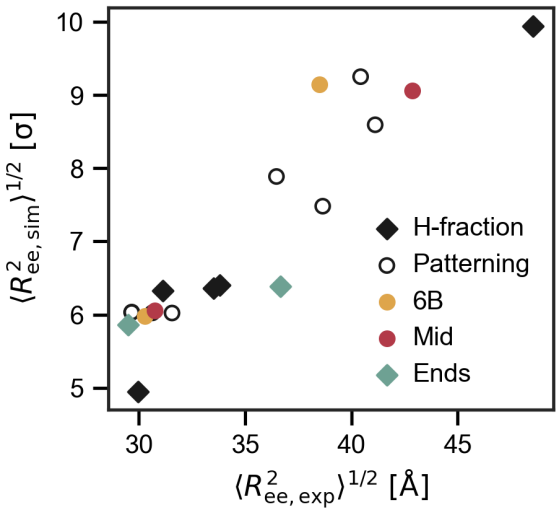

Figure 2.6. Low-cost bead model predicts conformational changes.

Trends in $\langle R_{ee}^2 \rangle^{\frac{1}{2}}$ generally agree with experiment, partially replicating experimental results for the patterned sequences. Because the model represents each monomer as a bead with size σ, computed $\langle R_{ee}^2 \rangle^{\frac{1}{2}}$ are plotted in units of σ, rather than Å.

Measurement of the entire P(R_{ee}) by DEER, rather than an average value, provides additional insights into the conformational ensembles as a function of polypeptoid sequence through analysis of higher order statistical moments of the distributions (e.g., width and skew). Due to the DEER cutoff, higher order moments are only calculated for the 38-mer polypeptoids, where an estimated 92% of P(R_{ee}) is estimated to reside within the measurable range.[163] Underlying variations in $\langle R_{ee}^2 \rangle^{\frac{1}{2}}$, the variance and skewness of the 38-mer P(R_{ee}) are sequence-dependent (**Figure 2.7**). Here, the variance (distribution width) and skewness (distribution symmetry) are calculated as the second central and third standardized moments, respectively, from P(R_{ee}) distributions above the 2 nm DEER cutoff. The variance is normalized by the first moment (distribution mean) squared to provide a size-independent metric of the distribution width. A positive skewness indicates a higher density of shorter conformations with a tail at higher R_{ee} values. Differences in variance between the sequences are small, consistent with the design that all of the polypeptoid ensembles studied here have significant disorder and hence access a similarly wide range of conformations. The measured variances are smaller than those computed from the excluded volume chain due to artificial reduction of the distribution width imposed by the DEER cutoff. The presence and sequence of hydrophobic moieties cause the ensemble to skew substantially from excluded volume behavior previously observed for hydrophilic polypeptoids.[87] In particular, the "ends" sequence shows the greatest skew because the hydrophobic chain ends give rise to a greater proportion of short R_{ee}. Shifting the position of the hydrophobic blocks closer to the center decreases skewness ("2B" and "mid"). Increasing the number of hydrophobic blocks also brings the skewness closer to that of ideal excluded volume polymers. As the number of hydrophobic blocks increases, the block size decreases, yielding a more homogenous

composition among each blob along the backbone. The decreasing skewness toward the excluded volume model limit hence provides experimental evidence of an upper limit on the level of sequence complexity that can tune chain shape of disordered polymers, where sequence features smaller than the polymer blob size become averaged out by neighboring residues. The blob size of disordered polypeptides has been estimated to be 5-7 residues, which reasonably matches the length scale over which the patterned polypeptoid sequences become more ideal.[164] This study observes conformational differences between polypeptoid sequences of equivalent overall composition, indicating an expected, but previously difficult to observe, sequence-induced deviation from Flory theory.[149]

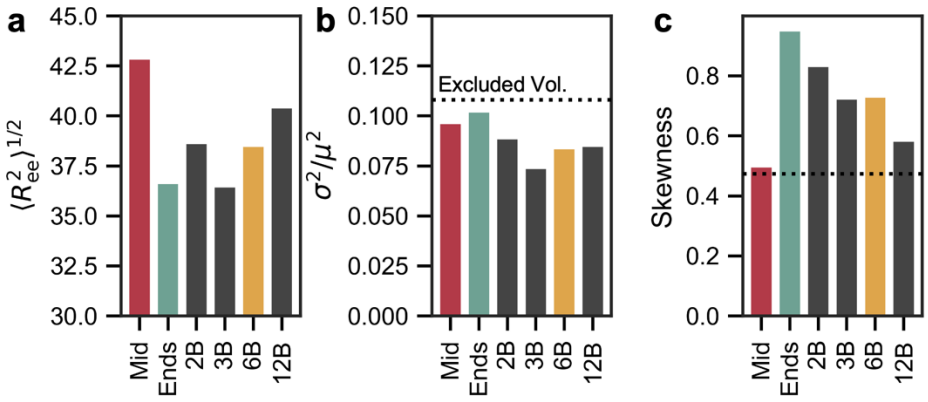

Figure 2.7. Measurement of full P(R_{ee}) enables analysis of higher order moments.

(a) Polymer conformations are often characterized in terms of average quantities such as R_g and $\langle R_{ee}^2 \rangle^{\frac{1}{2}}$. For the 38-mer sequences considered here, $\langle R_{ee}^2 \rangle^{\frac{1}{2}}$ is shortest when hydrophobes are placed at both ends ("Ends"), longest when all hydrophobes are placed at the center of the polymer chain ("Mid"), in between the two extremes when the hydrophobes are distributed into blocks ("2B" to "12B"). (b) Distribution variances show small sequence effects, and all are lower than that predicted for excluded volume chains, due in part to the lower limit of the DEER technique falling at 2nm. (c) Sequence more strongly impacts skewness with decreasing the block size of evenly distributed blocks ("2B" to "12B") generally leading to less positive skewness.

2.5 Conclusions

This study demonstrates that control over polypeptoid conformational ensembles can be achieved through precise monomer sequence patterning. Measurement of P(R_{ee}) and $\langle R_g^2 \rangle^{\frac{1}{2}}$ reveals that both chain composition and exact hydrophobe placement create deviations from classical polymer theory. Initial results agree qualitatively with theories and experimental observations of BAB triblock copolymers[155] and hydrophobic self-associating polymers[165] in selective solvents but demonstrate new capabilities for characterizing more complicated sequence-defined polymers. Past studies have been limited by indirect measures of chain conformation (e.g., viscometry) as well as poor sequence precision and high dispersity. The workflow presented here that relies on direct measurement of the full R_{ee} distribution by DEER overcomes these issues while generalizing to arbitrary sequence complexity. The low-cost computational model presented here produces trends that generally match experimental results, predicting both the compositional and patterning effects on chain conformations. This demonstrates the potential of high-throughput models to screen and predict sequence-encoded properties and motivates further development of coarse-grained models to improve resolution in nuanced sequence effects. Together, this work moves beyond analysis of averaged scaling laws to provide a powerful approach for elucidating sequence-structure relationships of synthetic polymers. Such capabilities are necessary for achieving chain shape design rivaling the structural complexity of proteins.

2.6 Acknowledgements

The polymer synthesis and characterization were supported by the National Science Foundation under Grant No. 2203179 (SDM, AJD, RAS) leveraging facilities and expertise from the BioPACIFIC Materials Innovation Platform of the National Science Foundation

under Award No. DMR-1933487 (MWB). Development of the DEER technique and computational model was supported by the Center for Materials for Water and Energy Systems (M-WET), an Energy Frontier Research Center funded by the U.S. Department of Energy, Office of Science, Basic Energy Sciences under Award #DE-SC0019272. SDM and SJ acknowledge support from the National Science Foundation Graduate Research Fellowship (DGE 2139319, DGE 1650114). AJD acknowledges support from the Department of Defense through the National Defense Science & Engineering Graduate (NDSEG) Fellowship Program. SH thanks the National Institute of General Medicine grant (R35GM126411) for support. We also thank Dr. Xiangxi (Zoey) Meng for optimizing the polypeptoid submonomer method for 2-CTC resin.

2.7 Appendix

Table 2.1. Polypeptoid sequence names, lengths, monomer order, and theoretical molecular weight.

Label	Chain Length	Sequence	Theoretical MW (g/mol)
0H	20	$TP_{18}T$	2555
1H	20	$THP_{16}HT$	2647
2H	20	$TH_2P_{14}H_2T$	2739
3H/Ends	20	$TH_3P_{12}H_3T$	2831
Mid	20	$TP_6H_6P_6T$	2831
4H	20	$TH_4P_{10}H_4T$	2923
AB	20	$TP_{12}H_6T$	2831
2B	20	$TP_2H_3P_8H_3P_2T$	2831
3B	20	$T(P_2H_2P_2)_3T$	2831
6B	20	$T(PHP)_6T$	2831
1+5	20	$THP_{12}H_5T$	2831
0H	38	$TP_{36}T$	4626
Mid	38	$TP_{12}H_{12}P_{12}T$	5180
Ends	38	$TH_6P_{24}H_6T$	5180
2B	38	$TP_4H_4P_{16}H_4P_4T$	5180
3B	38	$T(P_4H_4P_4)_3T$	5180
6B	38	$T(P_2H_2P_2)_6T$	5180
12B	38	$T(PHP)_{12}T$	5180
1+5	38	$TH_2P_{24}H_{10}T$	5180

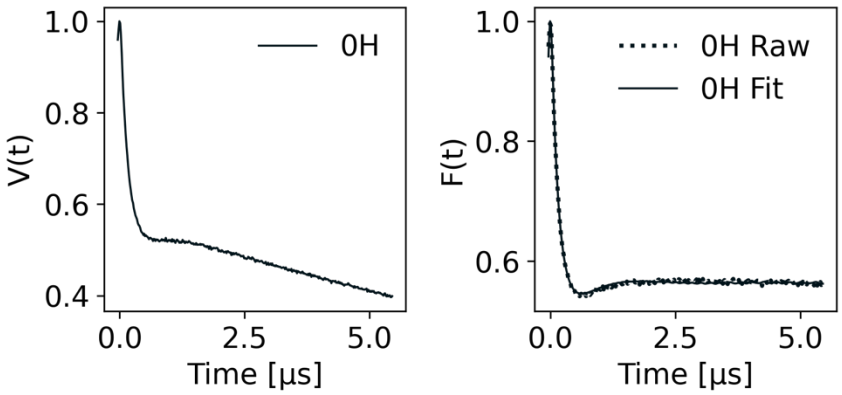

Figure 2.8. DEER time domain signal for 0H 20-mer.

Example of raw DEER time domain signal (left) and background corrected signal with fit (right) for the 0H 20-mer peptoid.

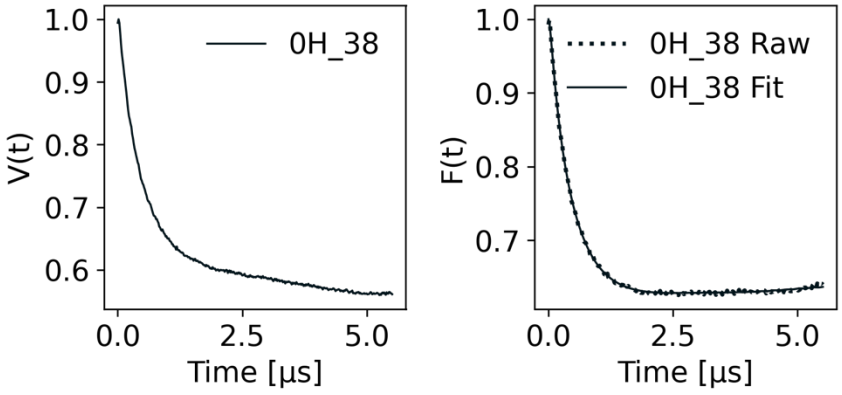

Figure 2.9. DEER time domain signal for 0H 38-mer.

Example of raw DEER time domain signal (left) and background corrected signal with fit (right) for the 0H 38-mer peptoid.

Chapter 3 – Measurement of Polymer End-to-end Distances Near the Lower DEER Cut-off

3.1 Abstract

Electron paramagnetic resonance enables determination of polymer conformations by measurement of intramolecular distances between two spin labels. In particular, double electron—electron resonance (DEER) spectroscopy is capable of measuring distributions of distances in the range of 20-80 Å. Many intramolecular distance distributions, however, extend below this sensitivity range. This work utilizes monodisperse polypeptoids with simulated conformational landscapes to determine how to interpret DEER measurements taken in this borderline distance regime. While DEER systematically overestimates label-label distances, trends obtained by DEER generally reflect those obtained by simulation, even when most distances reside below the DEER accessible range.

All synthesis was performed by Shawn Mengel (Segalman group). Daniela Rivera Mirabal (Shell group) performed all molecular dynamics simulations.

3.2 Introduction

Polymer chain conformation is central to the performance of both biological and synthetic polymers. Proteins, for example, fold into secondary structures capable of carrying out unique processes, such as phototropin light switches.[54] A protein's unique structure is encoded into the primary sequence of amino acid monomers that make up its polymer chain and changes in this sequence often lead to changes in protein folded structure. In the case of phototropin light switches, mutations have been engineered into the protein monomer sequence to fine-tune the switching range of the Jα-helix.[55, 56] While relationships connecting protein sequence to folded structure are well developed and often predictable for structured proteins,[57-59] intrinsically disordered regions remain challenging to predict and engineer.[166] Furthermore, generalization of protein-derived design rules to other polymer systems is challenging due to differences in backbone and side chain chemistry. As some level of disorder is intrinsic to most polymer systems, identifying relationships between polymer chemistry, chain conformation, and resulting functionality relies on developing generalizable methods for characterizing ensembles of polymer chain conformations.

Critically, recent advances in the synthesis of sequence-defined polymers have drastically increased the ability to produce materials with uniform chemical composition, thus simplifying identification of chemistry effects on polymer conformation and functionality.[133, 142] Sequence-defined polymers are characterized by precise control over the chemical identity of each monomer in the polymer chain, often resulting in nearly monodisperse materials.

Because function is enabled by structure, achieving protein-like control over polymer conformation could yield synthetic materials with functionalities akin to proteins while retaining the processing and scalability advantages of synthetic polymers.[127, 128] Identifying just what polymer to make for a given application, however, will rely on development of fundamental design rules connecting polymer chemical structure with conformation.

Central to determining how to control polymer conformation is the need for a method to measure conformational changes. Uniform protein structures are classically determined by X-ray diffraction,[167] but uncrystallized, non-uniform polymer conformations are not accessible by this method. At the other end of the spectrum, traditional measures of synthetic polymer conformation include metrics such as the radius of hydration, hydrodynamic ratio, and globularity obtained by small angle neutron scattering,[82, 83] small-angle X-ray scattering,[81, 82] and static light scattering.[80] These techniques often rely on model parameters and have a resolutions around 1-2 nm that are inadequate for capture minor conformation changes, especially for short polymer chains.[82] Furthermore, classical methods for defining chain conformation produce average quantities that may not capture nuanced shifts in conformational landscapes.

Label-based methods such as single molecule fluorescence resonance energy transfer (smFRET) and double electron-electron resonance (DEER) offer an intriguing route to provide detailed characterization of disordered systems.[88, 107] These techniques measure distances between experimental probes installed on polymer chains. Controlling spin probe locations enables measurement of well-defined intramolecular distances and, critically, the distribution of these distances. Of these methods, DEER is advantageous because it utilizes

smaller labels, probes far more molecules, and relies on fewer assumptions during data processing.[89-92]

DEER is a pulsed electron paramagnetic resonance (EPR) technique capable of measuring distributions of distances in the range of 20 and 80 Å between two spin labels on a macromolecule (**Figure 3.1**). [88, 108] While historically used to measure narrow distance distributions within structured biomacromolecules, application of DEER to less ordered systems such as intrinsically disordered proteins and polymers is being developed with great potential.[87, 95-106] One challenge of applying DEER to disordered polymer systems is that distance distributions may extend above or below the DEER accessible range.

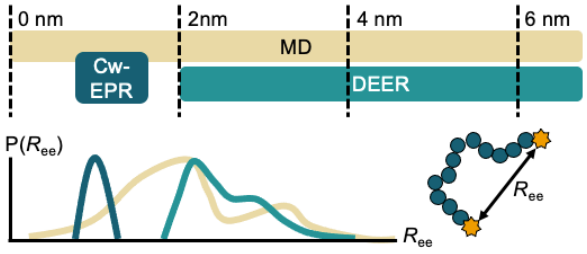

Figure 3.1. EPR techniques measure intramolecular distances.

Cw-EPR and DEER can measure distributions of distances between two spin labels, in this case end-to-end distances (R_{ee}). While cw-EPR utilizes dipolar broadening that does not occur past 2 nm, DEER uses microwave pulses to manipulate local magnetic fields and is sensitive to longer distances. Fully atomistic simulations offer the potential to draw connections between both experimental techniques to access the fully end-to-end distance distribution $P(R_{ee})$.

Another EPR technique, continuous wave EPR lineshape analysis, uses changes in lineshape broadening due to dipolar interactions to measure intramolecular distances in the range of 8-17 Å.[108, 115] Together, cw-EPR and DEER provide an extended range of sensitivity,

~8-80 Å. Consequently, combination of these techniques can accurately reflect intermediate distances.[108] Achieving the highest accuracy in this borderline region requires advanced data processing and EPR experience,[108] but EPR-based measurements are becoming increasingly accessible to users without extensive quantum mechanical backgrounds. Software packages such as DeerLab,[103] LongDistances,[159] and ShortDistances[116] have drastically lowered the barrier to entry and can implement advanced processing workflows. As access to EPR spectroscopy experiments increases, relatively simple workflows, sometimes with qualitative outcomes, may be more feasible for many users with recognition of the limitations of such analysis. Such simplified methods have already showed utility, such as revealing differences in polymer stiffness based on backbone identify.[95] Understanding what we can learn from simple analysis of EPR experiments for materials that span both cw-EPR and DEER regimes will help enable characterization of broad polymer conformational landscapes.

This study combines DEER and cw-EPR experiments with fully atomistic molecular dynamic simulations to determine the potential of combining EPR-based techniques to access full conformational landscapes of broad distributions. Polypeptoids with precisely controlled length, but disordered conformations, serve as a model platform to examine the applicability of DEER and cw-EPR lineshape analysis in measuring broad conformational landscapes that extend well outside the ideal range of each technique. In particular, hydrophilic polypeptoids with 6, 8, 14, and 20 monomers (H series, **Figure 3.2**) provide an example of a relatively simple homopolymer. A second amphiphilic series (A series) incorporates hydrophobic moieties on both ends of each sequence. All sequences contain a nitroxide spin label as the first and last monomer to enable measurement end-to-end distances. Comparison of P(R_{ee}) obtained by cw-EPR, DEER, and MD simulations reveal that DEER better represents trends

in conformation than cw-EPR and suggests its utility even in materials that largely extend below the lower limit of sensitivity.

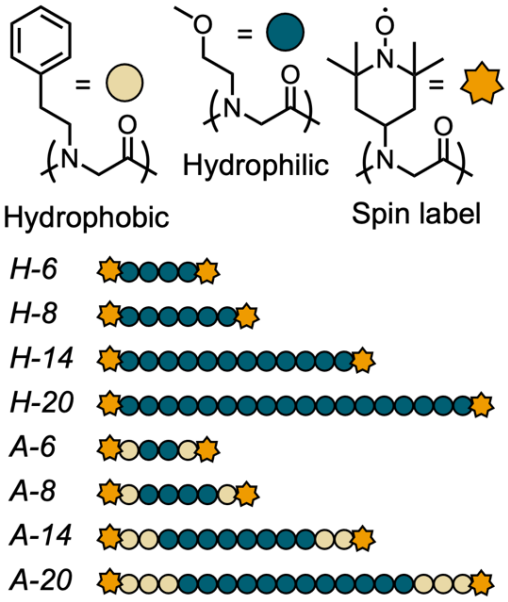

Figure 3.2. Polypeptoids span a range of backbone lengths with near monodispersity.

This study focuses on polypeptoids with precisely defined length and monomer order that span lengths from 6 to 20 monomers. The "H" series is fully hydrophilic while the "A" series is amphiphilic. All polypeptoids include nitroxide spin labels on both ends that are ideal for electron paramagnetic resonance spectroscopy experiments.

3.3 Methods

DEER measurement of P(R_{ee})

P(R_{ee}) are measured for polypeptoids dissolved in 37.5/37.5/30 v/v/v D_2O/*d*-THF/d-glycerol at a concentration of 140 µM. This concentration and solvent composition prevents polypeptoid aggregation and preserves polypeptoid conformation upon freezing. About 30 µL of solution is loaded into a 3 mm OD, 2 mm ID quartz tube and flash frozen in liquid nitrogen. Samples are maintained at 60 K using a Bruker/ColdEdge FlexLine Cryostat (Model

ER 4118HV-CF100). DEER experiments are conducted using a Bruker QT-II resonator with a pulsed Q-band Bruker E580 Elexsys spectrometer with an Applied Systems Engineering, Model 177 Ka 300 W TWT amplifier. A standard four pulse DEER sequence is applied to all samples: $\pi_{obs}/2$- τ_1-π_{obs}-(t-π_{pump})- (τ_2-t)-π_{obs}- τ_2-echo where π_{obs} is the observer pulse, π_{pump} is the pump pulse, t is the delay before the pump pulse, and τ_1 and τ_2 are pulse spacings. Optimal observer pulse lengths are determined by nutation experiments (~10 ns for 90 pulses and ~20 ns for 180 pulses). The linear chirp π_{pump} frequency width is set at 80 MHz and its duration at 100 ns, while π_{obs} is 90 MHz above the center of the pump frequency range. Artifacts from electron spin echo envelope modulation are suppressed by using a series of 8 τ_1 values in 16 ns increments. τ_2 was set at 6 μs for all experiments. All DEER experiments are signal averaged over at least 10 averages. "Model-free" Tikhonov regularization as executed by the LongDistances software[159] is used to produce P(R_{ee}) from the time-domain DEER data.

Cw-EPR measurement of P(R_{ee})

P(R_{ee}) are determined by comparing the frozen cw-EPR spectra of singly and doubly labeled polypeptoids using the ShortDistances software.[116] Polypeptoids are dissolved in 37.5/37.5/30 v/v/v D_2O/*d*-THF/d-glycerol at a concentration of 140 μM. A sample size of 30 μL is loaded into a 3 mm OD, 2 mm ID quartz tube and flash frozen in liquid nitrogen. Samples are maintained at 150 K using a nitrogen cryostat. Dispersive EPR spectra are obtain using a Bruker EMXplus X-band EPR spectrometer equipped with a Bruker ER4119DM resonator. All spectra are obtained using a fixed frequency of 9.8 GHz at 20dB, a modulation frequency of 140.0 kHz, and a modulation amplitude of 1.0 G. All cw-EPR spectra are plotted in **Figure 3.3**.

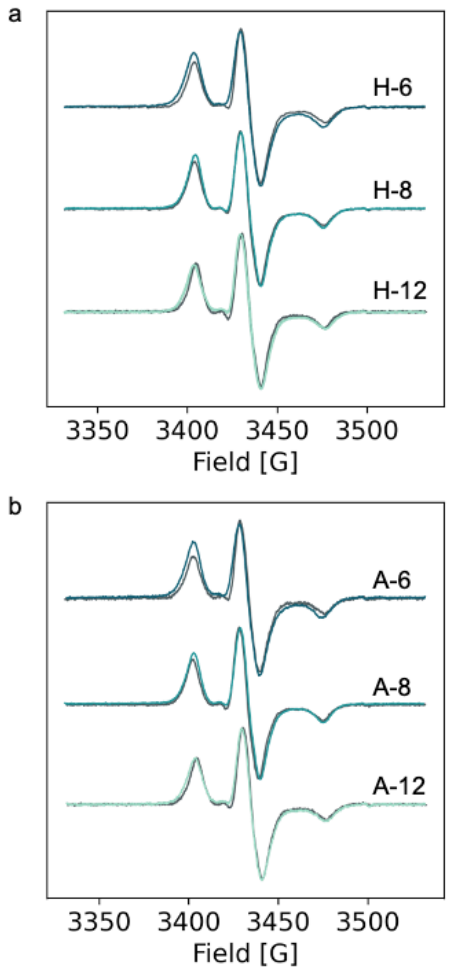

Figure 3.3. Dipolar interactions broaden cw-EPR spectra.

Low temperature cw-EPR spectra of doubly labeled polypeptoids (colored traces) are broadened compared to singly labeled polypeptoids (black traces) in both the (a) hydrophilic and (b) amphiphilic series. Because broadening due to dipolar interactions is stronger for shorter distances and unobservable for distances above 17 Å, this effect is most pronounced for conformational landscapes which primarily reside below 17 Å. Consequently, polypeptoids composed of the smallest number of monomers, in this case the H-6 and A-6 samples, show significant broadening compared to their singly labeled analogs. The longer samples considered (H-8, H-14, A-8, and A-14) produce less broadening because more of their $P(R_{ee})$ extends above the observable dipolar broadening limit.

3.4 Results and Discussion

To determine the efficacy of EPR methods for characterizing broad end-to-end distance distributions of short polymer chains, P(R_{ee}) are measured for hydrophilic polypeptoids ranging from 6 monomers in length to 20 monomers in length via DEER, cw-EPR, and MD simulations (**Figure 3.4a**). MD simulations can access the entire P(R_{ee}), whereas DEER is sensitive to distance above 20 Å and cw-EPR lineshapes broaden in response to distances below this lower DEER cut-off. Because of these experimental limitations, simulated P(R_{ee}) most accurately represent the entire P(R_{ee}) of these samples. For all chain lengths considered, DEER overestimates the presence of long R_{ee} while cw-EPR overemphasizes the presence of short R_{ee}. This result is expected because both techniques are only sensitive to one side of 20 Å while the true distributions span either side of 20 Å.[108] Increasing the polymer chain length from 6 monomers to 20 monomers shifts more of the P(R_{ee}) above this cut-off, so DEER more accurately portrays longer polymers. Cw-EPR, on the other hand, only reveals slight shifts in P(R_{ee}) for the shortest polymer lengths considered.

While at the surface neither cw-EPR or DEER can fully capture the conformational landscapes of polymers in their borderline region, more detailed analysis provides indicators of polymer chain shape. Measures of trends in conformational landscapes reflect those predicted by MD. For example, average end-to-end distances calculated from each distribution, $\langle R_{ee}^2 \rangle^{\frac{1}{2}}$, show excellent agreement in general trend between MD and DEER (**Figure 3.4a**). In particular, both MD and DEER show that $\langle R_{ee}^2 \rangle^{\frac{1}{2}}$ increases with chain length, as expected, but the exact distances are longer for DEER than for MD. Overestimation of the $\langle R_{ee}^2 \rangle^{\frac{1}{2}}$ by DEER makes sense, given that this technique is insensitive to the distances below

20 Å that contribute substantially to the true conformational landscape. $\langle R_{ee}^2 \rangle^{\frac{1}{2}}$ calculated from cw-EPR, however, show only slight changes with chain length, suggesting that DEER is better able to capture changes in broad distributions.

Conformational landscape changes also drive observables not reflected in the P(R_{ee}).[108] Specifically, P(R_{ee}) are calculated from oscillations in the time-domain spectra, but the modulation depth of this signal depends on the fraction of the P(R_{ee}) that falls within the DEER sensitive regime. **Figure 3.4b** plots background corrected time-domain data as well as the modulation depths of these spectra as a function of the portion of the MD P(R_{ee}) that falls below the DEER cut-off. Samples H-8, H-14, and H-20 follow the expectation that modulation depth decreases as the fraction of inaccessible spin-spin distances (R_{ee} below 20 Å) increases. The shortest polypeptoid considered, H-6, has a deeper modulation depth than H-8 despite simulation predicting that more of the distribution will be inaccessible. This inconsistency could be due to experimental factors such as imperfections in spin labeling or be a result of this relationship breaking down when the vast majority of expected distances fall below the DEER cut-off. As a result, modulation depth can be a useful indicator of the relative proportions of the P(R_{ee}) accessible to DEER but should be used in concert with simulation or other measures of conformation.

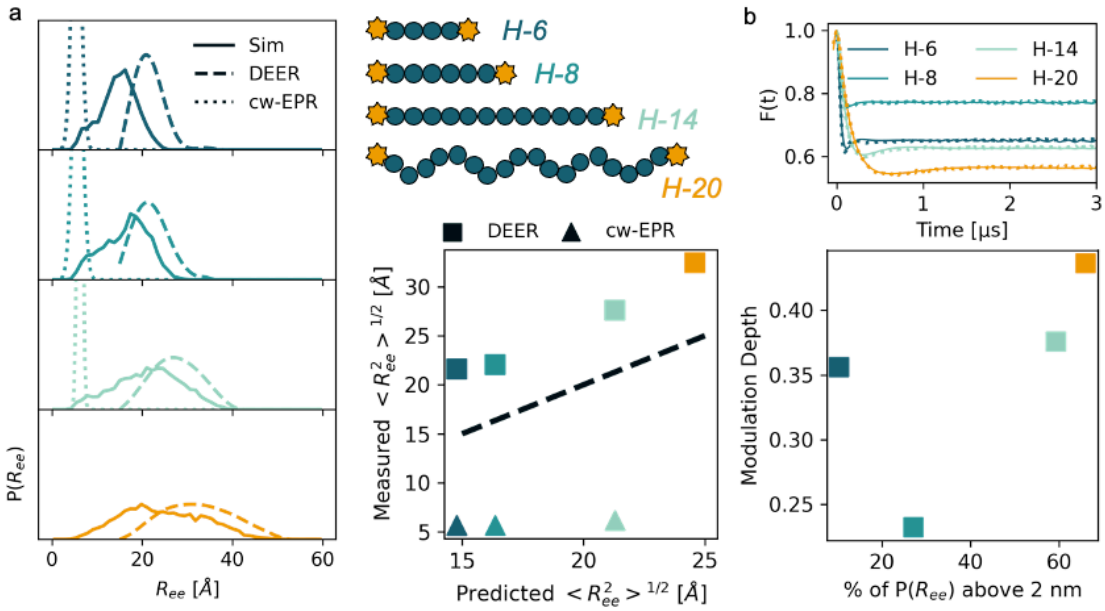

Figure 3.4. Multi-method characterization of polypeptoids that span the lower DEER cutoff.

(a) The $P(R_{ee})$ of fully hydrophilic polypeptoid are characterized by MD simulation, DEER, and cw-EPR for four chain lengths. While MD simulations capture the entire $P(R_{ee})$, neither experimental technique is sensitive to the full ensemble. DEER, however, better captures the increases in the average R_{ee} due to chain contour length predicted by simulation. (b) The modulation depths of time-domain DEER signals are sensitive to the number of spins being probed. As a result, for similar sample environments with consistent labeling efficiency, signal modulation depths will be larger when more of the population is above the lower cut-off of DEER. Samples H-8, H-14, and H-20 follow this trend, but the shortest chain length considered, H-6, does not. This suggests that modulation depth should be not relied upon when the vast majority of expected distances fall outside the DEER-resolvable range. For clarity, time-domain signals are truncated from 6 µs to 3 µs.

Fully hydrophilic polypeptoids follow classical excluded volume scaling,[87] but interest is increasing in co-polymers that deviate from classical scaling relationships, especially polymers with some level of sequence control.[142] These polymers have the potential to

achieve protein-like functionality, but their development is limited by a lack of understanding of how to control polymer conformation. To evaluate the potential of DEER to contribute to studies of short, multifunctional polypeptoids, we examined a series of amphiphilic polypeptoids (**Figure 3.5**). These polypeptoid sequences increase in length and contain hydrophobes divided evenly between both ends. As in the case of fully hydrophilic polypeptoids, the DEER P(R_{ee}) shows better agreement with the simulated P(R_{ee}) than cw-EPR and this agreement improves as the distribution shifts to longer distances. Also similar to the simpler polymers, trends in $\langle R_{ee}^2 \rangle^{\frac{1}{2}}$ extracted from DEER agree with those from simulation. While differences in modulation depth match the expected trend, these differences are minor. Clearer differences in $\langle R_{ee}^2 \rangle^{\frac{1}{2}}$ than in modulation depth suggest that $\langle R_{ee}^2 \rangle^{\frac{1}{2}}$ may the more useful measure of conformation.

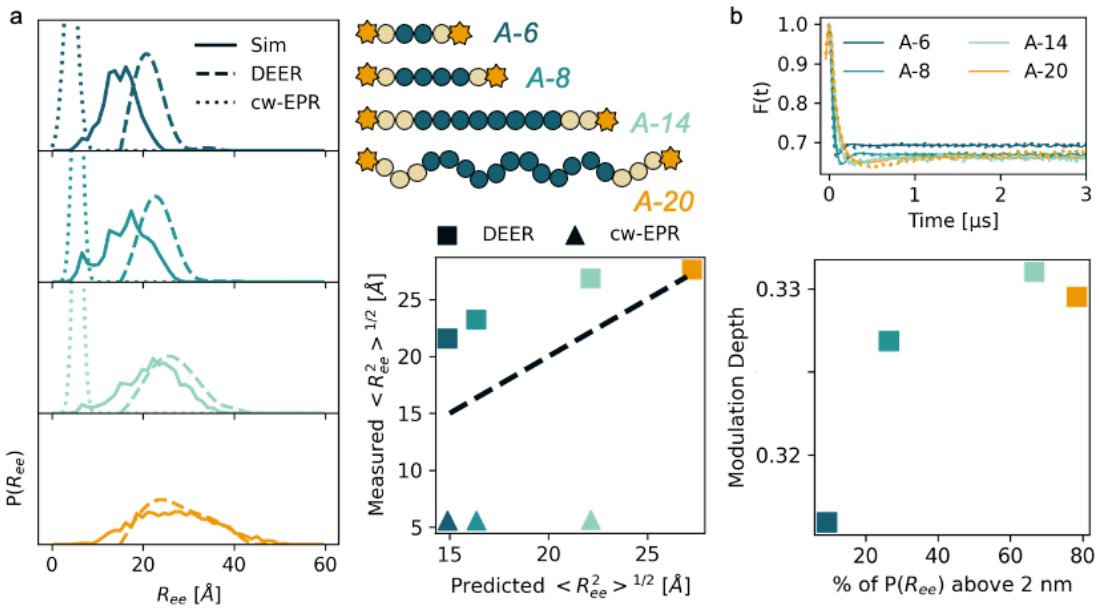

Figure 3. 5. Application of combined characterization approach to amphiphilic polypeptoids.

(a) The P(R_{ee}) of amphiphilic polypeptoid of increasing length are characterized by MD simulation, DEER, and cw-EPR. Average R_{ee} extracted from DEER increases with chain length, as expected based on MD simulations, but distances determined by cw-EPR vary little. These results suggest that cw-EPR is of limited utility for systems in which a large portion of the P(R_{ee}) extends above 1 nm. (b) Modulation depths show less variation for the amphiphilic series than for the fully hydrophilic series despite covering similar distribution ranges. These results suggest that interpretation of modulation depth as an indicator of the distribution portion below 2 nm is non-trivial. Overall, trends in average R_{ee} extracted from DEER are the most reflective experimental indicator examined here of trends in simulated distributions. For clarity, time-domain signals are truncated from 6 µs to 3 µs.

3.5 Conclusions

This work combines DEER and cw-EPR with MD simulations to characterize end-to-end distance distributions of monodisperse polypeptoid samples spanning a range of chain lengths and hydrophobic contents. While DEER and cw-EPR together span the entire range of

possible end-to-end distances, trends in DEER better align with those observed by simulation. This suggests that qualitative trends in intramolecular distances extracted from DEER can be useful indicators of polymer conformation, even when the distance distribution falls primarily below the lower limit of DEER.

3.6 Acknowledgements

Development of the DEER technique was supported by the Center for Materials for Water and Energy Systems (M-WET), an Energy Frontier Research Center funded by the U.S. Department of Energy, Office of Science, Basic Energy Sciences under Award #DE-SC0019272. Polymer synthesis and characterization was supported by the National Science Foundation under Grant No. 2203179 (AJD, SDM, RAS) leveraging facilities from the BioPACIFIC Materials Innovation Platform of the National Science Foundation under Award No. DMR-1933487. Computational work was supported by the BioPACIFIC Materials Innovation Platform of the National Science Foundation under Award No. DMR-1933487 (DRM, MSS). Use was made of computational facilities purchased with funds from the National Science Foundation (CNS-1725797) and administered by the Center for Scientific Computing (CSC). The CSC is supported by the California NanoSystems Institute and the Materials Research Science and Engineering Center (MRSEC; NSF DMR 2308708) at UC Santa Barbara. AJD acknowledges support from the Department of Defense through the National Defense Science & Engineering Graduate (NDSEG) Fellowship Program. DRM and SDM acknowledge support from the National Science Foundation Graduate Research Fellowship (DGE 1720256, DGE 2139319).

Chapter 4 – Design of Soft Materials with Rationally Tuned Water Diffusivity

4.1 Abstract

Water structure and dynamics can be key modulators of adsorption, separations, and reactions at soft material interfaces, but systematically tuning water environments in an aqueous, accessible, and functionalizable material platform has been elusive. This work leverages variations in excluded volume to control, and measure, water diffusivity as a function of position within polymeric micelles using Overhauser dynamic nuclear polarization spectroscopy. Specifically, a versatile materials platform consisting of sequence-defined polypeptoids simultaneously offers a route to control functional group position and a unique opportunity to generate a water diffusivity gradient extending away from the polymer micelle core. These results demonstrate an avenue to rationally design not only the chemical and structural property of polymer surfaces, but also design and tune the local water dynamics that, in turn, can adjust the local activity for solutes.

My Nguyen (Fredrickson group) performed all molecular dynamics simulations. This chapter was reproduced in part with permission from:

DeStefano, A. J.; Nguyen, M.; Fredrickson, G. H.; Han, S.; Segalman, R. A. Design of Soft Materials with Rationally Tuned Water Diffusivity. *ACS Central Science*, 2023, 9 (5), 1019-1024. DOI: 10.1021/acscentsci.3c00208. Copyright 2023 American Chemical Society.

4.2. Introduction

Equilibrium dynamics of hydration water mediate surface-solute interactions critical to sensing, catalysis, drug delivery, and advanced separations. Underlying water dynamics is the strong correlation between water diffusivity and local water structure, as well as solvation thermodynamic properties. Development of next generation functional materials for use in aqueous environments, therefore, necessitates the ability to design and tune surface water structure, dynamics, and thermodynamics.[53, 126, 168, 169] While some progress has been made in using surface chemistry and geometry to tune surface water properties,[169-173] the engineering of versatile surfaces capable of producing multiple water environments, i.e. with different water volume fraction, diffusivity and/or structure, that are readily accessible to solutes has not been achieved to date. This study demonstrates that water diffusivities can be made to vary as a function of radial distance in the fully hydrated corona of polymeric micelles, suggesting that incorporating functionalities at specific points within polymeric chains may enable us to access a range of user-defined water properties. The ability to access multiple water conditions within one material system will enable precise engineering of specialized and even multifunctional waterborne materials.

Bioinspired materials, much like enzymes, can offer a route to produce local environments capable of facilitating interactions or reactions that require an environment that is distinct from

bulk water. As one example, the amino acid L-proline catalyzes reactions that form carbon-carbon bonds via aldol condensation,[174] but the L-proline-catalyzed aldol condensation reaction is inactive in bulk water. Only when proline is incorporated on the surface of hydrophobic pockets formed by collapsed single-chain polymers, can such reactions proceed in water.[175] Critically, changing the chemistry of the hydrophobic monomers that line the folded hydrophobic pockets in which the reaction is carried out has been shown to tune the catalytic activity of L-proline while also decreasing the local water diffusivity.[123, 175] Water structuring has been proposed to stabilize transition states in aldol condensation reactions, but studies of how the water environment of catalyst surfaces tune broader classes of catalytic processes are only beginning.[175-179] Again, what is missing is a materials platform that allows access to multiple water environments, enabling a systematic investigation of water properties on catalytic processes. In this study, we focus on spatially and systematically tuning the local water density and diffusivity within the same soft material system.

Current theories suggest that the presence of a surface impacts water diffusivity by altering the governing hydrogen bond exchange mechanism in two ways.[180, 181] Bond exchange slows near interfaces due to (1) the steric hinderance of interacting with the surface and (2) the strength of hydrogen bonds between water and the surface.[180] This suggests that functional group position and chemistry on a surface or interface (or in this case within a polymer assembly) can tune local water diffusivity. Discussions on the extent or size of the hydration shell and the degree to which water slows within it remain active.[182] Differences in surface geometries, chemical compositions, and the sparsity of direct characterization techniques of hydration water make it highly challenging to generate a unified understanding of spatial variation of water properties with respect to materials or molecular surfaces. It is generally

agreed that water within the first few hydration layers (< 1nm) diffuses slower than bulk water, but few experiments offer the spatial resolution required to measure how far perturbations extend from a given surface.[183] The determination and tuning of an experimental profile of water dynamic relative to a hydrated surface has been, therefore, elusive.

Here, polypeptoids serve as a class of model polymers in which the sequence of monomers and, therefore, functional group or experimental probe position can be controlled.[134, 142] Indeed, Zhang and coworkers recently showed that the incorporation of charged groups at specific locations in polypeptoid amphiphiles allows for exquisite control over aqueous micelle size and structure.[136] Our incorporation of nitroxide radical-based spin probes enables the use of Overhauser dynamic nuclear polarization (ODNP), a magnetic resonance technique uniquely capable of mapping translational water dynamics with ~1 nm resolution. ODNP uses saturation of the electron paramagnetic resonance (EPR) signal of the spin probe to transfer polarization from the electron spin of the spin probe to nearby ^{1}H nuclear spins of water, and is described thoroughly elsewhere.[118, 119] Briefly, transferring electron spin polarization to nearby nuclei and subsequent exchange with bulk water enhances the ^{1}H nuclear magnetic resonance (NMR) signal of water. Because the polarization transfer requires direct and close interaction between the electron and ^{1}H nuclear spin and the transfer efficiency depends on the relative speed of movement of ^{1}H with respect to the electron spin, the signal amplification effect is exclusively due to the dynamics of water within about 1 nm of a spin probe. Critically, site directed spin labeling enables ODNP to characterize water diffusivity near specific regions of complex surfaces under ambient conditions. As a result, ODNP has, among other things, resolved spatial heterogeneities in protein hydration and demonstrated that changes in surface chemistry drive differences in surface water behavior

that impact protein and catalytic function.[53, 120-123] ODNP has also been successfully employed to map out the hydration profile across a peptide amphiphile (PA) fibril cross section, but the different water environments resolved in the study were focused on the water-depleted fibril interior, not the dynamic PA fibril surface accessible to interactions with various molecular constituents in solution.[124]

Measuring how water properties transition between the surface and bulk water, however, remains difficult even with ODNP because it is highly challenging to control the spatial location of the spin probe relative to the surface of interest. This study leverages the sequence-specificity of polypeptoids to control spin probe position within micelles formed from amphiphilic polypeptoid chains, and therefore enables measurements of water dynamics as a function of radial position within the micelle. Because the polypeptoid monomers are generally lacking in hydrogen bond donors (with the exception of a single monomer used to control micelle size), this model system allows hydrogen bond efficiency to be controlled by choice of side chain and, thereby, simplify polymer-water interactions to probe universal effects associated with polymer excluded volume.

4.3. Experimental Methods*Polypeptoid Synthesis*

Micelle-forming polypeptoids with precisely placed nitroxide spin labels are synthesized using established methods on an automated Prelude peptide synthesizer.[184] All polypeptoids are grown on a rink-amide resin (loading 0.62 mmol/g, 100 μmol scale). The resin is deprotected with 20% 4-methylpiperdine in dimethylformamide (DMF). Each monomer addition is then divided into two steps separated by DMF washes. All steps are performed at room temperature. The first a consists of bromoacetylation for 20 minutes with 1.2 M bromoacetic acid and 0.4 M N,N'-Dissopropylcarbodiimide in DMF. The second imparts

monomer functionality through incorporation of a primary amine (1 M in DMF) for 2 hours. A hydrophobic block of 5 monomers is first synthesized using N-decylamine (Ndc) followed by one monomer from N-methoxyethylamine (Nme) and one from β-Alanine tert-butyl ester (Nce). Finally, 18 monomers are incorporated from N-methyoxyethylamine. For each spin labeled sequence, a solution of 4-amino-2,2,6,6-tetramethylpiperidinyloxyl (Ntmp) is used rather than N-methoxyethylamine at the specified position with monomer one being the initial hydrophobic group. For example, sequence S-6 contains a spin label at position 6 rather than a methoxyethyl sidechain at the hydrophobic-hydrophilic interface. Upon completion of the polypeptoid sequence, the polypeptoids are acetylated for 30 minutes in 0.4 M pyridine and 0.4 M acetic anhydride. We note that formylation would likely be preferable to acetylation to prevent end group cleavage if it does not impact polypeptoid self-assembly.[184-186] β-Alanine tert-butyl ester is purchases as a hydrochloride and extracted from ethyl acetate and basic water. All other chemicals are used as received.

A cocktail of trifluoroacetic acid : water : triisopropylsilane (95 : 2.5 : 2.5, v/v/v) is used to cleave polypeptoids from the solid support. After immersion in the cocktail for 2 hours, the resin is filtered and washed with dichloromethane. The collected solution is dried under vacuum and lyophilized from acetonitrile and water (1 : 1, v/v). Because the cleavage process causes spin labels to disproportionate, polypeptoids are stirred in a 7 N ammonia in methanol : water (9 : 1, v/v) solution for 4-12 hours. The solutions is then removed by vacuum and the samples are lyophilized from acetonitrile and water (1 : 1, v/v). This method does not regenerate all radicals, but enables sufficient labeling for EPR and ODNP experiments.

To confirm the presence of the target compounds, polypeptoid samples are characterized with matrix-assisted laser desorption/ionization (MALDI) spectrometry and

high-pressure liquid chromatography (HPLC). MALDI is done on a Bruker Microflex LRF MALDI TOF mass spectrometer. Alpha-cyano matrix is prepared in tetrahydrofuran. Matrix-sample mixtures are spotted onto a polished steel MALDI target plate. Mass spectra are collected in positive reflectron mode. HPLC is done on a Waters Acquity H-class Ultra High Pressure Liquid Chromatography system. All samples are dissolved in acetonitrile and water (1 : 1, v/v) with 0.1% formic acid and separated using a 50-100% acetonitrile gradient. The detected wavelength is 214 nm.

Table 4. 1. Polypeptoid sequences and molecular weights.

Sample	Sequence	Calc (m/z)	Found (m/z)	Ion type
Unlabeled	$Nme_{18}NceNmeNdc_5$	3362.24	3363.6	$[M+H]^+$
C6	$Nme_{18}NceNtmpNdc_5$	3457.38	3482.6	$[M+Na]^+$
C8	$Nme_{17}NtmpNceNmeNdc_5$	3458.48	3481.1	$[M+Na]^+$
C10	$Nme_{15}NtmpNme_2NceNmeNdc_5$	3458.48	3481.2	$[M+Na]^+$
C12	$Nme_{13}NtmpNme_4NceNmeNdc_5$	3458.48	3482.3	$[M+Na]^+$
C18	$Nme_7NtmpNme_{10}NceNmeNdc_5$	3457.38	3482.0	$[M+Na]^+$
C24	$Nme_1NtmpNme_{16}NceNmeNdc_5$	3457.38	3481.2	$[M+Na]^+$
C26	$NtmpNme_{18}NceNmeNdc_5$	3572.53	3597.3	$[M+Na]^+$

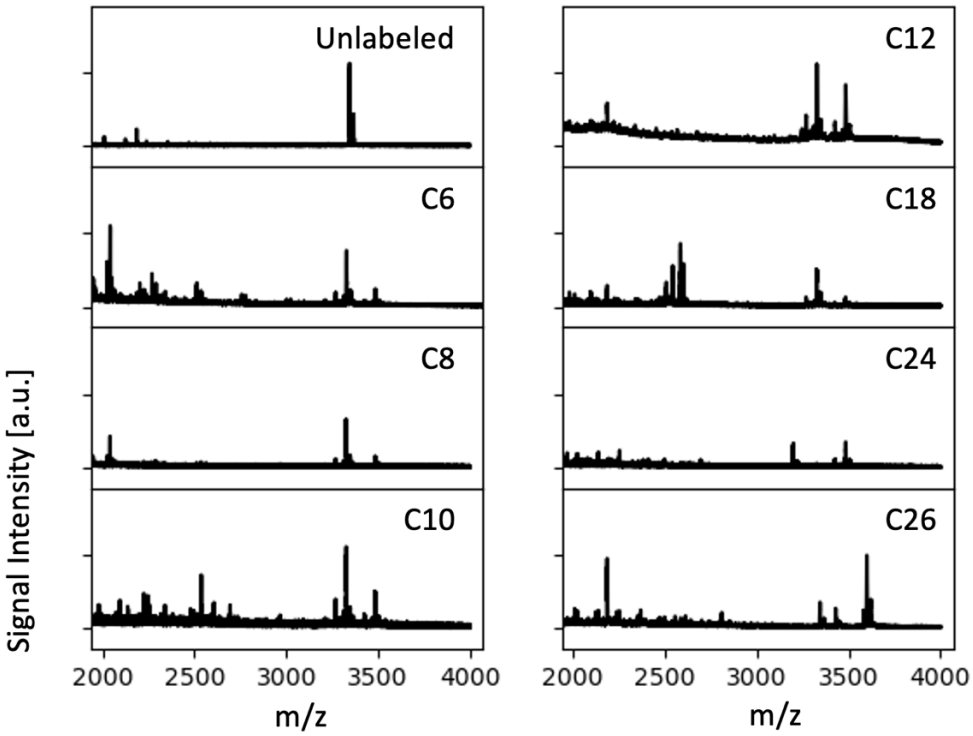

Figure 4.1. MALDI confirms presence of desired product.

The dominant biproduct for most samples is a sequence in which the terminal monomer is removed during the peptoid cleavage process.

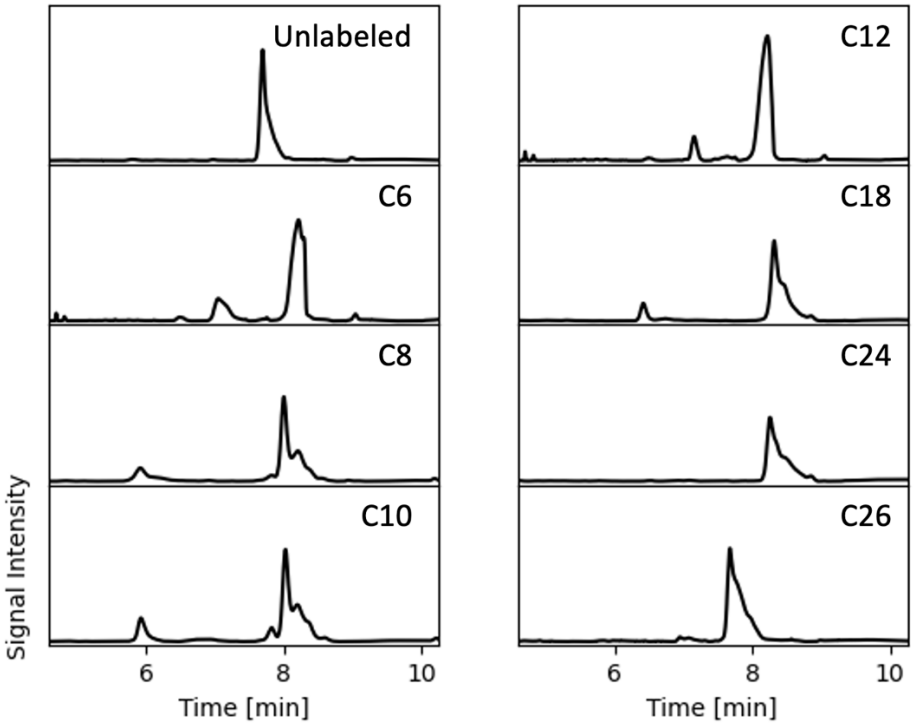

Figure 4. 2. HPLC traces for labeled and unlabeled polypeptoids.

Micelle AssemblyMicelles are prepared by suspending 5 mg/mL of polypeptoid in filtered, ultrapure water following the method described by Sternhagen et al.[136] Fewer than one spin label chain, on average, is incorporated into each micelle to target a spin concentration of 100-200 μM. The pH is adjusted to 9 using sodium chloride.

Hydrodynamic radii (R_h) are measured with light scattering to confirm that spin label incorporation does not change micelle size. All measurements are conducted at 20 °C at a concentration of 5 mg/mL using a Brookhaven Instruments BI-200SM goniometer with a scattering angle of 90°. The system utilizes a 500 mW dye-pumped solid state laser that operates at 532 nm. The unlabeled sample yielded a R_h of 33 nm while the C6 sample had a R_h of 30 nm. The R_h measured here are larger than those reported by Sternhagen et al.[136] This

is likely due to differences in filtering protocols during sample preparation or the presence of small numbers of worm-like micelles (also reported by Sternhagen et al).

Electron Paramagnetic Resonance (EPR)

Spin label concentrations and spin label mobilities are measured via cw-EPR on micelle solutions prepared at a concentration of 5 mg/mL in water with spin concentrations of 100-200 μM. A quartz round capillary tube of 0.60 mm inner diameter and 0.84 mm outer diameter is loaded with 3.5 μL of solution and sealed at one end with beeswax and at the other with Critoseal. The dispersive electron paramagnetic resonance (EPR) spectrum is obtained with a fixed frequency (9.8 GHz) at 20 dB, while the magnetic field is swept with a modulation frequency of 140.0 kHz and a modulation amplitude of 0.70 G. Spin concentrations were obtained by double integration of the spectrum. Lineshape analysis is performed using the Multicomponent software[187] to obtain rotational correlation times (τ_c) for each sample. Cw-EPR spectra and fits are shown in **Figure 4.3**.

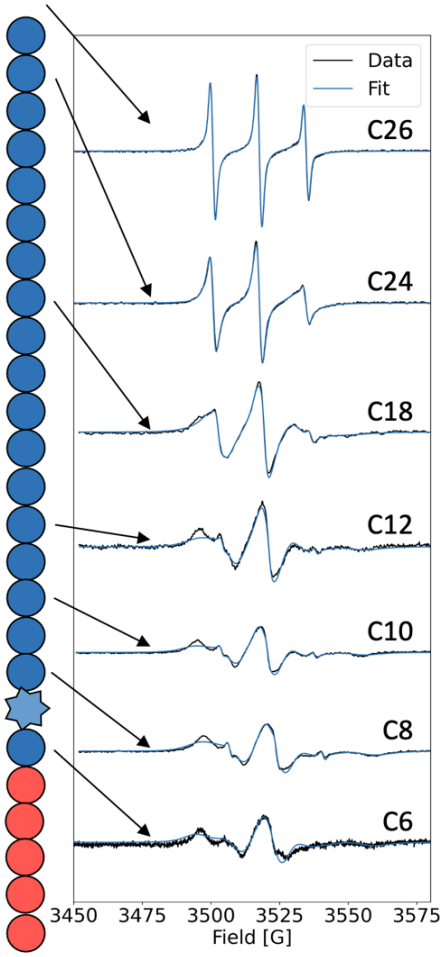

Figure 4.3. Continuous-wave electron paramagnetic resonance.

Raw cw-EPR spectra (black) and their corresponding fits (blue) for seven spin label positions within the polymeric micelles.

Overhauser Dynamic Nuclear Polarization (ODNP)

ODNP experiments utilize samples as prepared for EPR. Sample temperature is maintained at 18°C in the ER4123D dielectric resonator using a stream of compressed air. ODNP is performed at 0.35 T at a 14.8 MHz ^{1}H Larmor frequency and at 9.8 GHz electron spin Larmor frequency using a home-built U-shaped NMR coil. An inversion-recovery pulse sequence acquires proton spin-lattice relaxation times (T_1). Following the protocol described by Franck et al.,[119] $T_{1,0,0}$ is determined to be 2.37 for unlabeled micelles. Hydration parameters ($T_{1,0}$, $T_{1,0,0}$, k_σ, coupling factor (ξ), the translational correlation time of water interacting with the electron spin by dipolar cross-relaxation (τ_{corr}), and D_{local}) are calculated from ODNP experiments using previously established methods implemented through the Python-based software package called dnpLab.[125] In brief, the Overhauser effect causes an enhancement in NMR signal by saturation of the EPR signal by microwave irradiation. The electron-nuclear spin cross-relaxation rate, k_σ, is extracted from this saturation and combined with $T_{1,0,0}$ to determine the self-relaxation rate (k_ρ). Dividing k_σ by k_ρ yields ξ. ξ is combined with the analytical form of the spectral density function using the force free hard sphere model to calculate τ_{corr}. Finally, the local water diffusivity within 1 nm of the spin probe is calculated using equation 1 where $\tau_{\mathrm{corr,bulk}}$ is τ_{corr} for bulk water, $D_{\mathrm{H_2O}}$ is the diffusivity of water, and D_{SL} is the diffusivity of the spin label.

$$D_{\mathrm{local}} \equiv \frac{\tau_{\mathrm{corr,bulk}}}{\tau_{\mathrm{corr}}}(D_{\mathrm{H_2O}} + D_{\mathrm{SL}}) \qquad \text{(Eqn. 1)}$$

Hydration parameters ($T_{1,0}$, ξ, and D_{local}) are listed in **Table 4.2** for each sample. The environment of water can be estimated by τ_{corr} and ξ .

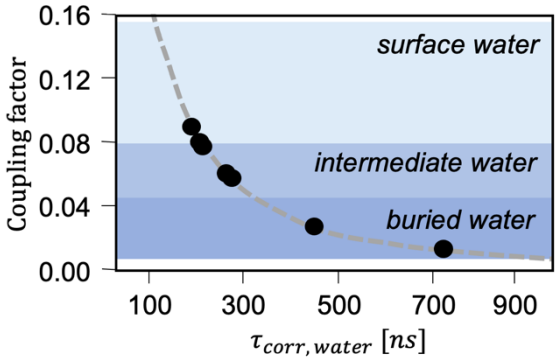

Figure 4.4. Micelle hydration parameters.

The buried, intermediate, or surface-like character of water is classified by the coupling factor (ξ) and the translational correlation time of water interacting with the electron spin by dipolar cross-relaxation (τ_{corr}). The dashed line represents the relationship between ξ and τ_{corr} as connected through the force-free hard sphere model at a field strength of 0.35 T.[119]

Table 4.2. Hydration parameters ($T_{1,0}$, ξ, and D_{local}) obtained via ODNP

Hydration parameters obtained via ODNP for micelle samples with varied spin probe position. Standard deviations are calculated based on three experimental trials.

Sample	$T_{1,0}$	ξ	D_{local} [10^{10} m^2/s]
C6	1.77 ± 0.01	0.014 ± 0.001	2.05 ± 0.09
C8	1.26 ± 0.01	0.028 ± 0.001	3.22 ± 0.06
C10	1.67 ± 0.09	0.056 ± 0.014	5.15 ± 0.91
C12	1.92 ± 0.06	0.053 ± 0.011	4.98 ± 0.75
C18	1.93 ± 0.13	0.083 ± 0.029	6.96 ± 1.98
C24	1.98 ± 0.08	0.081 ± 0.026	6.81 ± 1.71
C26	2.03 ± 0.03	0.93 ± 0.016	7.61 ± 1.08

4.4. Results and Discussion

In this study, the hydrophobic core of a polymeric micelle serves as a model surface surrounded by a water-rich corona. As shown in **Figure 4.5a**, spherical micelles are formed by amphiphilic polypeptoid chains containing hydrophobic and hydrophilic blocks, with the

hydrophobic block forming the dry core (pink in **Figure 4.5**) and the hydrophilic block spanning the hydrated corona (blue in **Figure 4.5**) of the micelle. The ether-like hydrophilic side chain is suitable for probing excluded volume effects because, despite containing one hydrogen bond acceptor, the side chain has shown very similar impacts on water behavior as those induced by nonpolar polypeptoids, suggesting inefficient hydrogen bonding.[126] The size of the micelle (in water at an adjusted pH of 9) can be further adjusted via the position of a single charged peptoid monomer within the sequence (light blue star in **Figure 4.5**) whose position is controlled by sequence specific polypeptoid synthesis.[136] In this work, the position of the charged peptoid monomer is held fixed to produce consistently sized micelles. To map water properties near the surface, we functionalize approximately one polypeptoid per micelle with a nitroxide spin label whose position is also precisely defined during synthesis (yellow star in **Figure 4.5b**). The position of the spin labeled monomer in terms of distance from the hydrophobic micelle core is determined by coarse-grained molecular dynamics (MD) simulations **(Figure 4.6**). The local water diffusivity near the specific spin probe within the micelle is measured via ODNP to determine how water properties vary with distance from the hydrophobic micelle core surface.

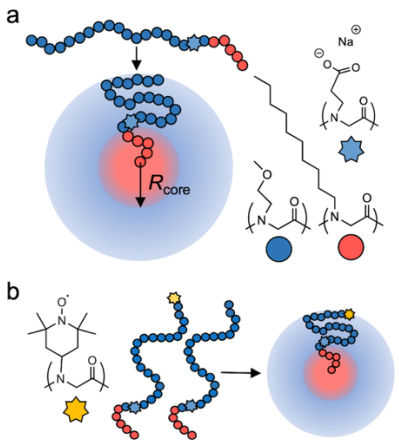

Figure 4.5. Sequence-defined polypeptoids enable spatial mapping of polymer and water properties.

(a) Polypeptoids containing a hydrophobic 5-mer block and a hydrophilic 20-mer block self-assemble into spherical micelles. (b) Approximately one polypeptoid with a paramagnetic spin label is incorporated into each micelle. Precisely controlling spin label position within the polypeptoid chain enables characterization of average segmental motion and local water dynamics throughout the micelle.

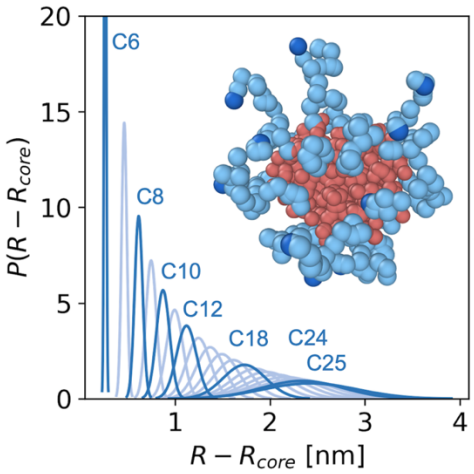

Figure 4.6. Distributions of monomer position relative to the micelle core ($R - R_{core}$) are determined by coarse-grained MD simulations.

Distributions are plotted for each hydrophilic peptoid monomer where C6 refers to the first hydrophilic monomer at the hydrophobic/hydrophilic transition and C25 represents the terminal hydrophilic monomer. The darker blue distributions represent distinct monomer positions within the polypeptoid chains at which local water dynamics are measured by ODNP. Because C26 utilizes a spin label attached to the hydrated chain end, C25 is used as an approximate position.

Combining knowledge of the position of the spin label within the micelle corona with sequence-controlled synthesis and ODNP experiments allow us to map out the water diffusivity gradient in the micelle corona. Specifically, local water diffusivities (D_{local}) are measured at seven distinct monomer positions. The measured local water diffusivities, D_{local}, normalized by the measured water diffusivity near the core, D_{core}, are plotted as a function of distance from the hydrophobic surface in **Figure 4.7**. The most dramatic retardation in water diffusivity occurs within about 1 nm of the hydrophobic micelle core surface. Beyond 1 nm, but still within the corona, water translational diffusivities are observed to reduce to about 1/3 of that of bulk water. **Figure 4.7** divides the corona into 3 regions (indicated in different shades of blue), based on ODNP hydration parameters from prior studies (**Figure 4.4**).[119] This

comparison suggests that water closest to the micelle core interacts strongly with the polymer chains, similar to buried water in polymers, proteins, and lipid vesicles. In contrast, water closest to the outside of the micelles shows surface-like water behavior, while water in between the two regimes exhibits intermediate dynamic characteristics. Previous studies also observed retarded water diffusivity near polymeric macromolecules and more extended soft surfaces,[53, 123, 126, 188] but spatially resolving water dynamics relied on the 3D structure of a protein scaffold and was never done as a function of distance from a surface within fully water accessible volumes.

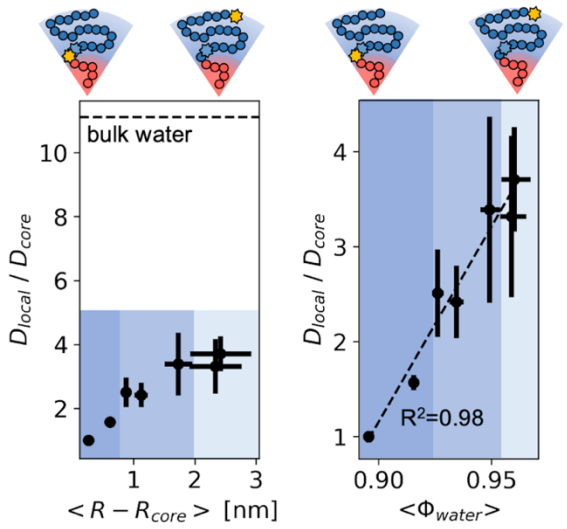

Figure 4.7. Water diffusivity is experimentally mapped throughout the micelle corona using seven distinct spin label positions.

D_{local} is slowest within about 1 nm of the hydrophobic surface and approaches a diffusivity about 1/3 of bulk water towards the outside of the corona. Water diffusivity correlates more closely with water volume fraction ($< \phi_{water} >$) within the corona than with distance from the surface. This suggests that excluded volume predicts water behavior near non-polar hydrophobic surfaces (hydrophobic micelle core here). The average distance from the core is calculated by coarse-grained MD simulations and the average water volume fraction is calculated by $< \phi_{water} > = 1 - \phi_{polymer}(< R >)$. The diffusivity of bulk water is obtained from ref 119. Dark blue shading represents water with buried character, while light blue shading denotes surface-like behavior.

Because both the micelle core and corona consist almost entirely of monomers that do not efficiently hydrogen bond, universal polymer brush physics are assumed to describe water behavior. **Figure 4.7** uses the volume fraction of water (ϕ_{water}) as a proxy for the local environment because ϕ_{water} will increase as ϕ_{polymer} decreases with distance from the micelle core. The radial distance from the center of the micelle core (R) relates to the polymer volume fraction (ϕ_{polymer}) at a given point within the corona of charge-neutral block copolymer micelles by Equation 4.1, [189-191]

$$\phi_{\text{polymer}}(R) \cong \left(\frac{\sqrt{s}}{a}\frac{R}{R_{\text{core}}}\right)^{-\frac{3\upsilon-1}{\upsilon}} \qquad \text{(Equation 4.1)}$$

For polypeptoid micelles bearing a single ionic group per chain, Sternhagen et al. found that the model shown in Eqn. 1 works well to describe corresponding neutron scattering data. Here we employ Eqn. 1 to relate distance from the hydrophobic micelle surface within the corona to water volume fraction, $\phi_{\text{water}}(R) = 1 - \phi_{\text{polymer}}(R)$. The specific parameters selected are R_{core}=1.8 nm (radius of the core) and s =3.1 nm^2 (interfacial area per polymer chain).[136] The Flory exponent, υ, is equal to 3/5 under good solvent conditions and the monomer size, a, is taken as 0.37 nm for polypeptoids in trans-amide conformations.[135]

When correlating the so obtained water volume fraction, ϕ_{water}, with the retardation of the ODNP-derived water diffusivity, $D_{\text{local}}/D_{\text{core}}$, we found a linear dependence as shown in **Figure 4.7**, validating our hypothesis that the excluded volume inside the hydrated micelle corona closely correlates with local water diffusivity. Our finding is consistent with previous observations that protein hydration water diffusivity correlates with excluded volume near hydrophilic sites.[53] This result suggests that enthalpic interactions between water and the polymer chains in polypeptoid micelles devoid of efficient hydrogen bond functionality is not the sole determinant of the water diffusivity gradient. Rather, steric effects play key roles in the inefficiently hydrogen bonding systems studied here. Consequently, changing the geometry of polymer assemblies and surfaces, such as by moving the charged monomer location in the corona of our material system to make larger micelles, will likely alter the range and location of accessible water environments. We expect that variation of polypeptoid chemistry to include specific interactions such as efficient hydrogen bonding or charged residues will impose further alterations in the water diffusivity landscape with respect to the micelle core surface. Nonetheless, our study demonstrates that proximity to a surface can be

employed to systematically and significantly tune water diffusivity, and so the water environment within water accessible locations in the micelle corona.

Because changes in water motion are often underpinned by variations in water structure,[183] confinement may cause differences in water structuring that most likely underpin water's reduced mobility near the hydrophobic surface. The structure of interfacial water balances packing forces with maximizing the number of hydrogen bonds, and has been proposed to form "dangling bonds" in which one bonding group orients towards the hydrophobic surface rather than interacting with nearby water molecules.[192] Because the polypeptoids used in this study do not hydrogen bond efficiently, the first hydration layer cannot form efficient hydrogen bonds with the surface and instead may reorient to form dangling bonds. Alternatively, water that do not efficiently bond to the polypeptoid surface may engage in stronger lateral interactions with neighboring water molecules, forming what has been introduced as a "wrap" water network in recent literature.[193] Differences in water orientation and packing influenced by interactions with nearby surfaces and chemical functionalities have been shown to consequently alter the water density and tetrahedrality that are descriptors of water structural property.[182, 183, 194] Indeed, molecular dynamics simulations predict increased water tetrahedrality with increasing hydrophobicity near single chain polypeptoids, i.e. small-scale hydrophobic sites below 1 nm, that has been shown to correlate with slowed local water diffusivity.[126] Furthermore, water with slowed local water diffusivity and increased tetrahedrality has also been shown to correlate with lower water entropy,[126, 183, 195-198] and hence can be exploited to tune solute-surface interaction.

Understanding how water diffusivity varies spatially necessitates knowledge of where each monomer, on average, is positioned. This study utilized coarse-grained molecular

dynamics simulations to estimate distance from the core, while EPR may provide an experimental tool to approximate relative spin label position. In addition to probing water properties with ODNP, spin labels enable polymer mobility mapping within assemblies by continuous wave EPR (cw-EPR).[199] Lineshape analysis of cw-EPR spectra can be used to extract the rotational correlation time (τ_c) of spin probes that correspond to the time that the probe loses correlation to its initial orientation due to rotational motion.[200] In the case of spin probes incorporated directly into the polypeptoid backbone, τ_c is expected to reflect site-specific polymer segmental mobility.[201, 202] Normalized τ_c's plotted in **Figure 4.8** demonstrate that mobility is most hindered closest to the micelle core, as expected. In fact, the monomer distance from the micelle core derived from MD simulation scales linearly with τ_c determined from cw-EPR lineshape analysis. Hence, cw-EPR provides a valuable experimental method to determine the relative position of the spin label from a surface within water accessible volumes.

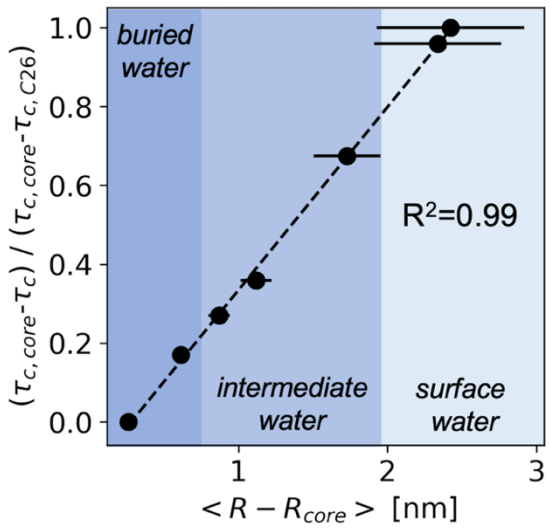

Figure 4.8. Spin label mobility serves as a proxy for distance from the surface.

Monomer distance from the micelle core (calculated by coarse-grained MD simulations) correlates linearly with the rotational correlation time (τ_c) of EPR spin probes at seven spin label positions. Because spin probes are incorporated into the polymer backbone, changes in rotational correlation times are expected to reflect changes in segmental motion. Close to the micelle core, polymer chains are highly hindered (large τ_c) due to dense packing in the core, while more water rich regions experience higher mobility (short τ_c). For each spin label position, τ_c is normalized to the range between the largest (edge of core, $\tau_{c,core}$) and shortest (hydrophilic chain end, $\tau_{c,C26}$) τ_c.

4.5. Conclusions

In this study, we demonstrate that variations in excluded volume within a micellar corona can be utilized to tune the translational water diffusivity to by up to a factor of 4 by combining sequence-defined polypeptoids capable of precisely defining functional group position with ODNP. Local water diffusivity slows dramatically in the immediate vicinity of a hydrophobic surface, but rapidly doubles within a distance of approximately 1 nm, likely due to increased free volume driving changes in water structure. This study showcases that controlling the proximity of functional groups to a surface offers a promising route to tuning material

interactions with aqueous solutes for applications ranging from catalysis to water purification. Functional handles, such as proline that can catalyze aldol condensation reactions, can be readily incorporated into polypeptoids, making them an intriguing platform for probing the effect of local water environments on material performance, such as catalytic activity.

4.6. Acknowledgements

This work was supported by the Center for Materials for Water and Energy Systems (M-WET), an Energy Frontier Research Center funded by the U.S. Department of Energy, Office of Science, Basic Energy Sciences under Award #DE-SC0019272. A.J.D. acknowledges support from the National Defense Science & Engineering Graduate (NDSEG) Fellowship Program. M.N. was supported by BASF Corporation through the California Research Alliance. Support for the ODNP studies was provided by the Deutsche Forschungsgemeinschaft (DFG, German Research Foundation) under Germany's Excellence Strategy─EXC-2033─Project number 390677874. This work makes use of Materials Research Lab (MRL) Shared Experimental Facilities that are supported by the MRSEC Program of the NSF under Award No. DMR 1720256; a member of the NSF-funded Materials Research Facilities Network (www.mrfn.org). Use was made of computational facilities purchased with funds from the National Science Foundation (OAC-1925717) and administered by the Center for Scientific Computing (CSC). The CSC is supported by the California NanoSystems Institute and the Materials Research Science and Engineering Center (MRSEC; NSF DMR 1720256) at UC Santa Barbara.

Chapter 5 – Sequence-defined Polymers as a Platform to Tune Catalytic Activity

5.1 Abstract

Polymeric supports create of hydration environments that enable selective solute interactions, such as catalysis. Current methods for designing polymeric supports result in statistically distributed functional groups. Sequence-defined polymers enable precise control over functional group position, thereby offering an opportunity to determine the potential benefits of finer synthetic control. This study utilizes a series of polypeptoid micelles with precisely defined catalyst positions to access multiple hydration environments within a single polymeric assembly. Our results demonstrate that catalyst position can be used as a tool to tune catalytic activity and provide design guidance for polymeric supports.

5.2 Introduction

Polymer-based catalyst carriers are advantageous for enabling reactions in water, in part due to their ability to create compartmentalized water environments in which water diffusivity and structure differ from bulk water.[123, 203, 204] These materials take inspiration from enzymes that leverage their often well-defined three-dimensional structures to facilitate selective solute interactions. Two of the main approaches for creating such water compartments with synthetic polymers are manipulating the conformations of single polymer chains (single chain nanoparticles)[175, 205-210] and incorporating multiple polymer chains into assemblies such as micelles.[211-218] Resulting "compartments" or "pockets" provide shielding and stabilization benefits as well as increasing the local concentration of reactants with poor solubility in water.[203]

While enzymes gain their functionality from precisely defined amino acid sequences, current polymer catalysts largely make use of co-polymers in which the position of each monomer type is controlled statistically. Such synthetic methods result in disperse polymer ensembles with chain-to-chain variations in molecular weight, monomer composition, and monomer arrangement. Precision polymers with readily controlled monomer arrangement and molecular weight could be transformative for advancing polymeric catalysts. Use of sequence-defined polymers, however, has been limited due to the challenge of synthesizing these materials on sufficient scales.[205] One class of sequence-controlled polymers, polypeptoids, presents a particularly viable model platform for catalyst development by coupling the scalability and processability of synthetic polymers with the monomer sequence control so crucial to many biological materials.[48, 142, 184]

Choosing where and how to incorporate catalytic moieties is of central importance to polymer catalyst design. In the case of single chain nanoparticles, catalytic functional groups are typically statistically distributed along the polymer backbone.[175, 205-210] For assemblies based on co-polymers, the catalyst is usually incorporated non-covalently into hydrophobic domains[216-218] or co-polymerized with one block.[211-215] More precisely controlling functional group position could improve catalyst performance and versatility. Tandem catalysis, for example, has been realized in polymeric micelles by separating two types of catalysts into the hydrophilic (corona) and hydrophobic (core) polymer domains.[219-221]

The effects of functional group position beyond simply hydrophilic or hydrophobic domains on polymer-solute interactions remain an open question. Does specific functional group position within a given domain matter? Differences in hydration environment impact catalytic activity[123] and polymer assemblies can access a range of water environments,[124, 222] suggesting the potential impact of precisely placing catalytic moieties. The water-rich corona of a polymeric micelle, in particular, spans a range of hydration water diffusivities that correlates with changes in water volume fraction throughout the corona cross-section.[222]

This study makes use of nearly monodisperse, sequence-defined polypeptoids to test the effect of catalyst position within the corona of polymer micelles on catalyst performance. The polypeptoid system used here consists of a 5-mer hydrophobic block (pink in **Figure 5.1**) and a 20-mer hydrophilic block (blue in **Figure 5.1**). These block sizes drive polymer self-assembly into micelles in water. The sequence-specificity of polypeptoids enables facile incorporation of catalytic piperidine side chains at user-defined locations (yellow star in **Figure 5.1**). Specifically, seven samples are prepared in which piperidine takes the place of one of the inert hydrophilic monomers. These catalyst positions within the polymer chains

correspond to a range of locations and hydration environments within the micelle corona, thus probing the effect of catalyst position on catalytic performance.

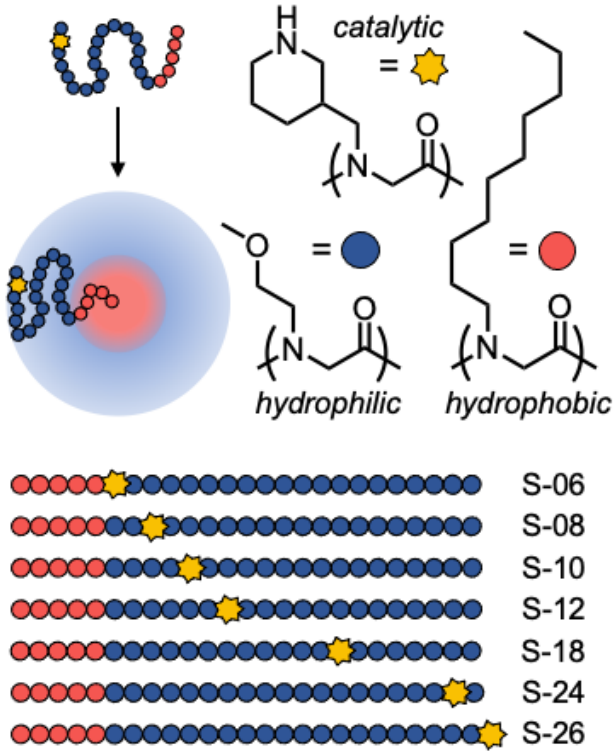

Figure 5.1. Catalyst-loaded polypeptoid micelles.

Polypeptoids containing hydrophilic (blue) and hydrophobic (pink) blocks self-assemble to form micelles in aqueous solution. To test the effect of catalyst location within polymeric assemblies on catalytic performance, the position of one catalytic monomer (yellow star) is shifted within a series of micelle-forming polypeptoids. Sample S-06 refers to the sequence in which a piperidine functionality is installed at the hydrophilic/hydrophobic interface whereas in S-26 the piperidine monomer is located at the other end of the hydrophilic block (furthest from the hydrophobic block).

5.3 Methods

Polypeptoid synthesis and purification

Polypeptoids with precisely defined catalyst positions are synthesized using a step-wise method implemented on an automated Prelude synthesizer.[184] All chemicals are used as received. Rink amide resin (loading 0.62 mmol/g, 100 μmol scale) is used as a substrate. A 20% 4-methylpiperidine in dimethylformamide (DMF) solution is used to deprotect the resin immediately prior to polymer synthesis. After deprotection, each monomer addition is separated into two self-limited reactions separated by DMF washes to attain sequence control. The first half reaction is bromoactylation with 0.6 M bromoacetic acid and 0.6 M N,N'-Dissopropylcarbodiimide (DIC) in DMF for 20 minutes. Bromoacetylation is repeated after the bulky hydrophobic monomers to improve reaction yield. Monomer functionality is then defined by incorporating an amine (1 M in DMF). The hydrophilic block is synthesized using N-methoxyethylamine (Nme) and 1 hour reaction times. Reaction times are extended to two hours for the bulkier hydrophobic (N-decylamine, Ndc) and catalytic (1-Boc-3-(aminomethyl)piperidine, Npip) monomers. Prior to removal from the resin, polypeptoids are formylated twice for 30 minutes using 1 M DIC and 1 M formic acid in N-methyl-2-pyrrolidone (NMP) so ensure full chain end termination. Polypeptoids are cleaved from the resin using a cocktail of trifluoroacetic acid (TFA) : water : triisopropylsilane (95 : 2.5 : 2.5, v/v/v) for 2 hours. Polypeptoids are then rinsed from the resin with dichloromethane (DCM). TFA and DCM are removed under vacuum and the polypeptoids are lyophilized from acetonitrile and water.

Polypeptoids are purified using preparative high performance liquid chromatography (HPLC) with a Shimadzu Nexera Hybride reverse phase HPLC coupled with a single quad

mass spectrometer. Samples are dissolved at 50 mg/mL in a 50 : 50 water : acetonitrile mixture then filtered through a 0.45 μm PVDF filter. Polypeptoids are separated on a C4 column (XBridge Protein BEH C4 OBD Column, 300 Å, 5 μm) using a 50-100% acetonitrile with 0.1% v/v TFA gradient over 30 minutes. Water with 0.1% v/v TFA was used as the second solvent. To confirm isolation of the targeted polypeptoid sequences, all purified polypeptoid samples are characterized by ultra-high-performance liquid chromatography-mass spectroscopy (UPLC-MS) (**Figure 5.2, Table 5.1**). A Waters Acquity H-class UPLC coupled with a Waters Xevo G2-XS time-of-flight mass spectrometer is utilized. Samples are dissolved in 1 : 1 water : acetonitrile with 0.1% formic acid and separated using a 20-100% acetonitrile gradient. Use of TFA during cleavage and purification results in polypeptoids in conjugate acid form, so polypeptoids are converted to their base form using Amberlyst A26 ion exchange beads prior to catalytic testing.

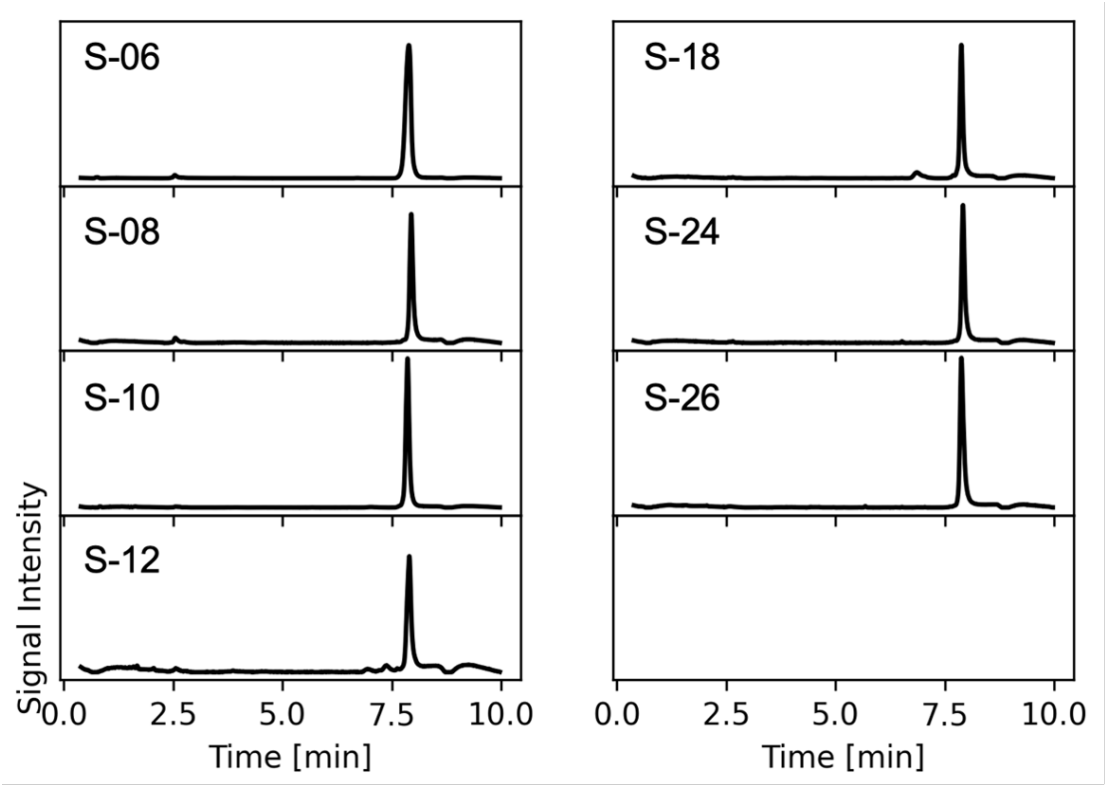

Figure 5.2. HPLC confirms sample purity.

Samples elute as a single peak after preparative HPLC, confirming isolation of a monodisperse product for all seven polypeptoid sequences.

Table 5.1. Polypeptoid sequences and molecular weights.

Sample	Sequence	Calc (m/z)	Found (m/z)	Ion type
S-06	Fm-Ndc_5-Npip-Nme_{19}	3371.2	1709.1	$[M/2+Na]^+$
S-08	Fm-Ndc_5-Nme_2-Npip-Nme_{17}	3371.2	1709.1	$[M/2+Na]^+$
S-10	Fm-Ndc_5-Nme_4-Npip-Nme_{15}	3371.2	1709.1	$[M/2+Na]^+$
S-12	Fm-Ndc_5-Nme_6-Npip-Nme_{13}	3371.2	1709.1	$[M/2+Na]^+$
S-18	Fm-Ndc_5-Nme_{12}-Npip-Nme_7	3371.2	1709.6	$[M/2+Na]^+$
S-24	Fm-Ndc_5-Nme_{23}-Npip-Nme	3371.2	1709.1	$[M/2+Na]^+$
S-26	Fm-Ndc_5-Nme_{25}-Npip	3486.3	1767.1	$[M/2+Na]^+$

Micelle Assembly

Polypeptoids are dissolved at a concentration of 5 mg/mL in water and stirred overnight to form micelles. Micelle formation is confirmed by dynamic light scattering (Malvern Zetasizer μV, model ZMV2000). A hydrodynamic radius of 5 ± 2 nm is observed for S-24. This size is within the range reported by Donghui Zhang and coworkers for similar polypeptoid micelles containing one charged group within the corona.[136]

Catalytic Testing

The aldol reaction between cyclohexanone and *p*-nitrobenzaldehyde (**Figure 5.3**) serves as a model reaction commonly used in the study of polymeric catalysts.[175, 211, 223, 224] Aldehyde (1 eq., 0.025 mmol) and ketone (5 eq., 0.125 mmol) are added to the catalytic micelle solution (0.5 mL, 0.03 equiv, 0.00074 mmol). Reaction mixtures are stirred at room temperature. Aldol products are extracted with diethyl ether. Products are dried under air and analyzed by ^{1}H NMR without further purification (**Figure 5.4**).

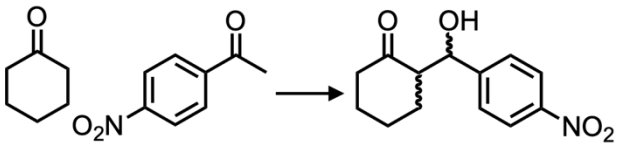

Figure 5.3. Model aldol reaction.

Piperidine containing micelles catalyze the reaction of cyclohexanone and p-nitrobenzaldehyde into an aldol product.

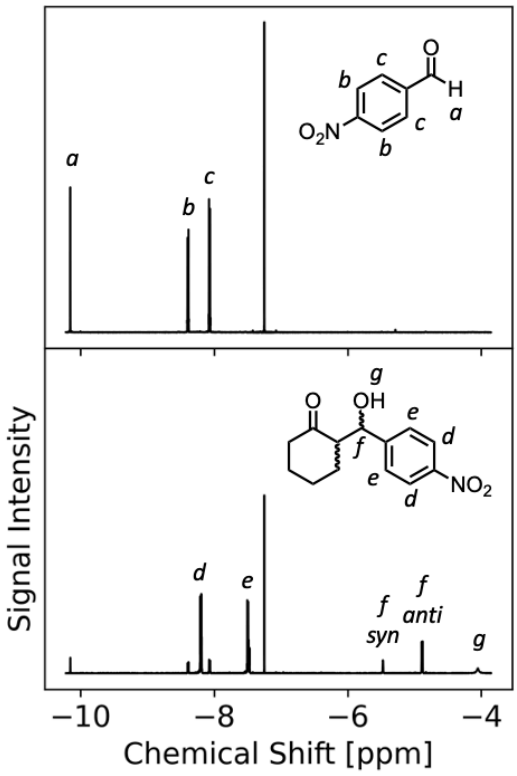

Figure 5.4. Reaction yields are determined by ^{1}H NMR.

Reaction conversion from p-nitrobenzaldehyde (top) to the aldol product (bottom) is monitored by ^{1}H NMR.

5.4 Results and Discussion

Local hydration environments change throughout the water-rich corona of polymeric micelles because polymer volume fraction increases close to the micelle core.[222] To determine if these hydration environments can be leveraged for catalysis, catalytic activity is mapped across the cross-section of a polymeric micelle using polypeptoids with precisely defined catalyst position. Specifically, piperidine moieties capable of catalyzing aldol reactions are incorporated at seven positions within the hydrophilic corona. Aldol reaction yields reveal a dependence on piperidine location, suggesting that catalyst position can be used as a handle to tune catalytic activity.

Micelles with a range of catalyst locations demonstrate site-dependent aldol product yields (**Figure 5.5**). Sample S-26 shows the lowest reaction yield but shifting the catalytic functional group away from the chain end by two monomer positions (S-24) more than doubles the reaction yield. Reaction yield further increases away from the micelle exterior until decreasing again for positions closest to the micelles core. Of the catalyst positions considered, sample S-12 results in the highest reaction yield. Reaction conversion between cyclohexanone and *p*-nitrobenzaldehyde is expected to increase with water content (**Figure 5.7** in the Appendix),[211, 225, 226] but improved solvent accessibility does not explain the superior performance of S-12 relative to S-18, S-14, and S-26. While the micelle corona is water rich, the S-12 catalyst position will correspond to slightly lower water volume fraction than catalyst position further from the micelle core.[222] Rather, variations in hydration environment likely underpin improved performance, as previously observed for catalytic single chain nanoparticles.[123]

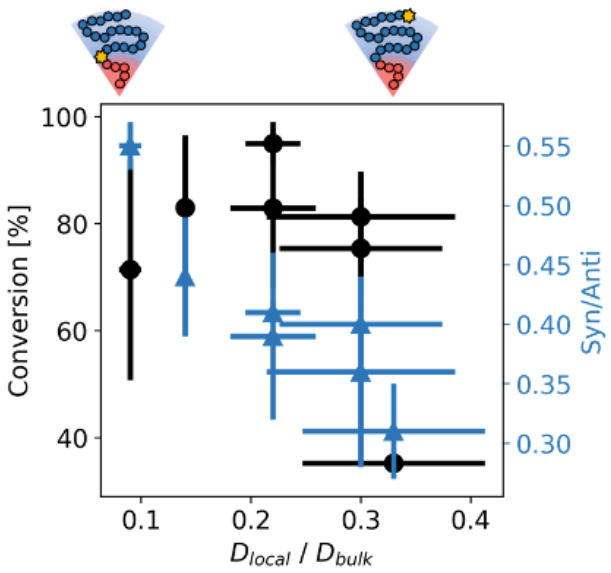

Figure 5.5. Intermediate monomer position enables highest aldol yield.

Conversion of aldehyde to an aldol product after 24 hours is highest for the S-12 sample. Samples in which the catalyst is closer to the core (S-06, S-08, S-10) or further from the core (S-18, S-24, S-26) result in lower reaction conversions. Interestingly, the ratio between syn- and anti- enantiomers in the product increases close to the micelle core, suggesting that catalyst position can tune enantioselection.

To demonstrate the effect of hydration environment on catalyst efficacy, reaction yields are plotted as a function of normalized local water diffusivity (D_{local}) in **Figure 5.6**. D_{local} and hydration environments (buried-, intermediate-, or surface-like) are approximated from Overhauser Dynamic Nuclear Polarization spectroscopy experiments of a closely related micelle system.[222] Water closest to the micelle core (S-06) moves about 10 times slower than bulk water and corresponds to a buried water character, while the S-26 sample is hydrated by more surface-like water.[222] Even this surface-like water diffuses at less than half the speed of bulk water (D_{bulk}). The maximum reaction yields observed in this system correspond to hydration environments with intermediate water characteristics. These intermediate regions

are likely advantageous because they balance solute accessibility with a stabilizing hydration environment.

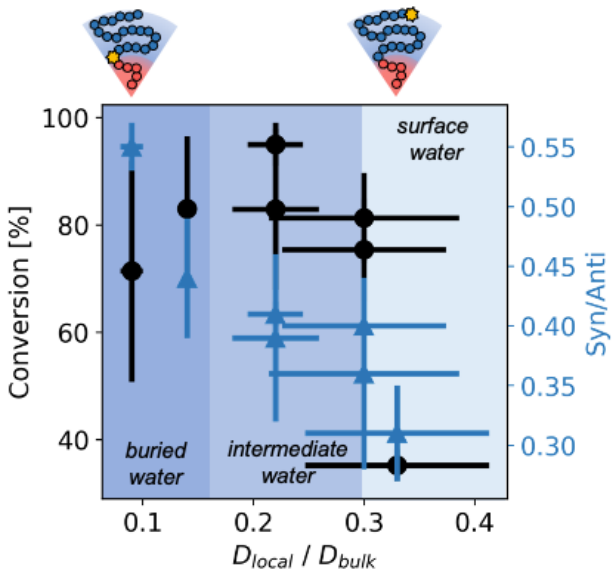

Figure 5.6. Slowed water diffusivity enhances catalytic activity.

Aldol yields are plotted as a function of normalized local water diffusivity (D_{local}/D_{bulk}). Catalyst positions corresponding to the slowest and fastest water D_{local} have lower aldol conversions than positions in more intermediate regions. Rather than benefitting from intermediate water dynamics, enantiomer selectivity correlates directly with water diffusivity, with slower water environments (higher polymer volume fraction) corresponding to larger syn enantiomer populations. These results confirm that hydration environment as controlled by local water volume fraction is central to catalyst performance and can be modulated within polymer assemblies.

5.5 Conclusions

This study demonstrates that catalytic performance can be tuned by precisely defining catalyst position within polymeric assemblies. Polymers self-assemble into multi-chain structures such as micelles and bilayers that contain water rich regions with distinct water properties. These hydration environments are elegantly accessed with polypeptoids because

sequence-specific synthesis enables control over catalytic moiety position. In the case of a model aldol reaction, reaction yield varied by more than two-fold depending on catalyst position within the micelle corona. The best performing catalyst are located in regions where local water diffusivity is about one quarter that of bulk water. The ability of sequence-specific polymers to control functional group position and access user-defined hydration environments opens the door for not only optimized and multifunctional polymer catalyst supports, but also other applications where selective interactions are desired at soft interfaces, such as water purification membranes.

5.6 Acknowledgements

This work was supported by the Center for Materials for Water and Energy Systems (M-WET), an Energy Frontier Research Center funded by the U.S. Department of Energy, Office of Science, Basic Energy Sciences under Award #DE-SC0019272. The research reported here made use of the shared facilities (NMR, UPLC-MS) of the Materials Research Science and Engineering Center (MRSEC) at UC Santa Barbara: NSF DMR–2308708. The UC Santa Barbara MRSEC is a member of the Materials Research Facilities Network (www.mrfn.org). This work also makes use of experimental facilities (prep-HPLC) that are supported by the BioPACIFIC Materials Innovation Platform of the National Science Foundation under Award No. DMR-1933487. A.J.D. acknowledges support from the National Defense Science & Engineering Graduate (NDSEG) Fellowship Program.

5.7 Appendix

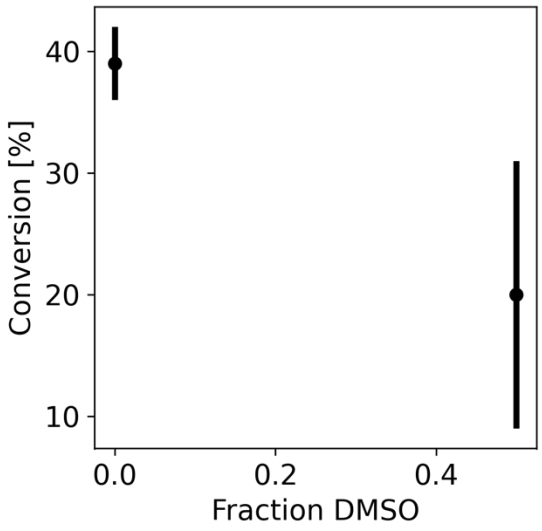

Figure 5.7. DMSO reduces reaction yield.

Reaction conversion between p-nitrobenzaldehyde *and cyclohexanone catalyzed by 4-methyl-piperidine is lower for a 50/50 water/DMSO than for pure water. Reactions are performed at room temperature over 6 hours with 1 equivalent aldehyde, 5 equivalents ketone, and 0.03 equivalent catalyst.*

Chapter 6 – Conclusions and Outlook

Sequence-defined polymer offer a promising route to produce soft materials that are able to selectively interact with solutes in water. This dissertation spans two elements of designing polymers with specific interactions: controlling polymer conformation (Chapters 2 and 3) and local water dynamics (Chapter 4). It then applies these concepts to design polymer micelles capable of catalyzing aldol reactions in water (Chapter 5). While promising, these results only scratch the surface of the potential for polymer sequence control to guide chain conformation and hydration. Likewise, the application of the electron paramagnetic resonance (EPR) techniques critical in this work to other polymeric systems is in its infancy.

Chapters 2 and 3 focused on controlling the conformation of polypeptoid chains in solution and measuring those conformational changes by double electron-electron resonance (DEER) spectroscopy. Ongoing work between the Segalman, Han, and Shell groups seeks to accelerate sequence discovery via a synthesis-characterization-simulation/machine learning workflow. Focusing these efforts on long polypeptoid chains (38-50mers) and strongly interacting or repulsing monomer types, such as charged monomers, will likely produce larger

conformational differences than shorter chains with similar side chain chemistries. Further extending capabilities to assembled systems, such as micelles or bilayers, will open more doors for accessing variations in polymer chain shape and provide insight into how polymer assembly impacts chain shape relative to dilute solution.

A natural extension of the micelle hydration (Chapter 4) and catalysis (Chapter 5) work will be to compare the excluded volume effects on hydration and catalysis observed for micelles to polymer systems with other geometries. Do these rules hold for bilayers or hydrogels, for example? In the case of bilayers, changing the hydrophilic/hydrophobic ratios of the micelle forming polypeptoids will enable analogous bilayer formation. For hydrogels, water volume fraction can be controlled by cross-linking density. Confirming that excluded volume predicts both water diffusivity and catalytic activity for multiple materials platforms will validate it as a design rule.

Water diffusivity near polymer surfaces is influenced by sterics and hydrogen bonding. The micelle hydration work of Chapter 4 utilized almost entirely non-polar hydrophilic monomers, but the polypeptoid platform is amenable to a wide range of chemistries. Varying the chemistry of the hydrophilic corona to include polar monomers could probe the effect of hydrogen bonding on local water behavior. Changes in side-chain chemistry will likely also drive differences in micelle morphology that must be controlled for to isolate effects associated with hydrogen bonding strength.

One intriguing area in which sequence-defined polymers and the DEER technique have enormous potential is in understanding chain conformations within hydrogels. Hydrogel networks are often highly heterogeneous, and DEER could provide insight on this disorder. Unlike techniques such as stimulated emission depletion microscopy that rely on tracer

molecules,[227] DEER directly measures chain shape. Furthermore, because EPR techniques can tolerate "dirty" samples, the effects of additives on chain conformation could easily be tracked. As with many EPR studies, preparing samples with optimal spin labeling will likely be challenging. Here, sequence-defined polymers could offer a way to produce hydrogel networks with precisely positioned spin labels. Another challenge associated with performing DEER on hydrogels will be achieving the correct sample geometry as samples must fit within a 3 mm OD and 2 mm ID tube. Advances in hydrogel microparticle synthesis make this form factor highly feasible.[228]

In conclusion, this thesis provides evidence for the synergistic potential of sequence-defined polymers and EPR techniques. Work presented here demonstrates that hydrophobic and hydrophilic sequencing can tune polymer chain conformation. It also maps out a water diffusivity gradient in polymeric micelles and leverages this to control catalytic activity for an aqueous reaction. Future work combining sequence-defined polymers and EPR techniques will produce further design rules for functional polymers and polymer surfaces, such as water filtration membranes and antifouling coatings.

Bibliography

(1) Bates, F. S.; Brant, P.; Coates, G. W.; Lipson, J.; Osuji, C.; Pablo, J. d.; Rowan, S.; Segalman, R.; Winey, K. I. *Frontiers in Polymer Science and Engineering*; NSF Workshop, University of Minnesota Twin Cities, 2016.

(2) Paabo, S.; Gifford, J. A.; Wilson, A. C. Mitochondrial-DNA Sequences from a 7000-Year Old Brain. *Nucleic Acids Res* **1988**, *16* (20), 9775-9787. DOI: DOI 10.1093/nar/16.20.9775.

(3) Bhattacharyya, R. P.; Remenyi, A.; Yeh, B. J.; Lim, W. A. Domains, motifs, and scaffolds: The role of modular interactions in the evolution and wiring of cell signaling circuits. *Annu Rev Biochem* **2006**, *75*, 655-680. DOI: 10.1146/annurev.biochem.75.103004.142710.

(4) Mann, S. Molecular Recognition in Biomineralization. *Nature* **1988**, *332* (6160), 119-124. DOI: DOI 10.1038/332119a0.

(5) Buehler, M. J.; Ackbarow, T. Nanomechanical strength mechanisms of hierarchical biological materials and tissues. *Comput Method Biomec* **2008**, *11* (6), 595-607. DOI: 10.1080/10255840802078030.

(6) Deming, T. J. Polypeptide materials: New synthetic methods and applications. *Adv Mater* **1997**, *9* (4), 299-+. DOI: DOI 10.1002/adma.19970090404.

(7) Blain, J. C.; Szostak, J. W. Progress Toward Synthetic Cells. *Annual Review of Biochemistry, Vol 83* **2014**, *83*, 615-640. DOI: 10.1146/annurev-biochem-080411-124036.

(8) Burkoth, T. S.; Beausoleil, E.; Kaur, S.; Tang, D. Z.; Cohen, F. E.; Zuckermann, R. N. Toward the synthesis of artificial proteins: The discovery of an amphiphilic helical peptoid assembly. *Chem Biol* **2002**, *9* (5), 647-654. DOI: Pii S1074-5521(02)00140-0 Doi 10.1016/S1074-5521(02)00140-0.

(9) Murnen, H. K.; Khokhlov, A. R.; Khalatur, P. G.; Segalman, R. A.; Zuckermann, R. N. Impact of Hydrophobic Sequence Patterning on the Coil-to-Globule Transition of Protein-like Polymers. *Macromolecules* **2012**, *45* (12), 5229-5236. DOI: 10.1021/ma300707t.

(10) Lutz, J. F. Coding Macromolecules: Inputting Information in Polymers Using Monomer-Based Alphabets. *Macromolecules* **2015**, *48* (14), 4759-4767. DOI: 10.1021/acs.macromol.5b00890.

(11) Colquhoun, H.; Lutz, J. F. Information-containing macromolecules. *Nat Chem* **2014**, *6* (6), 455-456. DOI: 10.1038/nchem.1958.

(12) Gentekos, D. T.; Sifri, R. J.; Fors, B. P. Controlling polymer properties through the shape of the molecular-weight distribution. *Nat Rev Mater* **2019**, *4* (12), 761-774. DOI: 10.1038/s41578-019-0138-8.

(13) Rosenbloom, S. I.; Gentekos, D. T.; Silberstein, M. N.; Fors, B. P. Tailor-made thermoplastic elastomers: customisable materials via modulation of molecular weight distributions. *Chem Sci* **2020**, *11* (5), 1361-1367. DOI: 10.1039/c9sc05278j.

(14) Sifri, R. J.; Padilla-Velez, O.; Coates, G. W.; Fors, B. P. Controlling the Shape of Molecular Weight Distributions in Coordination Polymerization and Its Impact on Physical Properties. *J Am Chem Soc* **2020**, *142* (3), 1443-1448. DOI: 10.1021/jacs.9b11462.

(15) Beckingham, B. S.; Sanoja, G. E.; Lynd, N. A. Simple and Accurate Determination of Reactivity Ratios Using a Nonterminal Model of Chain Copolymerization. *Macromolecules* **2015**, *48* (19), 6922-6930. DOI: 10.1021/acs.macromol.5b01631.

(16) Zhang, C.; Bates, M. W.; Geng, Z. S.; Levi, A. E.; Vigil, D.; Barbon, S. M.; Loman, T.; Delaney, K. T.; Fredrickson, G. H.; Bates, C. M.; et al. Rapid Generation of Block Copolymer Libraries Using Automated Chromatographic Separation. *J Am Chem Soc* **2020**, *142* (21), 9843-9849. DOI: 10.1021/jacs.0c04028.

(17) Patterson, A. L.; Yu, B.; Danielsen, S. P. O.; Davidson, E. C.; Fredrickson, G. H.; Segalman, R. A. Monomer Sequence Effects on Interfacial Width and Mixing in Self-Assembled Diblock Copolymers. *Macromolecules* **2020**, *53* (9), 3262-3272. DOI: 10.1021/acs.macromol.9b02426.

(18) Yu, B.; Li, R.; Segalman, R. A. Tuning the Double Gyroid Phase Window in Block Copolymers via Polymer Chain Conformation Near the Interface. *Macromolecules* **2021**, *54* (12), 5388-5396. DOI: 10.1021/acs.macromol.1c00048.

(19) Bates, F. S.; Schulz, M. F.; Khandpur, A. K.; Forster, S.; Rosedale, J. H.; Almdal, K.; Mortensen, K. Fluctuations, Conformational Asymmetry and Block-Copolymer Phase-Behavior. *Faraday Discuss* **1994**, *98*, 7-18. DOI: DOI 10.1039/fd9949800007.

(20) Bates, M. W.; Lequieu, J.; Barbon, S. M.; Lewis, R. M.; Delaney, K. T.; Anastasaki, A.; Hawker, C. J.; Fredrickson, G. H.; Bates, C. M. Stability of the A15 phase in diblock copolymer melts. *P Natl Acad Sci USA* **2019**, *116* (27), 13194-13199. DOI: 10.1073/pnas.1900121116.

(21) Olsen, B. D.; Segalman, R. A. Phase transitions in asymmetric rod-coil block copolymers. *Macromolecules* **2006**, *39* (20), 7078-7083. DOI: ARTN MA060994Z 10.1021/ma060994z.

(22) Armand, P.; Kirshenbaum, K.; Falicov, A.; Dunbrack, R. L.; Dill, K. A.; Zuckermann, R. N.; Cohen, F. E. Chiral N-substituted glycines can form stable helical conformations. *Fold Des* **1997**, *2* (6), 369-375. DOI: Doi 10.1016/S1359-0278(97)00051-5.

(23) Barbee, M. H.; Wright, Z. M.; Allen, B. P.; Taylor, H. F.; Patteson, E. F.; Knight, A. S. Protein-Mimetic Self-Assembly with Synthetic Macromolecules. *Macromolecules* **2021**, *54* (8), 3585-3612. DOI: 10.1021/acs.macromol.0c02826.

(24) Habchi, J.; Tompa, P.; Longhi, S.; Uversky, V. N. Introducing Protein Intrinsic Disorder. *Chem Rev* **2014**, *114* (13), 6561-6588. DOI: 10.1021/cr400514h.

(25) Dobson, C. M. Protein folding and misfolding. *Nature* **2003**, *426* (6968), 884-890. DOI: 10.1038/nature02261.

(26) Kramer, J. R.; Deming, T. J. Glycopolypeptides with a Redox-Triggered Helix-to-Coil Transition. *J Am Chem Soc* **2012**, *134* (9), 4112-4115. DOI: 10.1021/ja3007484.

(27) Rodriguez, A. R.; Kramer, J. R.; Deming, T. J. Enzyme-Triggered Cargo Release from Methionine Sulfoxide Containing Copolypeptide Vesicles. *Biomacromolecules* **2013**, *14* (10), 3610-3614. DOI: 10.1021/bm400971p.

(28) Shiraga, K.; Naito, H.; Suzuki, T.; Kondo, N.; Ogawa, Y. Hydration and Hydrogen Bond Network of Water during the Coil-to-Globule Transition in Poly(N-isopropylacrylamide) Aqueous Solution at Cloud Point Temperature. *J Phys Chem B* **2015**, *119* (17), 5576-5587. DOI: 10.1021/acs.jpcb.5b01021.

(29) Ndaya, D.; Bosire, R.; Vaidya, S.; Kasi, R. M. Molecular engineering of stimuli-responsive, functional, side-chain liquid crystalline copolymers: synthesis, properties and applications. *Polym Chem-Uk* **2020**, *11* (37), 5937-5954. DOI: 10.1039/d0py00749h.

(30) Wang, Y.; Chu, X. K.; Longhi, S.; Roche, P.; Han, W.; Wang, E. K.; Wang, J. Multiscaled exploration of coupled folding and binding of an intrinsically disordered molecular recognition element in measles virus nucleoprotein. *P Natl Acad Sci USA* **2013**, *110* (40), E3743-E3752. DOI: 10.1073/pnas.1308381110.

(31) Pelham, J. F.; Mosier, A. E.; Hurley, J. M. Characterizing Time-of-Day Conformational Changes in the Intrinsically Disordered Proteins of the Circadian Clock. *Intrinsically Disordered Proteins* **2018**, *611*, 503-529. DOI: 10.1016/bs.mie.2018.08.024.

(32) Haug, A.; Larsen, B.; Smidsrod, O. Uronic Acid Sequence in Alginate from Different Sources. *Carbohyd Res* **1974**, *32* (2), 217-225. DOI: Doi 10.1016/S0008-6215(00)82100-X.

(33) Jouenne, S.; Gonzalez-Leon, J. A.; Ruzette, A. V.; Lodefier, P.; Tence-Girault, S.; Leibler, L. Styrene/butadiene gradient block copolymers: Molecular and mesoscopic structures. *Macromolecules* **2007**, *40* (7), 2432-2442. DOI: 10.1021/ma062723u.

(34) Roy, R.; Park, J. K.; Young, W. S.; Mastroianni, S. E.; Tureau, M. S.; Epps, T. H. Double-Gyroid Network Morphology in Tapered Diblock Copolymers. *Macromolecules* **2011**, *44* (10), 3910-3915. DOI: 10.1021/ma1025847.

(35) Bates, F. S.; Fredrickson, G. H. Block copolymers - Designer soft materials. *Phys Today* **1999**, *52* (2), 32-38. DOI: Doi 10.1063/1.882522.

(36) Wagener, K. B.; Boncella, J. M.; Nel, J. G. Acyclic Diene Metathesis (Admet) Polymerization. *Macromolecules* **1991**, *24* (10), 2649-2657. DOI: DOI 10.1021/ma00010a001.

(37) Pribyl, J.; Wagener, K. B.; Rojas, G. ADMET polymers: synthesis, structure elucidation, and function. *Mater Chem Front* **2021**, *5* (1), 14-43. DOI: 10.1039/d0qm00273a.

(38) Baughman, T. W.; Chan, C. D.; Winey, K. I.; Wagener, K. B. Synthesis and morphology of well-defined poly(ethylene-co-acrylic acid) copolymers. *Macromolecules* **2007**, *40* (18), 6564-6571. DOI: 10.1021/ma070841r.

(39) Chen, Y. L.; Guan, Z. B. Bioinspired Modular Synthesis of Elastin-Mimic Polymers To Probe the Mechanism of Elastin Elasticity. *J Am Chem Soc* **2010**, *132* (13), 4577-+. DOI: 10.1021/ja9104446.

(40) Gutekunst, W. R.; Hawker, C. J. A General Approach to Sequence-Controlled Polymers Using Macrocyclic Ring Opening Metathesis Polymerization. *J Am Chem Soc* **2015**, *137* (25), 8038-8041. DOI: 10.1021/jacs.5b04940.

(41) Zhang, J. H.; Matta, M. E.; Hillmyer, M. A. Synthesis of Sequence-Specific Vinyl Copolymers by Regioselective ROMP of Multiply Substituted Cyclooctenes. *Acs Macro Letters* **2012**, *1* (12), 1383-1387. DOI: 10.1021/mz300535r.

(42) Wu, Y. H.; Zhang, J.; Du, F. S.; Li, Z. C. Dual Sequence Control of Uniform Macromolecules through Consecutive Single Addition by Selective Passerini Reaction. *Acs Macro Letters* **2017**, *6* (12), 1398-1403. DOI: 10.1021/acsmacrolett.7b00863.

(43) Kreye, O.; Toth, T.; Meier, M. A. R. Introducing Multicomponent Reactions to Polymer Science: Passerini Reactions of Renewable Monomers. *J Am Chem Soc* **2011**, *133* (6), 1790-1792. DOI: 10.1021/ja1113003.

(44) Jiang, Y.; Golder, M. R.; Nguyen, H. V. T.; Wang, Y. F.; Zhong, M. J.; Barnes, J. C.; Ehrlich, D. J. C.; Johnson, J. A. Iterative Exponential Growth Synthesis and Assembly of Uniform Diblock Copolymers. *J Am Chem Soc* **2016**, *138* (30), 9369-9372. DOI: 10.1021/Jacs.6b04964.

(45) Binauld, S.; Damiron, D.; Connal, L. A.; Hawker, C. J.; Drockenmuller, E. Precise Synthesis of Molecularly Defined Oligomers and Polymers by Orthogonal Iterative Divergent/Convergent Approaches. *Macromol Rapid Comm* **2011**, *32* (2), 147-168. DOI: 10.1002/marc.201000548.

(46) Leibfarth, F. A.; Johnson, J. A.; Jamison, T. F. Scalable synthesis of sequence-defined, unimolecular macromolecules by Flow-IEG. *P Natl Acad Sci USA* **2015**, *112* (34), 10617-10622. DOI: 10.1073/pnas.1508599112.

(47) Konrad, W.; Fengler, C.; Putwa, S.; Barner-Kowollik, C. Protection-Group-Free Synthesis of Sequence-Defined Macromolecules via Precision lambda-Orthogonal Photochemistry. *Angew Chem Int Edit* **2019**, *58* (21), 7133-7137. DOI: 10.1002/anie.201901933.

(48) Zuckermann, R. N.; Kerr, J. M.; Kent, S. B. H.; Moos, W. H. Efficient Method for the Preparation of Peptoids [Oligo(N-Substituted Glycines)] by Submonomer Solid-Phase Synthesis. *J Am Chem Soc* **1992**, *114* (26), 10646-10647. DOI: DOI 10.1021/ja00052a076.

(49) Merrifield, R. B. Solid Phase Peptide Synthesis .1. Synthesis of a Tetrapeptide. *J Am Chem Soc* **1963**, *85* (14), 2149-&. DOI: DOI 10.1021/ja00897a025.

(50) Espeel, P.; Carrette, L. L. G.; Bury, K.; Capenberghs, S.; Martins, J. C.; Du Prez, F. E.; Madder, A. Multifunctionalized Sequence-Defined Oligomers from a Single Building Block. *Angew Chem Int Edit* **2013**, *52* (50), 13261-13264. DOI: 10.1002/anie.201307439.

(51) Dill, K. A.; Ozkan, S. B.; Shell, M. S.; Weikl, T. R. The protein folding problem. *Annu Rev Biophys* **2008**, *37*, 289-316. DOI: 10.1146/annurev.biophys.37.092707.153558.

(52) Baneyx, F.; Matthaei, J. F. Self-assembled two-dimensional protein arrays in bionanotechnology: from S-layers to designed lattices. *Curr Opin Biotech* **2014**, *28*, 39-45. DOI: 10.1016/j.copbio.2013.11.001.

(53) Barnes, R.; Sun, S.; Fichou, Y.; Dahlquist, F. W.; Heyden, M.; Han, S. I. Spatially Heterogeneous Surface Water Diffusivity around Structured Protein Surfaces at Equilibrium. *J Am Chem Soc* **2017**, *139* (49), 17890-17901. DOI: 10.1021/jacs.7b08606.

(54) Harper, S. M.; Neil, L. C.; Gardner, K. H. Structural basis of a phototropin light switch. *Science* **2003**, *301* (5639), 1541-1544. DOI: DOI 10.1126/science.1086810.

(55) Kuhlman, B. Designing protein structures and complexes with the molecular modeling program Rosetta. *J Biol Chem* **2019**, *294* (50), 19436-19443. DOI: 10.1074/jbc.AW119.008144.

(56) Guntas, G.; Hallett, R. A.; Zimmerman, S. P.; Williams, T.; Yumerefendi, H.; Bear, J. E.; Kuhlman, B. Engineering an improved light-induced dimer (iLID) for controlling the localization and activity of signaling proteins. *P Natl Acad Sci USA* **2015**, *112* (1), 112-117. DOI: 10.1073/pnas.1417910112.

(57) Baek, M.; DiMaio, F.; Anishchenko, I.; Dauparas, J.; Ovchinnikov, S.; Lee, G. R.; Wang, J.; Cong, Q.; Kinch, L. N.; Schaeffer, R. D.; et al. Accurate prediction of protein structures and interactions using a three-track neural network. *Science* **2021**, *373* (6557), 871-+. DOI: 10.1126/science.abj8754.

(58) Baker, D. What has de novo protein design taught us about protein folding and biophysics? *Protein Sci* **2019**, *28* (4), 678-683. DOI: 10.1002/pro.3588.

(59) Jumper, J.; Evans, R.; Pritzel, A.; Green, T.; Figurnov, M.; Ronneberger, O.; Tunyasuvunakool, K.; Bates, R.; Zidek, A.; Potapenko, A.; et al. Highly accurate protein structure prediction with AlphaFold. *Nature* **2021**, *596* (7873), 583-+. DOI: 10.1038/s41586-021-03819-2.

(60) Crapster, J. A.; Guzei, I. A.; Blackwell, H. E. A Peptoid Ribbon Secondary Structure. *Angew Chem Int Edit* **2013**, *52* (19), 5079-5084. DOI: 10.1002/anie.201208630.

(61) Shin, S. B. Y.; Yoo, B.; Todaro, L. J.; Kirshenbaum, K. Cyclic peptoids. *J Am Chem Soc* **2007**, *129* (11), 3218-3225. DOI: 10.1021/ja066960o.

(62) Shah, N. H.; Butterfoss, G. L.; Nguyen, K.; Yoo, B.; Bonneau, R.; Rabenstein, D. L.; Kirshenbaum, K. Oligo(N-aryl glycines): A New Twist on Structured Peptoids. *J Am Chem Soc* **2008**, *130* (49), 16622-16632. DOI: 10.1021/ja804580n.

(63) Wu, C. W.; Sanborn, T. J.; Zuckermann, R. N.; Barron, A. E. Peptoid oligomers with alpha-chiral, aromatic side chains: Effects of chain length on secondary structure. *J Am Chem Soc* **2001**, *123* (13), 2958-2963. DOI: 10.1021/ja003153v.

(64) Murnen, H. K.; Rosales, A. M.; Jaworsk, J. N.; Segalman, R. A.; Zuckermann, R. N. Hierarchical Self-Assembly of a Biomimetic Diblock Copolypeptoid into Homochiral Superhelices. *J Am Chem Soc* **2010**, *132* (45), 16112-16119. DOI: 10.1021/ja106340f.

(65) Robertson, E. J.; Battigelli, A.; Proulx, C.; Mannige, R. V.; Haxton, T. K.; Yun, L. S.; Whitelam, S.; Zuckermann, R. N. Design, Synthesis, Assembly, and Engineering of Peptoid Nanosheets. *Accounts Chem Res* **2016**, *49* (3), 379-389. DOI: 10.1021/acs.accounts.5b00439.

(66) Mannige, R. V.; Haxton, T. K.; Proulx, C.; Robertson, E. J.; Battigelli, A.; Butterfoss, G. L.; Zuckermann, R. N.; Whitelam, S. Peptoid nanosheets exhibit a new secondary-structure motif. *Nature* **2015**, *526* (7573), 415-+. DOI: 10.1038/nature15363.

(67) Olivier, G. K.; Cho, A.; Sanii, B.; Connolly, M. D.; Tran, H.; Zuckermann, R. N. Antibody-Mimetic Peptoid Nanosheets for Molecular Recognition. *Acs Nano* **2013**, *7* (10), 9276-9286. DOI: 10.1021/nn403899y.

(68) Nam, K. T.; Shelby, S. A.; Choi, P. H.; Marciel, A. B.; Chen, R.; Tan, L.; Chu, T. K.; Mesch, R. A.; Lee, B. C.; Connolly, M. D.; et al. Free-floating ultrathin two-dimensional crystals from sequence-specific peptoid polymers. *Nat Mater* **2010**, *9* (5), 454-460. DOI: 10.1038/Nmat2742.

(69) Shendure, J.; Balasubramanian, S.; Church, G. M.; Gilbert, W.; Rogers, J.; Schloss, J. A.; Waterston, R. H. DNA sequencing at 40: past, present and future. *Nature* **2017**, *550* (7676), 345-353. DOI: 10.1038/nature24286.

(70) Stark, R.; Grzelak, M.; Hadfield, J. RNA sequencing: the teenage years. *Nat Rev Genet* **2019**, *20* (11), 631-656. DOI: 10.1038/s41576-019-0150-2.

(71) Restrepo-Perez, L.; Joo, C.; Dekker, C. Paving the way to single-molecule protein sequencing. *Nat Nanotechnol* **2018**, *13* (9), 786-796. DOI: 10.1038/s41565-018-0236-6.

(72) De Vlaminck, I.; Dekker, C. Recent Advances in Magnetic Tweezers. *Annual Review of Biophysics, Vol 41* **2012**, *41*, 453-472. DOI: 10.1146/annurev-biophys-122311-100544.

(73) Earl, L. A.; Falconieri, V.; Milne, J. L. S.; Subramaniam, S. Cryo-EM: beyond the microscope. *Curr Opin Struc Biol* **2017**, *46*, 71-78. DOI: 10.1016/j.sbi.2017.06.002.

(74) Gurarslan, R.; Hardrict, S.; Roy, D.; Galvin, C.; Hill, M. R.; Gracz, H.; Sumerlin, B. S.; Genzer, J.; Tonelli, A. Beyond Microstructures: Using the Kerr Effect to Characterize the Macrostructures of Synthetic Polymers. *J Polym Sci Pol Phys* **2015**, *53* (3), 155-166. DOI: 10.1002/polb.23598.

(75) Hardrict, S. N.; Gurarslan, R.; Galvin, C. J.; Gracz, H.; Roy, D.; Sumerlin, B. S.; Genzer, J.; Tonelli, A. E. Characterizing polymer macrostructures by identifying and locating microstructures along their chains with the kerr effect. *J Polym Sci Pol Phys* **2013**, *51* (9), 735-741. DOI: 10.1002/polb.23248.

(76) Floris, F.; Vallotto, C.; Chiron, L.; Lynch, A. M.; Barrow, M. P.; Delsuc, M. A.; O'Connor, P. B. Polymer Analysis in the Second Dimension: Preliminary Studies for the Characterization of Polymers with 2D MS. *Anal Chem* **2017**, *89* (18), 9892-9899. DOI: 10.1021/acs.analchem.7b02086.

(77) Laure, C.; Karamessini, D.; Milenkovic, O.; Charles, L.; Lutz, J. F. Coding in 2D: Using Intentional Dispersity to Enhance the Information Capacity of Sequence-Coded Polymer Barcodes. *Angew Chem Int Edit* **2016**, *55* (36), 10722-10725. DOI: 10.1002/anie.201605279.

(78) Thakkar, A.; Cohen, A. S.; Connolly, M. D.; Zuckermann, R. N.; Pei, D. High-Throughput Sequencing of Peptoids and Peptide-Peptoid Hybrids by Partial Edman Degradation and Mass Spectrometry. *J Comb Chem* **2009**, *11* (2), 294-302. DOI: 10.1021/cc8001734.

(79) Paulick, M. G.; Hart, K. M.; Brinner, K. M.; Tjandra, M.; Charych, D. H.; Zuckermann, R. N. Cleavable hydrophilic linker for one-bead-one-compound sequencing of oligomer libraries by tandem mass spectrometry. *J Comb Chem* **2006**, *8* (3), 417-426. DOI: 10.1021/cc0501460.

(80) Zimm, B. H. The Scattering of Light and the Radial Distribution Function of High Polymer Solutions. *J Chem Phys* **1948**, *16* (12), 1093-1099. DOI: Doi 10.1063/1.1746738.

(81) Chu, B.; Hsiao, B. S. Small-angle X-ray scattering of polymers. *Chem Rev* **2001**, *101* (6), 1727-1761. DOI: 10.1021/cr9900376.

(82) Svergun, D. I.; Koch, M. H. J. Small-angle scattering studies of biological macromolecules in solution. *Rep Prog Phys* **2003**, *66* (10), 1735-1782. DOI: Pii S0034-4885(03)12688-7
Doi 10.1088/0034-4885/66/10/R05.

(83) Ullman, R. Small-Angle Neutron-Scattering of Polymers. *Annu Rev Mater Sci* **1980**, *10*, 261-285. DOI: DOI 10.1146/annurev.ms.10.080180.001401.

(84) Krishnan, V. V.; Bentley, T.; Xiong, A.; Maitra, K. Conformational Ensembles by NMR and MD Simulations in Model Heptapeptides with Select Tri-Peptide Motifs. *Int J Mol Sci* **2021**, *22* (3). DOI: ARTN 1364 10.3390/ijms22031364.

(85) Guerry, P.; Herrmann, T. Advances in automated NMR protein structure determination. *Q Rev Biophys* **2011**, *44* (3), 257-309. DOI: 10.1017/S0033583510000326.

(86) Schuler, B.; Soranno, A.; Hofmann, H.; Nettels, D. Single-Molecule FRET Spectroscopy and the Polymer Physics of Unfolded and Intrinsically Disordered Proteins. *Annual Review of Biophysics, Vol 45* **2016**, *45*, 207-231. DOI: 10.1146/annurev-biophys-062215-010915.

(87) Jiao, S.; DeStefano, A.; Monroe, J. I.; Barry, M.; Sherck, N.; Casey, T.; Segalman, R. A.; Han, S.; Shell, M. S. Quantifying Polypeptoid Conformational Landscapes through Integrated Experiment and Simulation. *Macromolecules* **2021**, *54* (11), 5011-5021. DOI: 10.1021/acs.macromol.1c00550.

(88) Jeschke, G. DEER Distance Measurements on Proteins. *Annu Rev Phys Chem* **2012**, *63*, 419-446. DOI: 10.1146/annurev-physchem-032511-143716.

(89) Watkins, H. M.; Simon, A. J.; Sosnick, T. R.; Lipman, E. A.; Hjelm, R. P.; Plaxco, K. W. Random coil negative control reproduces the discrepancy between scattering and FRET measurements of denatured protein dimensions. *P Natl Acad Sci USA* **2015**, *112* (21), 6631-6636. DOI: 10.1073/pnas.1418673112.

(90) Qu, S. Y.; Liu, C. B.; Liu, Q.; Wu, W.; Du, B. J.; Wang, J. Solvent effect on FRET spectroscopic ruler. *J Chem Phys* **2018**, *148* (12). DOI: Artn 123331 10.1063/1.5004205.

(91) Riback, J. A.; Bowman, M. A.; Zmyslowski, A. M.; Plaxco, K. W.; Clark, P. L.; Sosnick, T. R. Commonly used FRET fluorophores promote collapse of an otherwise disordered protein. *P Natl Acad Sci USA* **2019**, *116* (18), 8889-8894. DOI: 10.1073/pnas.1813038116.

(92) Best, R. B.; Merchant, K. A.; Gopich, I. V.; Schuler, B.; Bax, A.; Eaton, W. A. Effect of flexibility and cis residues in single-molecule FRET studies of polyproline. *P Natl Acad Sci USA* **2007**, *104* (48), 19064-19066.

(93) Chiang, Y. W.; Borbat, P. P.; Freed, J. H. The determination of pair distance distributions by pulsed ESR using Tikhonov regularization. *J Magn Reson* **2005**, *172* (2), 279-295. DOI: 10.1016/j.jmr.2004.10.012.

(94) Sezer, D.; Freed, J. H.; Roux, B. Parametrization, molecular dynamics simulation, and calculation of electron spin resonance spectra of a nitroxide spin label on a polyalanine alpha-helix. *J Phys Chem B* **2008**, *112* (18), 5755-5767. DOI: 10.1021/jp711375x.

(95) Kaminker, R.; Kaminker, I.; Gutekunst, W. R.; Luo, Y.; Lee, S.; Niu, J.; Han, S.; Hawker, C. J. Tuning conformation and properties of peptidomimetic backbones through dual N/Cα-substitution. *Chem Commun* **2018**, *54* (41), 5237-5240. DOI: 10.1039/c8cc01356j.

(96) Morimoto, J.; Fukuda, Y.; Kuroda, D.; Watanabe, T.; Yoshida, F.; Asada, M.; Nakamura, T.; Senoo, A.; Nagatoishi, S.; Tsumoto, K.; et al. A Peptoid with Extended Shape in Water. *J Am Chem Soc* **2019**, *141* (37), 14612-14623. DOI: 10.1021/jacs.9b04371.

(97) Kotler, S. A.; Tugarinov, V.; Schmidt, T.; Ceccon, A.; Libich, D. S.; Ghirlando, R.; Schwieters, C. D.; Clore, G. M. Probing initial transient oligomerization events facilitating Huntingtin fibril nucleation at atomic resolution by relaxation-based NMR. *P Natl Acad Sci USA* **2019**, *116* (9), 3562-3571. DOI: 10.1073/pnas.1821216116.

(98) Schmidt, T.; Schwieters, C. D.; Clore, G. M. Spatial domain organization in the HIV-1 reverse transcriptase p66 homodimer precursor probed by double electron-electron resonance EPR. *P Natl Acad Sci USA* **2019**, *116* (36), 17809-17816. DOI: 10.1073/pnas.1911086116.

(99) Schmidt, T.; Jeon, J.; Okuno, Y.; Chiliveri, S. C.; Clore, G. M. Submillisecond Freezing Permits Cryoprotectant-Free EPR Double Electron-Electron Resonance Spectroscopy. *Chemphyschem* **2020**, *21* (12), 1224-1229. DOI: 10.1002/cphc.202000312.

(100) Schmidt, T.; Louis, J. M.; Clore, G. M. Probing the Interaction between HIV-1 Protease and the Homodimeric p66/p66' Reverse Transcriptase Precursor by Double Electron-Electron Resonance EPR Spectroscopy. *Chembiochem* **2020**, *21* (21), 3051-3055. DOI: 10.1002/cbic.202000263.

(101) Sherck, N.; Webber, T.; Brown, D. R.; Keller, T.; Barry, M.; DeStefano, A.; Jiao, S.; Segalman, R. A.; Fredrickson, G. H.; Shell, M. S.; et al. End-to-End Distance Probability Distributions of Dilute Poly(ethylene oxide) in Aqueous Solution. *J Am Chem Soc* **2020**, *142* (46), 19631-19641. DOI: 10.1021/jacs.0c08709.

(102) Edwards, T. H.; Stoll, S. A Bayesian approach to quantifying uncertainty from experimental noise in DEER spectroscopy. *J Magn Reson* **2016**, *270*, 87-97. DOI: 10.1016/j.jmr.2016.06.021.

(103) Fabregas Ibanez, L.; Jeschke, G.; Stoll, S. DeerLab: a comprehensive software package for analyzing dipolar electron paramagnetic resonance spectroscopy data. *Magn Reson (Gott)* **2020**, *1* (2), 209-224. DOI: 10.5194/mr-1-209-2020 From NLM PubMed-not-MEDLINE.

(104) Edwards, T. H.; Stoll, S. Optimal Tikhonov regularization for DEER spectroscopy. *J Magn Reson* **2018**, *288*, 58-68. DOI: 10.1016/j.jmr.2018.01.021.

(105) Srivastava, M.; Freed, J. H. Singular Value Decomposition Method to Determine Distance Distributions in Pulsed Dipolar Electron Spin Resonance. *Journal of Physical Chemistry Letters* **2017**, *8* (22), 5648-5655. DOI: 10.1021/acs.jpclett.7b02379.

(106) Srivastava, M.; Freed, J. H. Singular Value Decomposition Method To Determine Distance Distributions in Pulsed Dipolar Electron Spin Resonance: II. Estimating Uncertainty. *Journal of Physical Chemistry A* **2019**, *123* (1), 359-370. DOI: 10.1021/acs.jpca.8b07673.

(107) de Souza, E. S.; Hirata, I. Y.; Juliano, L.; Ito, A. S. End-to-end distance distribution in bradykinin observed by Forster resonance energy transfer. *Bba-Gen Subjects* **2000**, *1474* (2), 251-261. DOI: Doi 10.1016/S0304-4165(00)00004-0.

(108) Banham, J. E.; Baker, C. M.; Ceola, S.; Day, I. J.; Grant, G. H.; Groenen, E. J. J.; Rodgers, C. T.; Jeschke, G.; Timmel, C. R. Distance measurements in the borderline region of applicability of CW EPR and DEER: A model study on a homologous series of spin-labelled peptides. *J Magn Reson* **2008**, *191* (2), 202-218. DOI: 10.1016/j.jmr.2007.11.023.

(109) Worswick, S. G.; Spencer, J. A.; Jeschke, G.; Kuprov, I. Deep neural network processing of DEER data. *Sci Adv* **2018**, *4* (8). DOI: ARTN eaat5218 10.1126/sciadv.aat5218.

(110) Merz, G. E.; Borbat, P. P.; Muok, A. R.; Srivastava, M.; Bunck, D. N.; Freed, J. H.; Crane, B. R. Site-Specific Incorporation of a Cu2+ Spin Label into Proteins for Measuring Distances by Pulsed Dipolar Electron Spin Resonance Spectroscopy. *J Phys Chem B* **2018**, *122* (41), 9443-9451. DOI: 10.1021/acs.jpcb.8b05619.

(111) Dikiy, I.; Edupuganti, U. R.; Abzalimov, R. R.; Borbat, P. P.; Srivastava, M.; Freed, J. H.; Gardner, K. H. Insights into histidine kinase activation mechanisms from the monomeric blue light sensor EL346. *P Natl Acad Sci USA* **2019**, *116* (11), 4963-4972. DOI: 10.1073/pnas.1813586116.

(112) Srivastava, M.; Georgieva, E. R.; Freed, J. H. A New Wavelet Denoising Method for Experimental Time-Domain Signals: Pulsed Dipolar Electron Spin Resonance. *Journal of Physical Chemistry A* **2017**, *121* (12), 2452-2465. DOI: 10.1021/acs.jpca.7b00183.

(113) Doll, A.; Qi, M.; Godt, A.; Jeschke, G. CIDME: Short distances measured with long chirp pulses. *J Magn Reson* **2016**, *273*, 73-82. DOI: 10.1016/j.jmr.2016.10.011.

(114) Steinhoff, H. J.; Radzwill, N.; Thevis, W.; Lenz, V.; Brandenburg, D.; Antson, A.; Dodson, G.; Wollmer, A. Determination of interspin distances between spin labels attached to insulin: Comparison of electron paramagnetic resonance data with the x-ray structure. *Biophys J* **1997**, *73* (6), 3287-3298. DOI: Doi 10.1016/S0006-3495(97)78353-X.

(115) Rabenstein, M. D.; Shin, Y. K. Determination of the Distance between 2 Spin Labels Attached to a Macromolecule. *P Natl Acad Sci USA* **1995**, *92* (18), 8239-8243. DOI: DOI 10.1073/pnas.92.18.8239.

(116) *ShortDistances*; 2014. https://sites.google.com/site/altenbach/labview-programs/epr-programs/short-distances (accessed Jan 2020).

(117) Altenbach, C.; Oh, K. J.; Trabanino, R. J.; Hideg, K.; Hubbell, W. L. Estimation of inter-residue distances in spin labeled proteins at physiological temperatures: Experimental strategies and practical limitations. *Biochemistry-Us* **2001**, *40* (51), 15471-15482. DOI: 10.1021/bi011544w.

(118) Franck, J. M.; Han, S. Overhauser Dynamic Nuclear Polarization for the Study of Hydration Dynamics, Explained. *Biological Nmr, Pt B* **2019**, *615*, 131-175. DOI: 10.1016/bs.mie.2018.09.024.

(119) Franck, J. M.; Pavlova, A.; Scott, J. A.; Han, S. Quantitative cw Overhauser effect dynamic nuclear polarization for the analysis of local water dynamics. *Prog Nucl Mag Res Sp* **2013**, *74*, 33-56. DOI: 10.1016/j.pnmrs.2013.06.001.

(120) Armstrong, B. D.; Choi, J.; Lopez, C.; Wesener, D. A.; Hubbell, W.; Cavagnero, S.; Han, S. Site-Specific Hydration Dynamics in the Nonpolar Core of a Molten Globule by Dynamic Nuclear Polarization of Water. *J Am Chem Soc* **2011**, *133* (15), 5987-5995. DOI: 10.1021/ja111515s.

(121) Pavlova, A.; Cheng, C. Y.; Kinnebrew, M.; Lew, J.; Dahlquist, F. W.; Han, S. Protein structural and surface water rearrangement constitute major events in the earliest aggregation stages of tau. *P Natl Acad Sci USA* **2016**, *113* (2), E127-E136. DOI: 10.1073/pnas.1504415113.

(122) Stone, K. M.; Voska, J.; Kinnebrew, M.; Pavlova, A.; Junk, M. J. N.; Han, S. G. Structural Insight into Proteorhodopsin Oligomers. *Biophys J* **2013**, *104* (2), 472-481. DOI: 10.1016/j.bpj.2012.11.3831.

(123) Stals, P. J. M.; Cheng, C. Y.; van Beek, L.; Wauters, A. C.; Palmans, A. R. A.; Han, S. G.; Meijer, E. W. Surface water retardation around single-chain polymeric nanoparticles: critical for catalytic function? *Chem Sci* **2016**, *7* (3), 2011-2015. DOI: 10.1039/c5sc02319j.

(124) Ortony, J. H.; Qiao, B. F.; Newcomb, C. J.; Keller, T. J.; Palmer, L. C.; Deiss-Yehiely, E.; de la Cruz, M. O.; Han, S.; Stupp, S. I. Water Dynamics from the Surface to the Interior of a Supramolecular Nanostructure. *J Am Chem Soc* **2017**, *139* (26), 8915-8921. DOI: 10.1021/jacs.7b02969.

(125) *DNPLab*; 2021. http://dnplab.net/ (accessed February 4, 2021).

(126) Jiao, S.; Mirabal, D. M. R.; DeStefano, A. J.; Segalman, R. A.; Han, S.; Shell, M. S. Sequence Modulates Polypeptoid Hydration Water Structure and Dynamics. *Biomacromolecules* **2022**, *23* (4), 1745-1756. DOI: 10.1021/acs.biomac.1c016137.

(127) Polymeropoulos, G.; Zapsas, G.; Ntetsikas, K.; Bilalis, P.; Gnanou, Y.; Hadjichristidis, N. 50th Anniversary Perspective: Polymers with Complex Architectures. *Macromolecules* **2017**, *50* (4), 1253-1290. DOI: 10.1021/acs.macromol.6b02569.

(128) Bates, F. S.; Hillmyer, M. A.; Lodge, T. P.; Bates, C. M.; Delaney, K. T.; Fredrickson, G. H. Multiblock Polymers: Panacea or Pandora's Box? *Science* **2012**, *336* (6080), 434-440. DOI: 10.1126/science.1215368.

(129) Korendovych, I. V.; DeGrado, W. F. De novo protein design, a retrospective. *Q Rev Biophys* **2020**, *53*. DOI: ARTN e3
PII S0033583519000131
10.1017/S0033583519000131.

(130) Pan, X. J.; Kortemme, T. Recent advances in de novo protein design: Principles, methods, and applications. *J Biol Chem* **2021**, *296*. DOI: ARTN 100558
10.1016/j.jbc.2021.100558.

(131) Kuhlman, B.; Bradley, P. Advances in protein structure prediction and design. *Nat Rev Mol Cell Bio* **2019**, *20* (11), 681-697. DOI: 10.1038/s41580-019-0163-x.

(132) Schadler, V.; Wiesner, U. Salt-controlled lamellar spacing in ionically end-capped symmetric diblock copolymers. *Macromolecules* **1997**, *30* (21), 6698-6701. DOI: DOI 10.1021/ma9707852.

(133) Perry, S. L.; Sing, C. E. 100th Anniversary of Macromolecular Science Viewpoint: Opportunities in the Physics of Sequence-Defined Polymers. *ACS Macro Lett* **2020**, *9* (2), 216-225. DOI: 10.1021/acsmacrolett.0c00002 From NLM PubMed-not-MEDLINE.

(134) Rosales, A. M.; Segalman, R. A.; Zuckermann, R. N. Polypeptoids: a model system to study the effect of monomer sequence on polymer properties and self-assembly (vol 9, pg 8400, 2013). *Soft Matter* **2013**, *9* (48), 11713-11713.

(135) Murnen, H. K.; Rosales, A. M.; Dobrynin, A. V.; Zuckermann, R. N.; Segalman, R. A. Persistence length of polyelectrolytes with precisely located charges. *Soft Matter* **2013**, *9* (1), 90-98. DOI: 10.1039/c2sm26849c.

(136) Sternhagen, G. L.; Gupta, S.; Zhang, Y. H.; John, V.; Schneider, G. J.; Zhang, D. H. Solution Self-Assemblies of Sequence-Defined Ionic Peptoid Block Copolymers. *J Am Chem Soc* **2018**, *140* (11), 4100-4109. DOI: 10.1021/jacs.8b00461.

(137) Kang, L.; Chao, A.; Zhang, M.; Yu, T.; Wang, J.; Wang, Q.; Yu, H.; Jiang, N.; Zhang, D. Modulating the Molecular Geometry and Solution Self-Assembly of Amphiphilic Polypeptoid Block Copolymers by Side Chain Branching Pattern. *J Am Chem Soc* **2021**, *143* (15), 5890-5902. DOI: 10.1021/jacs.1c01088.

(138) Jiang, N. S.; Yu, T. Y.; Darvish, O. A.; Qian, S.; Tsengam, I. K. M.; John, V.; Zhang, D. H. Crystallization-Driven Self-Assembly of Coil-Comb-Shaped Polypeptoid Block Copolymers: Solution Morphology and Self-Assembly Pathways. *Macromolecules* **2019**, *52* (22), 8867-8877. DOI: 10.1021/acs.macromol.9b01546.

(139) Hudson, B. C.; Battigelli, A.; Connolly, M. D.; Edison, J.; Spencer, R. K.; Whitelam, S.; Zuckermann, R. N.; Paravastu, A. K. Evidence for cis Amide Bonds in Peptoid

Nanosheets. *Journal of Physical Chemistry Letters* **2018**, *9* (10), 2574-2578. DOI: 10.1021/acs.jpclett.8b01040.

(140) Cheng, Y. K.; Rossky, P. J. Surface topography dependence of biomolecular hydrophobic hydration. *Nature* **1998**, *392* (6677), 696-699. DOI: Doi 10.1038/33653.

(141) Kauzmann, W. Some Factors in the Interpretation of Protein Denaturation. *Adv Protein Chem* **1959**, *14*, 1-63. DOI: Doi 10.1016/S0065-3233(08)60608-7.

(142) DeStefano, A. J.; Segalman, R. A.; Davidson, E. C. Where Biology and Traditional Polymers Meet: The Potential of Associating Sequence-Defined Polymers for Materials Science. *Jacs Au* **2021**, *1* (10), 1556-1571. DOI: 10.1021/jacsau.1c00297.

(143) Hiemenz, P. C.; Lodge, T. P. *Polymer Chemistry*; CRC Press, 2007.

(144) Schäfer, L. Dilute Limit: Details on the Internal Structure of Isolated Coils. In *Excluded Volume Effects in Polymer Solutions*, Springer, 1999; p 311.

(145) Bernado, P.; Svergun, D. I. Structural analysis of intrinsically disordered proteins by small-angle X-ray scattering. *Mol Biosyst* **2012**, *8* (1), 151-167. DOI: 10.1039/c1mb05275f From NLM Medline.

(146) Kosol, S.; Contreras-Martos, S.; Cedeno, C.; Tompa, P. Structural characterization of intrinsically disordered proteins by NMR spectroscopy. *Molecules* **2013**, *18* (9), 10802-10828. DOI: 10.3390/molecules180910802 From NLM Medline.

(147) Moeglich, A.; Joder, K.; Kiefhaber, T. End-to-end distance distributions and intrachain diffusion constants in unfolded polypeptide chains indicate intramolecular hydrogen bond formation (vol 103, pg 12394, 2006). *P Natl Acad Sci USA* **2008**, *105* (18), 6787-6787. DOI: 10.1073/pnas.0803144105.

(148) Merchant, K. A.; Best, R. B.; Louis, J. M.; Gopich, I. V.; Eaton, W. A. Characterizing the unfolded states of proteins using single-molecule FRET spectroscopy and molecular simulations. *P Natl Acad Sci USA* **2007**, *104* (5), 1528-1533. DOI: 10.1073/pnas.0607097104.

(149) Flory, P. J. *Principles of Polymer Chemistry*; Cornell University Press, 1953.

(150) Ewart, R. H.; Roe, C. P.; Debye, P.; Mccartney, J. R. The Determination of Polymeric Molecular Weights by Light Scattering in Solvent-Precipitant Systems. *J Chem Phys* **1946**, *14* (11), 687-695. DOI: Doi 10.1063/1.1724085.

(151) Li, B.; Madras, N.; Sokal, A. D. Critical Exponents, Hyperscaling, and Universal Amplitude Ratios for 2-Dimensional and 3-Dimensional Self-Avoiding Walks. *J Stat Phys* **1995**, *80* (3-4), 661-754. DOI: Doi 10.1007/Bf02178552.

(152) Duplantier, B. Geometrical properties of a Kuhnian polymer chain. *Journal de Physique* **1986**, *47* (10), 1633-1656. DOI: 10.1051/jphys:0198600470100163300.

(153) Tanaka, T.; Kotaka, T.; Ban, K.; Hattori, M.; Inagaki, H. Conformation of Block Copolymers in Dilute-Solution - Molecular Dimension-Block Architecture Relationships. *Macromolecules* **1977**, *10* (5), 960-967. DOI: DOI 10.1021/ma60059a014.

(154) Tanaka, T.; Omoto, M.; Inagaki, H. Conformation of Block Copolymers in Dilute-Solution .3. Determination of the Center-to-Center Distance between the 2 Blocks by Light-Scattering. *Macromolecules* **1979**, *12* (1), 146-152. DOI: DOI 10.1021/ma60067a030.

(155) Kotaka, T.; Tanaka, T.; Inagaki, H. Thermodynamic and Conformational Properties of Styrene-Methyl Methacrylate Block Copolymers in Dilute-Solution .4. Behavior of Diblock and Triblock Copolymers in Selective Solvents. *Polym J* **1972**, *3* (3), 327-&. DOI: DOI 10.1295/polymj.3.327.

(156) Tanaka, T.; Kotaka, T.; Inagaki, H. Conformation of Block Copolymers in Dilute-Solution - Monte-Carlo Calculations and Light-Scattering-Studies on Di-Block Copolymer Systems. *Macromolecules* **1976**, *9* (4), 561-568. DOI: DOI 10.1021/ma60052a006.

(157) Dondos, A.; Rempp, P.; Benoit, H. Investigations on Conformations of Block and of Random Copolymers in Dilute Solution. *Makromolekul Chem* **1969**, *130* (Dec), 233-&.

(158) Pfannebecker, V.; Klos, H.; Hubrich, M.; Volkmer, T.; Heuer, A.; Wiesner, U.; Spiess, H. W. Determination of end-to-end distances in oligomers by pulsed EPR. *J Phys Chem-Us* **1996**, *100* (32), 13428-13432. DOI: DOI 10.1021/jp960895v.

(159) *LongDistances*; 2022. https://sites.google.com/site/altenbach/labview-programs/epr-programs/long-distances (accessed May 2022).

(160) Lau, K. F.; Dill, K. A. Theory for Protein Mutability and Biogenesis. *P Natl Acad Sci USA* **1990**, *87* (2), 638-642. DOI: DOI 10.1073/pnas.87.2.638.

(161) Khokhlov, A. R.; Khalatur, P. G. Protein-like copolymers: Computer simulation. *Physica A* **1998**, *249* (1-4), 253-261. DOI: Doi 10.1016/S0378-4371(97)00473-1.

(162) Khokhlov, A. R.; Khalatur, P. G. Conformation-dependent sequence design (engineering) of AB copolymers. *Phys Rev Lett* **1999**, *82* (17), 3456-3459. DOI: DOI 10.1103/PhysRevLett.82.3456.

(163) Schäfer, L. *Excluded Volume Effects in Polymer Solutions*; Springer Berlin, Heidelberg, 1999. DOI: 10.1007/978-3-642-60093-7.

(164) Pappu, R. V.; Wang, X.; Vitalis, A.; Crick, S. L. A polymer physics perspective on driving forces and mechanisms for protein aggregation. *Arch Biochem Biophys* **2008**, *469* (1), 132-141. DOI: 10.1016/j.abb.2007.08.033.

(165) Bock, J.; Siano, D. B.; Valint, P. L.; Pace, S. J. Structure and Properties of Hydrophobically Associating Polymers. *Adv Chem Ser* **1989**, (223), 411-424.

(166) Ruff, K. M.; Pappu, R. V. AlphaFold and Implications for Intrinsically Disordered Proteins. *J Mol Biol* **2021**, *433* (20), 167208. DOI: 10.1016/j.jmb.2021.167208 From NLM Medline.

(167) Kendrew, J. C.; Bodo, G.; Dintzis, H. M.; Parrish, R. G.; Wyckoff, H.; Phillips, D. C. 3-Dimensional Model of the Myoglobin Molecule Obtained by X-Ray Analysis. *Nature* **1958**, *181* (4610), 662-666. DOI: DOI 10.1038/181662a0.

(168) Fisette, O.; Paslack, C.; Barnes, R.; Isas, J. M.; Langen, R.; Heyden, M.; Han, S.; Schafer, L. V. Hydration Dynamics of a Peripheral Membrane Protein. *J Am Chem Soc* **2016**, *138* (36), 11526-11535. DOI: 10.1021/jacs.6b07005 From NLM Medline.

(169) Moon, H.; Collanton, R. P.; Monroe, J. I.; Casey, T. M.; Shell, M. S.; Han, S.; Scott, S. L. Evidence for Entropically Controlled Interfacial Hydration in Mesoporous Organosilicas. *J Am Chem Soc* **2022**, *144* (4), 1766-1777. DOI: 10.1021/jacs.1c11342.

(170) Schrader, A. M.; Monroe, J. I.; Sheil, R.; Dobbs, H. A.; Keller, T. J.; Li, Y. X.; Jain, S.; Shell, M. S.; Israelachvili, J. N.; Han, S. G. Surface chemical heterogeneity modulates silica surface hydration. *P Natl Acad Sci USA* **2018**, *115* (12), 2890-2895. DOI: 10.1073/pnas.1722263115.

(171) Moon, H.; Han, S.; Scott, S. L. Tuning molecular adsorption in SBA-15-type periodic mesoporous organosilicas by systematic variation of their surface polarity. *Chem Sci* **2020**, *11* (14), 3702-3712. DOI: 10.1039/d0sc00168f.

(172) Chatzichristos, A.; Hassan, J. Current Understanding of Water Properties inside Carbon Nanotubes. *Nanomaterials-Basel* **2022**, *12* (1), 174. DOI: 10.3390/nano12010174.

(173) Jiao, S.; Katz, L. E.; Shell, M. S. Inverse Design of Pore Wall Chemistry To Control Solute Transport and Selectivity. *Acs Central Sci* **2022**, *8*, 1609-1617. DOI: 10.1021/acscentsci.2c01011.

(174) Sakthivel, K.; Notz, W.; Bui, T.; Barbas, C. F. Amino acid catalyzed direct asymmetric aldol reactions: A bioorganic approach to catalytic asymmetric carbon-carbon bond-forming reactions. *J Am Chem Soc* **2001**, *123* (22), 5260-5267. DOI: 10.1021/ja010037z.

(175) Huerta, E.; Stals, P. J. M.; Meijer, E. W.; Palmans, A. R. A. Consequences of Folding a Water-Soluble Polymer Around an Organocatalyst. *Angew Chem Int Edit* **2013**, *52* (10), 2906-2910. DOI: 10.1002/anie.201207123.

(176) Kandel, K.; Althaus, S. M.; Peeraphatdit, C.; Kobayashi, T.; Trewyn, B. G.; Pruski, M.; Slowing, I. I. Solvent-Induced Reversal of Activities between Two Closely Related Heterogeneous Catalysts in the Aldol Reaction. *Acs Catal* **2013**, *3* (2), 265-271. DOI: 10.1021/cs300748g.

(177) Saito, S.; Yamamoto, H. Design of acid - Base catalysis for the asymmetric direct aidol reaction. *Accounts Chem Res* **2004**, *37* (8), 570-579. DOI: 10.1021/ar030064p.

(178) Singappuli-Arachchige, D.; Manzano, J. S.; Sherman, L. M.; Slowing, I. I. Polarity Control at Interfaces: Quantifying Pseudo-solvent Effects in Nano-confined Systems. *Chemphyschem* **2016**, *17* (19), 2982-2986. DOI: 10.1002/cphc.201600740.

(179) Singappuli-Arachchige, D.; Kobayashi, T.; Wang, Z. R.; Burkhow, S. J.; Smith, E. A.; Pruski, M.; Slowing, I. I. Interfacial Control of Catalytic Activity in the Aldol Condensation: Combining the Effects of Hydrophobic Environments and Water. *Acs Catal* **2019**, *9* (6), 5574-5582. DOI: 10.1021/acscatal.9b00195.

(180) Laage, D.; Elsaesser, T.; Hynes, J. T. Water Dynamics in the Hydration Shells of Biomolecules. *Chem Rev* **2017**, *117* (16), 10694-10725. DOI: 10.1021/acs.chemrev.6b00765 From NLM Medline.

(181) Gomez, A.; Piskulich, Z. A.; Thompson, W. H.; Laage, D. Water Diffusion Proceeds via a Hydrogen-Bond Jump Exchange Mechanism. *J Phys Chem Lett* **2022**, *13* (21), 4660-4666. DOI: 10.1021/acs.jpclett.2c00825 From NLM Medline.

(182) Duboue-Dijon, E.; Laage, D. Characterization of the Local Structure in Liquid Water by Various Order Parameters. *J Phys Chem B* **2015**, *119* (26), 8406-8418. DOI: 10.1021/acs.jpcb.5b02936.

(183) Monroe, J.; Barry, M.; DeStefano, A.; Gokturk, P. A.; Jiao, S.; Robinson-Brown, D.; Webber, T.; Crumlin, E. J.; Han, S.; Shell, M. S. Water Structure and Properties at Hydrophilic and Hydrophobic Surfaces. *Annu Rev Chem Biomol* **2020**, *11*, 523-557. DOI: 10.1146/annurev-chembioeng-120919-114657.

(184) Connolly, M. D.; Xuan, S. T.; Molchanova, N.; Zuckermann, R. N. Submonomer synthesis of sequence defined peptoids with diverse side-chains. *Method Enzymol* **2021**, *656*, 241-270. DOI: 10.1016/bs.mie.2021.04.022.

(185) Kim, S.; Biswas, G.; Park, S.; Kim, A.; Park, H.; Park, E.; Kim, J.; Kwon, Y. U. Unusual truncation of N-acylated peptoids under acidic conditions. *Org Biomol Chem* **2014**, *12* (28), 5222-5226. DOI: 10.1039/c3ob42572j.

(186) Wijaya, A. W.; Nguyen, A. I.; Roe, L. T.; Butterfoss, G. L.; Spencer, R. K.; Li, N. K.; Zuckermann, R. N. Cooperative Intramolecular Hydrogen Bonding Strongly Enforces cis-Peptoid Folding. *J Am Chem Soc* **2019**, *141* (49), 19436-19447. DOI: 10.1021/jacs.9b10497.

(187) *Multicomponent*; 2021. https://sites.google.com/site/altenbach/labview-programs/epr-programs/multicomponent (accessed January 15, 2022).

(188) Song, J.; Franck, J.; Pincus, P.; Kim, M. W.; Han, S. Specific Ions Modulate Diffusion Dynamics of Hydration Water on Lipid Membrane Surfaces. *J Am Chem Soc* **2014**, *136* (6), 2642-2649. DOI: 10.1021/ja4121692.

(189) Daoud, M.; Cotton, J. P. Star shaped polymers : a model for the conformation and its concentration dependence. *Journal de Physique* **1982**, *43* (3), 531-538. DOI: 10.1051/jphys:01982004303053100.

(190) Birshtein, T. M.; Zhulina, E. B. Conformations of Star-Branched Macromolecules. *Polymer* **1984**, *25* (10), 1453-1461. DOI: Doi 10.1016/0032-3861(84)90109-5.

(191) Zhulina, E. B.; Borisov, O. V. Theory of Block Polymer Micelles: Recent Advances and Current Challenges. *Macromolecules* **2012**, *45* (11), 4429-4440. DOI: 10.1021/ma300195n.

(192) Lee, C. Y.; Mccammon, J. A.; Rossky, P. J. The Structure of Liquid Water at an Extended Hydrophobic Surface. *J Chem Phys* **1984**, *80* (9), 4448-4455. DOI: Doi 10.1063/1.447226.

(193) Nibali, V. C.; Pezzotti, S.; Sebastiani, F.; Galimberti, D. R.; Schwaab, G.; Heyden, M.; Gaigeot, M. P.; Havenith, M. Wrapping Up Hydrophobic Hydration: Locality Matters. *Journal of Physical Chemistry Letters* **2020**, *11* (12), 4809-4816. DOI: 10.1021/acs.jpclett.0c00846.

(194) Merzel, F.; Smith, J. C. Is the first hydration shell of lysozyme of higher density than bulk water? *Proc Natl Acad Sci U S A* **2002**, *99* (8), 5378-5383. DOI: 10.1073/pnas.082335099 From NLM Medline.

(195) Scala, A.; Starr, F. W.; La Nave, E.; Sciortino, F.; Stanley, H. E. Configurational entropy and diffusivity of supercooled water. *Nature* **2000**, *406* (6792), 166-169. DOI: Doi 10.1038/35018034.

(196) Agarwal, M.; Singh, M.; Sharma, R.; Alam, M. P.; Chakravarty, C. Relationship between Structure, Entropy, and Diffusivity in Water and Water-Like Liquids. *J Phys Chem B* **2010**, *114* (20), 6995-7001. DOI: 10.1021/jp101956u.

(197) Chopra, R.; Truskett, T. M.; Errington, J. R. On the Use of Excess Entropy Scaling to Describe the Dynamic Properties of Water. *J Phys Chem B* **2010**, *114* (32), 10558-10566. DOI: 10.1021/jp1049155.

(198) Nayar, D.; Chakravarty, C. Water and water-like liquids: relationships between structure, entropy and mobility. *Phys Chem Chem Phys* **2013**, *15* (34), 14162-14177. DOI: 10.1039/c3cp51114f.

(199) Ortony, J. H.; Newcomb, C. J.; Matson, J. B.; Palmer, L. C.; Doan, P. E.; Hoffman, B. M.; Stupp, S. I. Internal dynamics of a supramolecular nanofibre. *Nat Mater* **2014**, *13* (8), 812-816. DOI: 10.1038/Nmat3979.

(200) Budil, D. E.; Lee, S.; Saxena, S.; Freed, J. H. Nonlinear-least-squares analysis of slow-motion EPR spectra in one and two dimensions using a modified Levenberg-Marquardt algorithm. *J Magn Reson Ser A* **1996**, *120* (2), 155-189. DOI: DOI 10.1006/jmra.1996.0113.

(201) Bullock, A. T.; Cameron, G. G.; Smith, P. M. Electron-Spin Resonance Studies of Spin-Labeled Polymers .7. Dependence of Rotational Correlation Times on Solvent

Properties and Polymer Concentration. *J Chem Soc Farad T 2* **1974**, *70* (7), 1202-1210. DOI: DOI 10.1039/f29747001202.

(202) Bullock, A. T.; Cameron, G. G.; Krajewski, V. Electron-Spin Resonance Studies of Spin-Labeled Polymers .11. Segmental and End-Group Mobility of Some Acrylic Ester Polymers. *J Phys Chem-Us* **1976**, *80* (16), 1792-1797. DOI: DOI 10.1021/j100557a011.

(203) Eisenreich, F.; Palmans, A. R. A. Compartmentalized Polymers for Catalysis in Aqueous Media. In *Supramolecular Catalysis*, 2022; pp 489-506.

(204) Serrano-Luginbuhl, S.; Ruiz-Mirazo, K.; Ostaszewski, R.; Gallou, F.; Walde, P. Soft and dispersed interface-rich aqueous systems that promote and guide chemical reactions. *Nat Rev Chem* **2018**, *2* (10), 306-327. DOI: 10.1038/s41570-018-0042-6.

(205) Rothfuss, H.; Knofel, N. D.; Roesky, P. W.; Barner-Kowollik, C. Single-Chain Nanoparticles as Catalytic Nanoreactors. *J Am Chem Soc* **2018**, *140* (18), 5875-5881. DOI: 10.1021/jacs.8b02135.

(206) Azuma, Y.; Terashima, T.; Sawamoto, M. Self-Folding Polymer Iron Catalysts for Living Radical Polymerization. *Acs Macro Letters* **2017**, *6* (8), 830-835. DOI: 10.1021/acsmacrolett.7b00498.

(207) Chen, J. F.; Wang, J.; Bai, Y. G.; Li, K.; Garcia, E. S.; Ferguson, A. L.; Zimmerman, S. C. Enzyme-like Click Catalysis by a Copper-Containing Single-Chain Nanoparticle. *J Am Chem Soc* **2018**, *140* (42), 13695-13702. DOI: 10.1021/jacs.8b06875.

(208) Chen, J. F.; Wang, J.; Li, K.; Wang, Y. H.; Gruebele, M.; Ferguson, A. L.; Zimmerman, S. C. Polymeric "Clickase" Accelerates the Copper Click Reaction of Small Molecules, Proteins, and Cells. *J Am Chem Soc* **2019**, *141* (24), 9693-9700. DOI: 10.1021/jacs.9b04181.

(209) Eisenreich, F.; Meijer, E. W.; Palmans, A. R. Amphiphilic Polymeric Nanoparticles for Photoredox Catalysis in Water. *Chem-Eur J* **2020**, *26* (45), 10355-10361. DOI: 10.1002/chem.202001767.

(210) Kroger, A. P. P.; Paats, J. W. D.; Boonen, R. J. E. A.; Hamelmann, N. M.; Paulusse, J. M. J. Pentafluorophenyl-based single-chain polymer nanoparticles as a versatile platform towards protein mimicry. *Polym Chem-Uk* **2020**, *11* (37), 6056-6065. DOI: 10.1039/d0py00922a.

(211) Lu, A.; Smart, T. P.; Epps, T. H.; Longbottom, D. A.; O'Reilly, R. K. L-Proline Functionalized Polymers Prepared by RAFT Polymerization and Their Assemblies as Supported Organocatalysts. *Macromolecules* **2011**, *44* (18), 7233-7241. DOI: 10.1021/ma201256m.

(212) Lu, A.; Cotanda, P.; Patterson, J. P.; Longbottom, D. A.; O'Reilly, R. K. Aldol reactions catalyzed by L-proline functionalized polymeric nanoreactors in water. *Chem Commun* **2012**, *48* (78), 9699-9701. DOI: 10.1039/c2cc35170f.

(213) Liu, K.; Xu, W. W.; Wang, Q. Y.; Tang, Y.; Sheng, W. B.; Shen, Y. H.; Shi, L. J. Self-assembly of L-proline functional thermoresponsive double hydrophlic block copolymers for aldol reaction in water: the influence of POEGA block content. *Colloid Polym Sci* **2018**, *296* (7), 1109-1117. DOI: 10.1007/s00396-018-4327-6.

(214) Liu, K. Y.; Ye, L.; Wang, Y.; Du, G. H.; Jiang, L. M. A Pseudopeptide Polymer Micelle Used for Asymmetric Catalysis of the Aldol Reaction in Water. *Polymers-Basel* **2018**, *10* (9). DOI: ARTN 1004 10.3390/polym10091004.

(215) Cotanda, P.; Lu, A.; Patterson, J. P.; Petzetakis, N.; O'Reilly, R. K. Functionalized Organocatalytic Nanoreactors: Hydrophobic Pockets for Acylation Reactions in Water. *Macromolecules* **2012**, *45* (5), 2377-2384. DOI: 10.1021/ma2027462.

(216) Boucher-Jacobs, C.; Rabnawaz, M.; Katz, J. S.; Even, R.; Guironnet, D. Encapsulation of catalyst in block copolymer micelles for the polymerization of ethylene in aqueous medium. *Nat Commun* **2018**, *9*. DOI: ARTN 841 10.1038/s41467-018-03253-5.

(217) Liu, Y.; Wang, Y.; Wang, Y. F.; Lu, J.; Pinon, V.; Weck, M. Shell Cross-Linked Micelle-Based Nanoreactors for the Substrate-Selective Hydrolytic Kinetic Resolution of Epoxides. *J Am Chem Soc* **2011**, *133* (36), 14260-14263. DOI: 10.1021/ja206644d.

(218) Kim, K. T.; Cornelissen, J. J. L. M.; Nolte, R. J. M.; van Hest, J. C. M. A Polymersome Nanoreactor with Controllable Permeability Induced by Stimuli-Responsive Block Copolymers. *Adv Mater* **2009**, *21* (27), 2787-+. DOI: 10.1002/adma.200900300.

(219) Lu, J.; Dimroth, J.; Weck, M. Compartmentalization of Incompatible Catalytic Transformations for Tandem Catalysis. *J Am Chem Soc* **2015**, *137* (40), 12984-12989. DOI: 10.1021/jacs.5b07257.

(220) Qu, P. Y.; Kuepfert, M.; Jockusch, S.; Weck, M. Compartmentalized Nanoreactors for One-Pot Redox-Driven Transformations. *Acs Catal* **2019**, *9* (4), 2701-2706. DOI: 10.1021/acscatal.8b04667.

(221) Qu, P. Y.; Kuepfert, M.; Ahmed, E.; Liu, F. B.; Weck, M. Cross-Linked Polymeric Micelles as Catalytic Nanoreactors. *Eur J Inorg Chem* **2021**, *2021* (15), 1420-1427. DOI: 10.1002/ejic.202100013.

(222) DeStefano, A. J.; Nguyen, M.; Fredrickson, G. H.; Han, S. G.; Segalman, R. A. Design of Soft Material Surfaces with Rationally Tuned Water Diffusivity. *Acs Central Sci* **2023**, *9* (5), 1019-1024. DOI: 10.1021/acscentsci.3c00208.

(223) Evans, A. C.; Lu, A.; Ondeck, C.; Longbottom, D. A.; O'Reilly, R. K. Organocatalytic Tunable Amino Acid Polymers Prepared by Controlled Radical Polymerization. *Macromolecules* **2010**, *43* (15), 6374-6380. DOI: 10.1021/ma1008447.

(224) Kleinschmidt, D.; Fernandes, M. S.; Mork, M.; Meyer, A. A.; Krischel, J.; Anakhov, M. V.; Gumerov, R. A.; Potemkin, I. I.; Rueping, M.; Pich, A. Enhanced catalyst performance through compartmentalization exemplified by colloidal L-proline modified microgel catalysts. *J Colloid Interf Sci* **2020**, *559*, 76-87. DOI: 10.1016/j.jcis.2019.10.005.

(225) Gruttadauria, M.; Giacalone, F.; Marculescu, A. M.; Lo Meo, P.; Riela, S.; Noto, R. Hydrophobically directed aldol reactions: Polystyrene-supported l-proline as a recyclable catalyst for direct asymmetric aldol reactions in the presence of water. *Eur J Org Chem* **2007**, *2007* (28), 4688-4698. DOI: 10.1002/ejoc.200700586.

(226) Hayashi, Y.; Itoh, T.; Nagae, N.; Ohkubo, M.; Ishikawa, H. The effectiveness of proteinogenic amino acids in the asymmetric aldol reaction in DMSO and aqueous DMSO. *Synlett* **2008**, (10), 1565-1570. DOI: 10.1055/s-2008-1077789.

(227) Kenath, G. S.; Karanastasis, A. A.; Ullal, C. K. Super-Resolution Imaging of Spatial Heterogeneities in Model Thermosensitive Hydrogels with Implications for Their Origins. *Macromolecules* **2021**, *54* (17), 7743-7753. DOI: 10.1021/acs.macromol.1c00754.

(228) Daly, A. C.; Riley, L.; Segura, T.; Burdick, J. A. Hydrogel microparticles for biomedical applications. *Nat Rev Mater* **2020**, *5* (1), 20-43. DOI: 10.1038/s41578-019-0148-6.